UNIVERSIDAD DE CHILE
FACULTAD DE CIENCIAS FÍSICAS Y MATEMÁTICAS
DEPARTAMENTO DE ASTRONOMÍA

# GAP FORMATION AND ITS CONSECUENCE IN THE EVOLUTION OF SMBHS BINARIES IN GALAXY MERGERS

TESIS PARA OPTAR AL GRADO DE
DOCTOR EN CIENCIAS CON MENCIÓN EN ASTRONOMÍA

**LUCIANO NOE DEL VALLE BERTONI**

PROFESOR GUÍA:
DR. ANDRÉS ESCALA ASTORQUIZA

MIEMBROS DE LA COMISIÓN:
DR. JORGE CUADRA STIPETICH
DR. DIEGO MARDONES PÉREZ
DR. PAU AMARO SEOANE
DR. CESAR FUENTES GONZÁLEZ

SANTIAGO DE CHILE
DICIEMBRE, 2015

# RESUMEN

En el contexto del modelo de formacion jerárquico, las galaxias son esculpidas por una secuencia de colisiones y eventos de acreción. En algunas de estas colisiones los núcleos de cada galaxia migran a la región central del nuevo sistema y se fusionan, formando un nuevo núcleo virializado. Dentro de este nuevo núcleo los agujeros negros super masivos (SMBHs) de cada galaxia migran hacia el centro debido a la fricción dinámica, formando un sistema binario de SMBHs. Entender la evolución de estas binarias es crucial ya que si la separacion de los SMBHs se reduce a un tamaño comparable con $a_{\rm GW} \sim 10^{-3}(M_{\rm MBHs}/10^6 M_\odot)$ pc, entonces la binaria se convierte en una fuente intensa de ondas gravitacionales (GW) lo cual permite la coalescencia de los SMBHs en $10^{10}$ años. Por lo tanto, si somos capaces de determinar que le ocurrirá a las binarias de SMBH después de una colisión de galaxias, seremos capaces de determinar la cantidad de fuentes intensas de GW en el Universo y comprenderemos mejor la evolución cósmica de la población de SMBHs. Si las galaxias involucradas en una colisión tienen una fracción de gas de al menos 1 %, esperamos que se forme un disco de gas masivo en el kiloparsec central del remanente de la colisón, con una masa $\sim 1-10$ veces la masa de los SMBHs. Este gas puede extraer eficientemente el momento angular de la binaria, haciendo que su separación disminuya hasta un valor comparable con $a_{\rm GW}$, en una escala de tiempo del orden de $10^7$ años. Sin embargo, si el gas no es capaz de redistribuir de manera eficiente el momento angular extraído de la binaria entonces se alejara de esta, generando un vacío de baja densidad (gap) alrededor de la binaria. En este caso la binaria entrara en un régimen de contracción lenta cuya escala de tiempo es comparable con la edad del Universo.

Motivado por este escenario, en esta tesis derivo un criterio analítico para determinar la formación de gap en estos sistemas, es decir, bajo que condiciones una binaria experimentará una contracción rápida o una lenta. Las estimaciones derivadas de mi criterio son concordantes con los resultados de simulaciones numéricas de sistemas binaria/disco.

Realice simulaciones numéricas de colisiones de galaxias para determinar la probabilidad de que se cumplan las condiciones para una contracción rapida de la binaria, en sistemas astrofísicos reales. En todas las simulaciones observe que la formación de un gap es poco probable. Estime que la formación de gap sería posible sólo si el gas tiene una velocidad turbulenta igual o menor a la del centro de galaxias espirales locales (10 km $\rm s^{-1}$). Otra posibilidad sería que los SMBHs acreten una masa mayor al 2 % de la masa del núcleo de la galaxia remanente, lo que implica que los SMBHs deberían acretar a un ritmo mucho mayor que el derivado de observaciones. Además, use simulaciones numéricas para estudiar el efecto de la formación estrelar en la evolución dinámica de un par de SMBHs en la época pre-binaria y concluí que si la eficiencia de la formación estrelar cambia en un factor $\sim 20$, entonces el tiempo de migración de los SMBHs cambia sólo en un factor 2.

De mi resultados concluyo que es probable que las binarias de SMBHs experimenten una contracción rápida. Esto implica que el número de binarias de SMBHs en el Universo debiera ser muy bajo. Esta restricción es muy importante para la evolución de la población cósmica de SMBHs, el número esperado de binarias de SMBH en el Universo y la cantidad de fuentes de GW que esperamos observar con futuras misiones.

# ABSTRACT

In the context of hierarchical structure formation galaxies are sculpted by a sequence of mergers and accretion events. In some of these mergers, the core of each galaxy will sink to the central region of the new system, until they coalesce forming a new virialized core. Inside this new core the SMBHs of each galaxy will sink by dynamical friction until they form a SMBH binary. Understand the further evolution of these SMBH binaries is crucial because if they are able to shrink their separation down to $a_{\rm GW} \sim 10^{-3}(M_{\rm MBHs}/10^6 M_{\odot})$ pc, then the binary becomes an intensive emitter of gravitational waves (GW) which allows the binary to coalescence within $10^{10}$ years. Therefore, if we are able to determine what happens to SMBH binaries after galaxy mergers we will be able to determine the amount of sources of GW in the Universe and understand better the cosmic evolution of the population of SMBHs. If the galaxies involved in these mergers have a gas fraction of at least 1 %, we expect that a massive gaseous disk with a mass $\sim 1-10$ times the mass of the SMBHs will form in the central kiloparsec of the merger remnant. This gas can efficiently extract angular momentum from the binary making the shrinking timescale, down to a separation comparable with $a_{\rm GW}$, as short as $10^7$ years. However, if the gas does not efficiently redistribute the extracted angular momentum from the binary then it will be pushed away, generating a gap of low density around the binary. In this case the binary will shift to a regime of slow shrinking which has a shrinking timescale comparable with the age of the Universe.

Motivated by this scenario, In this thesis I derive an analytical criterion to determine when this gap will form. This criterion will allow me to determine in which conditions a binary will experience a fast or slow shrinking. I successfully test this analytical criterion against several numerical simulations of binaries embedded in isothermal gaseous disks.

I perform simulations of galaxy merges to determine how likely is that the conditions for a fast shrinking are fulfilled in real astrophysical systems. In all these simulations I find that the formation of a gap is unlikely. Moreover, I estimate that gap formation would be possible only if the gas has a turbulent velocity of the order of 10 km $s^{-1}$, which is comparable with the turbulent velocity in the inner region of local spiral galaxies. Also, the gap formation would be possible if the SMBHs accrete a mass that is of the order of 2 % the mass of the bulge of the remnant galaxy before they form a bound binary, this implies that the SMBHs have to accrete mass at a rate much greater than the derived from observations.

Also, using numerical simulations I study the effect of star formation in the dynamical evolution of a pair of SMBHs in the pre-binary epoch and I prove that for a difference of two order of magnitude in the star formation efficiency the migration timescale of the SMBHs change only in factor of two.

From my result I conclude that is likely that SMBH binaries will experience a fast shrinking. This means that the number of SMBH binaries in the Universe should be very low, setting important constraints to the evolution of the cosmic population of SMBHs, the expected number of SMBH binaries in the Universe and the amount of GW sources that we expect to observe with future missions.

# Tabla de contenido

# Capítulo 1

# Introduction

Black holes are one of the most interesting predictions of the general relativity theory of Einstein (GR). Their gravitational force is so strong that even light can be captured by it. We find indications of the existence of these objects in the Universe in three different regimes of mass; the lightest ones have masses between 5-30 $M_{\odot}$ and they are the relic of massive stars (Ozel et al. 2010), the intermediate ones with masses of the order of $10^2 - 10^5$ $M_{\odot}$ are suggested to have been formed in the collapse of population III stars (Madau & Rees 2001) and the heaviest ones have masses of the order of $10^6 - 10^9\, M_{\odot}$ and they are known as super massive black holes (SMBH). These extreme massive objects are found in the central region of practically every galaxy (Richstone et al. 1998, Magorrian et al. 1998, Gultekin et al. 2009) and they were first proposed in 1960s to explain the enormous luminosities of quasars (Salpeter 1964, ZelDovich & Novikov 1964) which we believed to be powered by the accretion of gas and stars onto SMBHs. If massive galaxies host a SMBH at their center, we expect that a pair of bound SMBHs will be form in the course of a galaxy merger (Kazanrzidis et al. 2005; Khan et al. 2012; Chapon, Mayer & Teyssier 2012). In this thesis we study the evolution of pairs of SMBHs in the nuclear region of mergers remnants to estimate how likely is the coalescence of two SMBH after the merger of their host galaxies.

### 1.0.1. Super massive black holes and galaxies

Active galactic nucleus (AGN) are very bright compact sources at the center of some galaxies. Their luminosities can be as large as $10^{47}$ erg $s^{-1}$ (Hopkins, Richards & Hernquist 2007) and their spectrum can be very wide, covering a large range of frequencies from radio to x-rays and even up to the gamma range. Also, their spectrum exhibits very broad emission lines. The width of these lines when interpreted as Doppler broadening, yields values of up to $\Delta v \sim 8500$ km $s^{-1}$. The high luminosity of AGNs, the large broadening of their spectrum and the fact that the luminosities of some AGNs changes by more than 50 % on time-scale of a day, are all evidences that support the model where these extreme objects are powered by the accretion of material onto SMBHs (Hoyle & Fowler 1963; Salpeter 1964; Zeldovich 1964; Lynden-Bell 1969, 1978; Lynden-Bell & Rees 1971).

There is also dynamical evidence of the existence of SMBHs at the center of practically every galaxy with a significant bulge (Richstone et al. 1998), which comes from the measurement of the velocity dispersion of stars at the nuclei of galaxies. There is typically

found that the velocity dispersion of the host galaxy bulge $\sigma_*$ is tightly correlated with the mass of the SMBH $m_{\rm bh}$ (Ferrarese & Merrit 2000; Marconi & Hunt 2003; Ferrarese & Ford 2005, Kormendy & Ho 2013). Similarly, the bulge (or spheroid) luminosity is correlated with the mass of the SMBH. These correlations indicate that for some galaxies their properties are interwined with the growth of their central SMBH.

Observations of the cosmic evolution of the quasars population can give us hints about the coupled evolution of SMBHs and galaxies. We observed that the space density of quasars increases with redshift, until it reaches a prominent peak at redshift $z \sim 2.5$ and then, for larger redshifts, it drops again (Richards et al. 2006). As the typical estimates of a quasar lifetime lie in the range of $10^6 - 10^8$ yrs (Salpeter 1964; Yu & Tremaine 2002), the cosmic evolution of the luminosity of the quasar population $L^*(z)$ does not indicate that the luminosity of every quasar varies in time following the same trend that the evolution of $L^*(z)$. Therefore, the cosmic evolution of quasars population has to be triggered by an external process. A plausible trigger of this cosmic evolution is the interaction and mergers between galaxies that can feed the central region of the remnant galaxy with large amount of stars and gas (Barnes 2002; Mayer et al. 2010; Ueda et al. 2014). Indeed, the cosmic star formation activity (see figure 1.1), that trace predominately interacting galaxies and mergers, evolve in a similar way than the quasar population with a peak at $z \sim 3$ (Boyle et al. 2000).

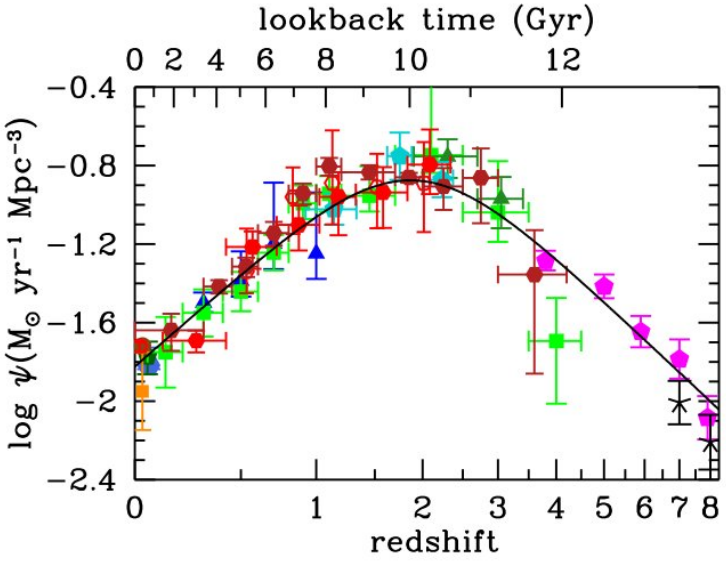


Figura 1.1: The history of cosmic star formation from FUV (blue, green and magenta points) and IR (red, brown and orange points) rest-frame measurements (Madau & Dickinson 2015).

Also, supporting the merger scenario, there is evidence that dusty ultra-luminous infrared galaxies (ULIRGs, $L_{\rm IR} > 10^{12} L_\odot$) in the local universe are invariably major mergers of gas-rich disk galaxies (Sanders et al. 1988). Therefore, an interpretation for the redshift evolution of the quasar space density is that, at early times the merger and interaction between galaxies were significantly more frequent than today, triggering a larger number of quasars. However, at very large redshift the number of quasars decrease

because SMBHs first need to form, which happens in the first $10^9$ years after the Big Bang (this is explained deeply below in the text).

In this picture, the evolution of SMBHs is tightly coupled with the evolution of galaxies, however, this does not necessarily means that the evolution of galaxies is tightly coupled with the evolution of their central massive black holes. In fact, observations tell us that MBH masses correlate tightly with classical bulges and ellipticals (see figure 1.2) but they correlate weakly with pseudo-bulges and dark halos. This weak dependence implies no relationship closer than the fact that it is easier to grow bigger BHs in bigger galaxies because they contain more fuel (Kormendy & Ho 2013). On the other hand, semi-analytical models and numerical simulations need some form of feedback from AGN to successfully reproduce the properties of massive galaxies (Fabian 2002), however, a precise description of how this feedback works and how it affects galaxies is still missing (Kormendy & Ho 2013, Heckman & Best 2014).

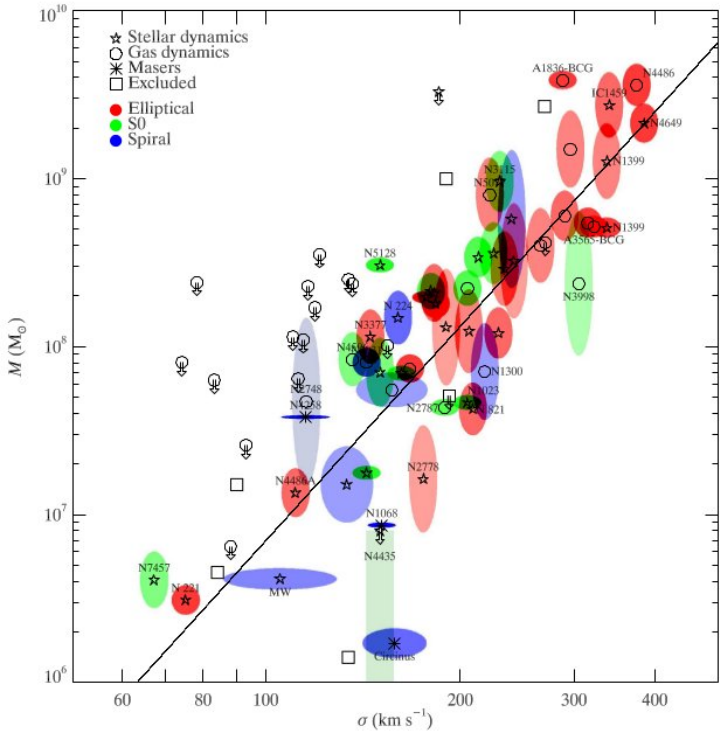


Figura 1.2: SMBH masses as function of velocity dispersion $\sigma$ based on the measurements of 49 galaxies (Gultekin et al. 2009).

Even though we are not sure of how the evolution of galaxies is related to the evolution of SMBHs and vice-versa, the more accepted picture of the cosmic evolution of SMBHs is: Black holes first appeared at large redshift $z > 9$ inside low mass ($M_{\rm halo} < 10^8 M_\odot$) dark matter halos (Volonteri, Haardt & Madau 2003). Then, in concordance with hierarchical structure formation (model in which small gravitationally bound objects form first and continuously evolve via merging activity, e.g: White & Frenk 1991, Springel et al. 2005), galaxies are sculpted by a sequence of mergers and accretion events (see figure 1.3), and the black holes inside these galaxies are expected to grow in mass in these events by

accretion and/or merging with other black holes (Volonteri, Haardt & Madau 2003; Merloni 2004; Merloni & Heinz 2008). Hereafter, MBHs accreting at high rates evolve in a population of bright quasars, with a peak at redshift $z \sim 2.5$, and then latter in time they pass to a more quiescent state possibly with much less accretion, like the one observed in SMBHs in the nuclei of local galaxies (Soltan 1982, Shaver et al. 1996; Yu & Tremaine 2002). In this picture, an important part of the evolution of SMBHs is the coalescence of MBHs after two galaxies merge, an issue that we discuss in subsection §1.0.3.

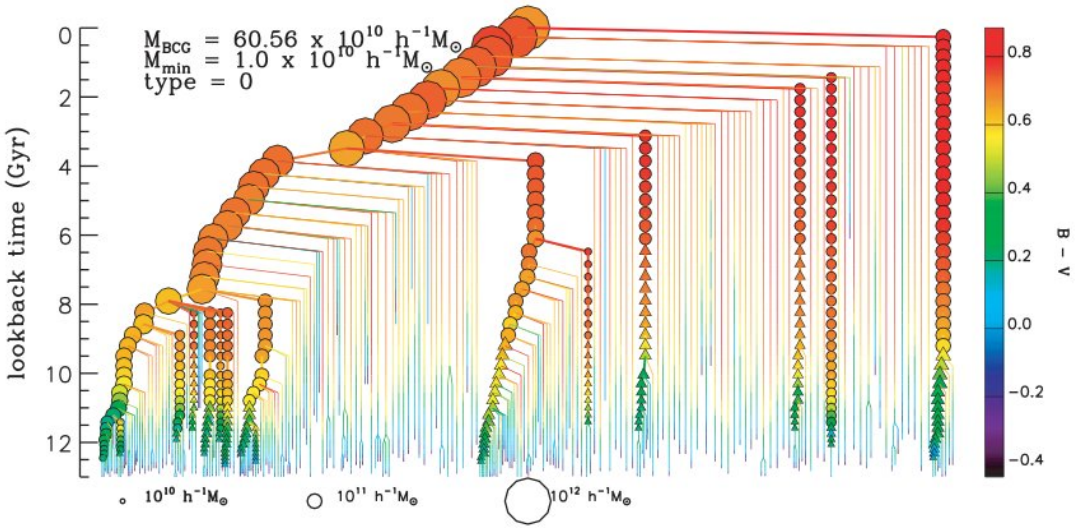


Figura 1.3: Example of a galaxy merger tree. Symbols are colour coded as function of B-V colour and their area scales with the stellar mass. Only progenitors more massive than $10^{10}$ $M_\odot$ are shown with symbols because in this particular case the merger tree correspond to the merger tree of bright cluster galaxies (Lucia & Blaizot 2007). From this figure is clear how galaxies are form via major and minor mergers as proposed by the hierarchical structure formation model.

### 1.0.2. Observational evidence of SMBHs pairs

In the context of hierarchical structure formation, the formation of SMBHs binaries after a major merger of galaxies should be a common event. Although to date there is not conclusive evidence of gravitational bound SMBHs binaries, in this subsection we will review some direct observational evidence of unbound pairs of SMBHs (and maybe one bound pair) and indirect evidence of objects that can be interpreted as unresolved bound SMBH binaries[1].

There are several indirect observations of unbound pairs of SMBHs. An example is the star-burst galaxy NGC 6240 (see figure 1.4), this galaxy is the result of the merger of two galaxies and is considered an ULIRG with a very high star formation rate. We observe two optical nuclei inside NGC 6240. As NGC 6240 is a galaxy with a large amount

[1]Here I use the following nomenclature. *SMBH pair*: one pair of two SMBHs that eventually will be very likely gravitationally bound but are not yet.*SMBH binary*: are two SMBH which are already bound.

of gas in the central region, we need x-rays observations to observe clearly this region. From observations with the space observatory Chandra it is found that, inside the central kilo parsec of NGC 6240, there are two SMBHs with a projected separation of $\sim$ 700 pc (Komossa et al. 2003; Max et al. 2007).

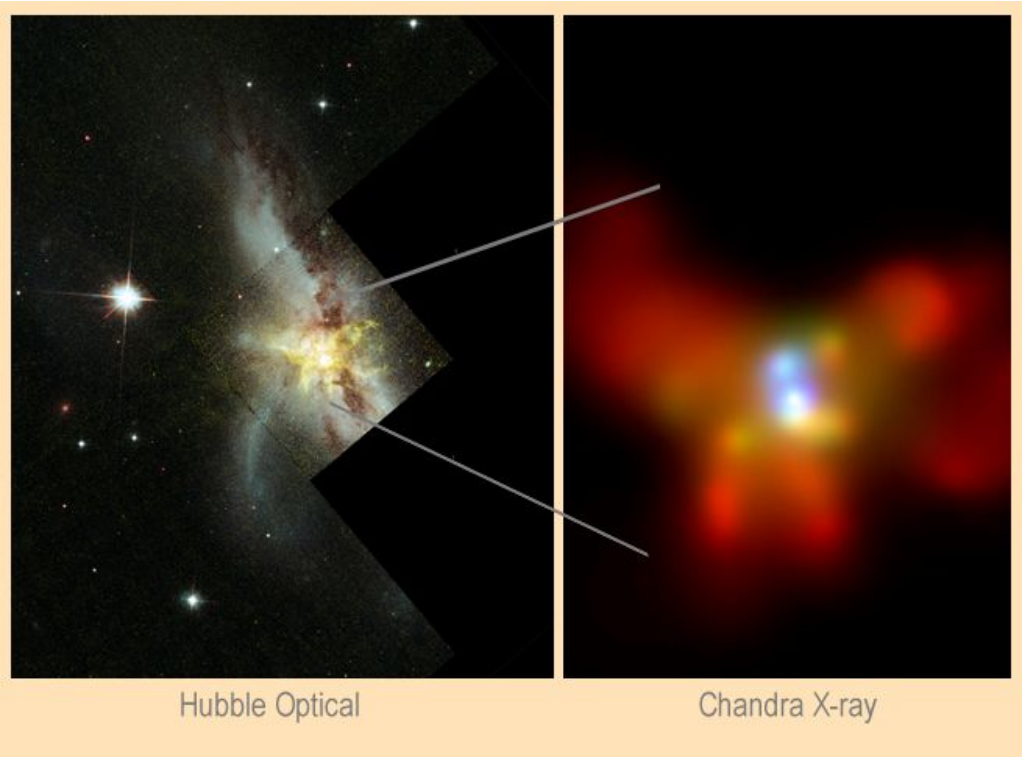


Figura 1.4: Hubble optical image and Chandra x-ray image of the galaxy NGC 6240. Credits: Optical: R.P.van der Marel & J.Gerssen(STScI),NASA; X-ray: S.Komossa & G.Hasinger(MPE) et al. ,CXC,NASA

An interesting example is the radio elliptical galaxy 0402+379. Mannes et al. (2004) reported that, using multi-frequency very long baseline array (VLBA) observations, they found two compact flat-spectrum components inside 0402+379. After this report, Rodriguez et al. (2006) observed in more detail the same galaxy with VLBA and concluded that the two components were two SMBHs of mass $\sim 10^8$ $M_\odot$ with a projected separation of 7.3 pc (see figure 1.5).

Another evidence of the existence of pairs of SMBHs comes from the observation of the optical spectre of AGNs. The AGNs optical spectra is typically characterised by a combination of narrow and broad emission lines. The narrow emission lines are generated by gas around the accreting SMBH that has less kinetic energy (narrow line region) and broad emission lines are generated by gas around the SMBHs that has greater kinetic energy (broad line region, see figure 1.6).

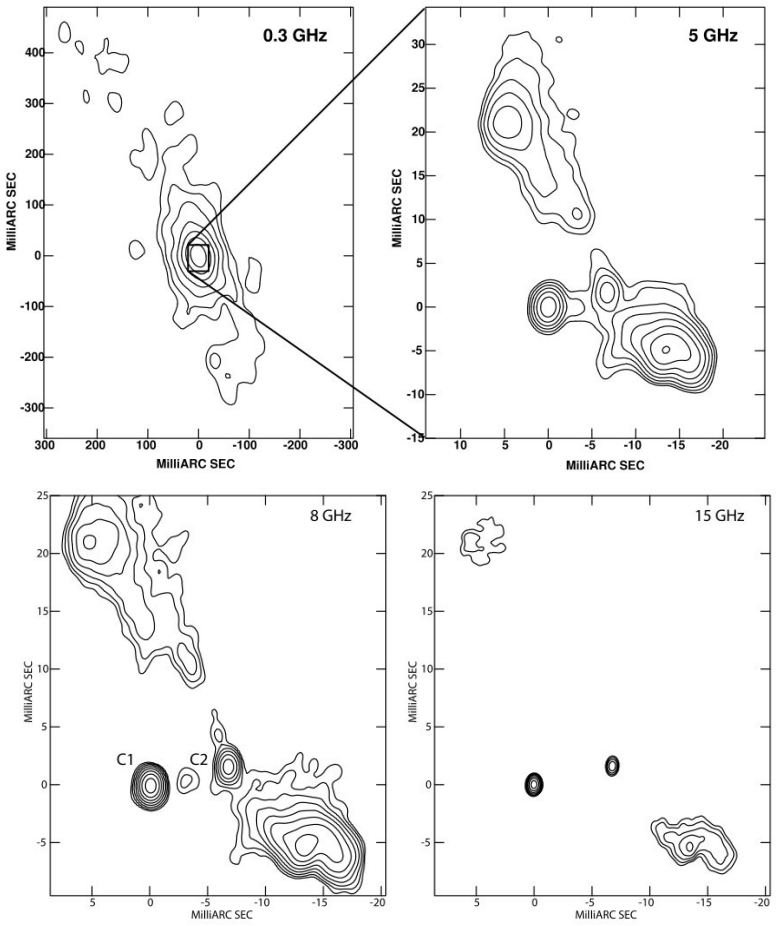


Figura 1.5: VLBA image of the radio elliptical galaxy 0402+379 (Rodriguez et al. 2006).

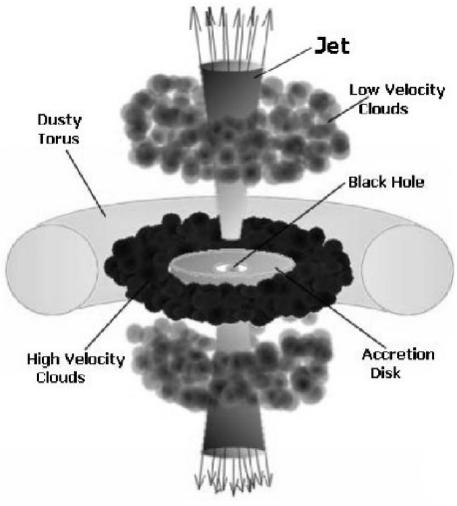


Figura 1.6: Caricature of an AGN. The accreting SMBHs is located in the center of an accretion disk and a dusty torus. Further away we identify the broad line region consistent of high velocity clouds and the narrow line region consistent of low velocity clouds.

In some peculiar cases these emission lines appear double and some authors study the possibility that this double emission are caused by the presences of two accreting SMBHs. In this scenario each SMBHs carries his own narrow and broad line region and the orbit of the two SMBHs around each other cause a blue and red shift in these emission lines, which can be reflected as a double peaked AGN. In recent years several double peaked lines candidates have been identified in surveys like SDSS, LAMOST and AGES (double narrow lines: Liu et al. 2010; Comerford et al. 2013; Barrows et al. 2013; Shi et al. 2014, double broad lines: Eracleous et al. 2012; Decarli et al. 2013; Shen et al. 2013). However, for double narrow lines emitters it is shown that only a small fraction (2 % -10 %) harbour an AGN pair (Liu et al. 2011). From these small fraction of systems one confirmed AGN pair is SDSSJ1502+1115 which, with high-resolution radio images from the Expanded Very Large Array, is revealed as two steep-spectrum compact radio sources separated by 7.4 kiloparsecs (see figure 1.7, Fu et al. 2011). Also, Liu et al. (2010) using deep near-infrared images and optical slit spectra obtained from the Magellan 6.5 m and the Apache point Observatory 3.5 m telescopes, discovered four kiloparsecs scale pair of AGNs in a sample of 43 AGNs selected from the Sloan Digital Sky Survey based on double-peaked $[O_{III}]$ $\lambda\lambda$ 4959, 5007 emission lines.

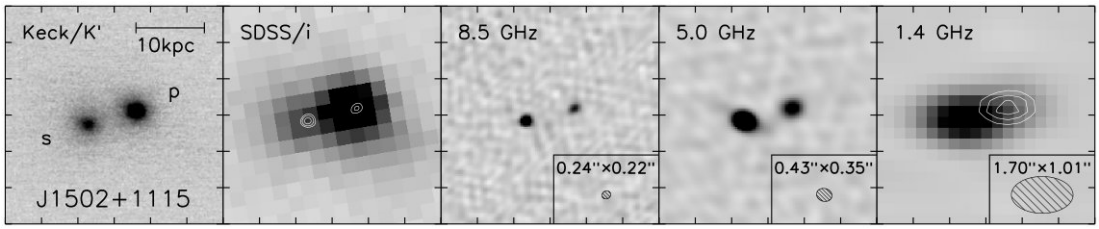


Figura 1.7: Keck K band, SDSS i band and EVLA X C L bands of SDSSJ1502+1115 (Fu et al. 2011).

Also interesting is the case of the Seyfert galaxy NGC 4151 for which Bon et al. (2012) present a model of an eccentric subparsec SMBHB with an orbital period of 16 years based on the variability observed in the $H_\alpha$ emission line (broad emission region) in many years of spectroscopic monitoring (see figure 1.8).

An indirect evidence of the existence of SMBH binaries comes from the bright quasar OJ 287. This quasar has been observed since the late nineteenth century and shows quasi periodic pattern of prominent outbursts in its light curve (Valtonen et al. 2008, see figure 1.9). Several authors had proposed different scenarios for the variability of OJ 287 that invoke the presence of a SMBH binary (Sillanpaa et al. 1988; Lehto & Valtonen 1996; Katz 1997). More recently Valtonen et al. (2008) argue that a plausible scenario is that the variability is caused by the impact of the secondary SMBH on the accretion disk of the primary SMBH. In their model, the mass of the primary is $18 \times 10^9 M_\odot$ and for the secondary is about $10^7 M_\odot$. With this model Valtonen et al. 2008 predicts the next outburst of activity of OJ 287 and they obtain a good agreement with observations. However OJ 287 is a blazar ( i.e. a quasar which relativistic jet is pointing towards the Earth) and therefore OJ 287, as all the blazars, has a very large optical variability, which in principle means that we can adjust any type of model to the variability of the optical spectrum of OJ 287.

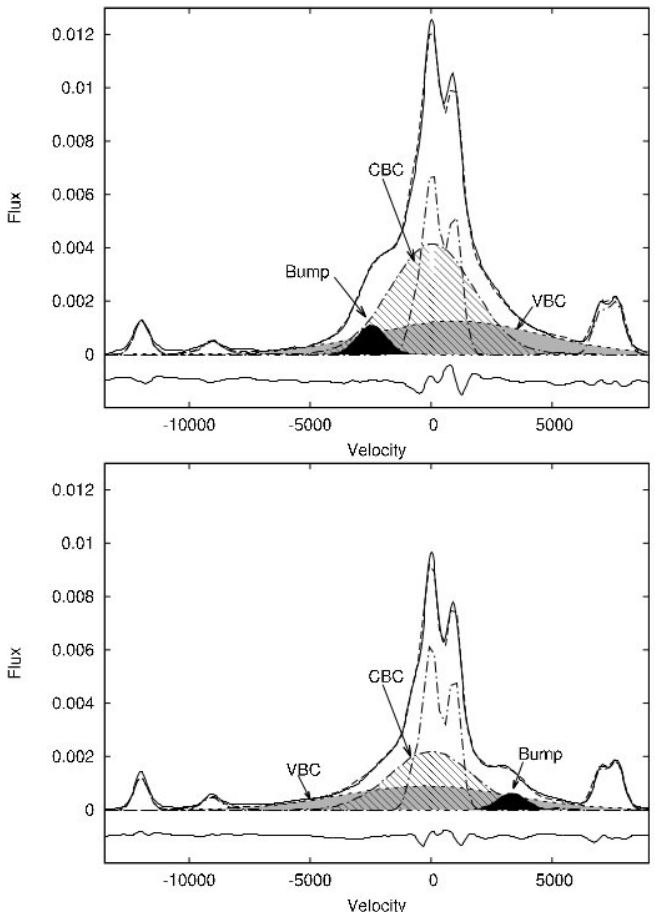


Figura 1.8: The $H_\alpha$ emission line of the core of the Seyfert galaxy NGC 4151. Each panel correspond to a different epoch. The best fit of $H_\alpha$ line are show as dashed lines (Bon et al. 2012).

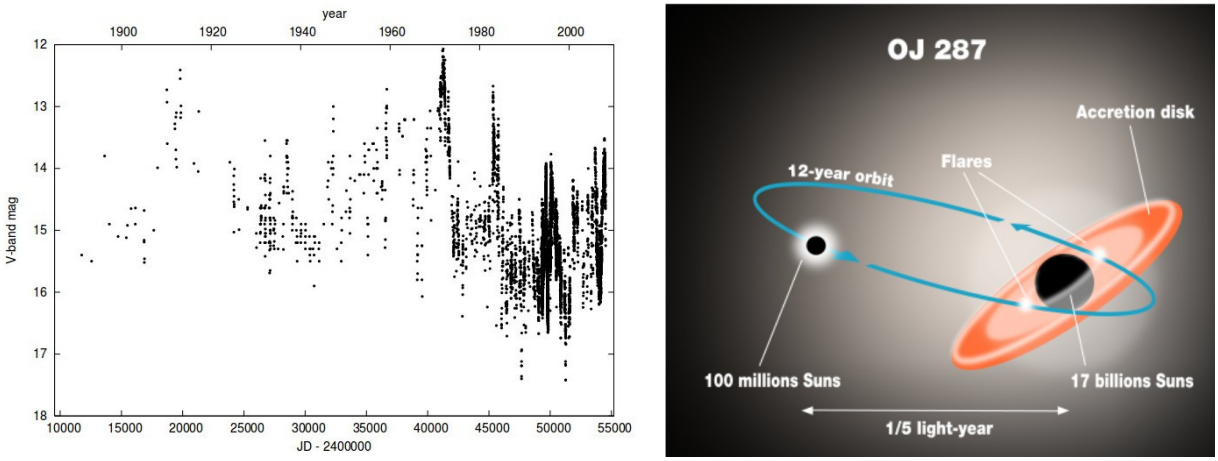


Figura 1.9: Variability of the quasar OJ 2087 and the model proposed to explain the variability (Valtonen et al. 2008).

Recently, Graham et al. (2015) reported the indirect observation of a sub-parsec scale SMBH binary in the quasar PG 1302-102. They found that this quasar has a smooth periodic signal in the optical variability with a mean period of 1884±88 days (see figure 1.10). They argue that even when the interpretation of this phenomenon is still uncertain, the more plausible mechanism to drive this variability is a SMBH binary with a mass on the order of $10^{8.5}$ $M_{\odot}$ and a projected separation of $\sim$ 0.01-0.1 parsecs. For this same object D'Orazion, Haiman & Schiminovich (2015) show that the sinusoidal like shape of the variability of PG 1302-102 can be fit by relativistic Doppler boosting of emission from a compact, steadily accreting, unequal-mass binary (see figure 1.11).

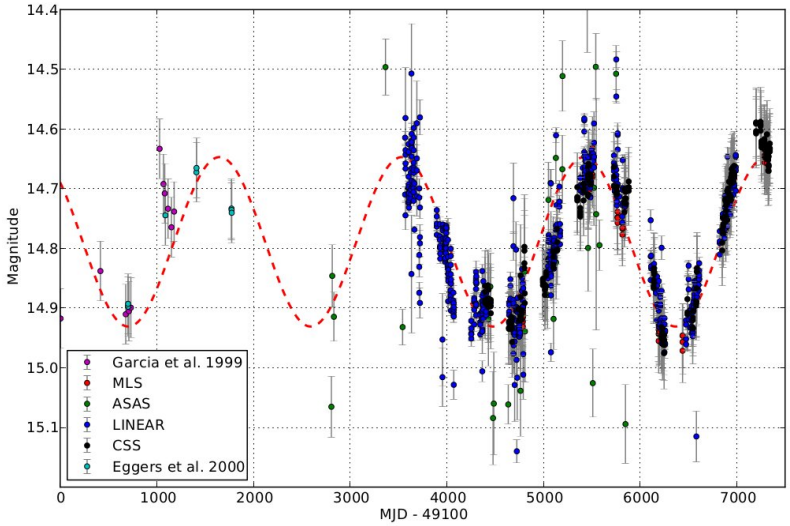


Figura 1.10: Optical variability of the quasar PG 1302-102 (Graham et al. 2015).

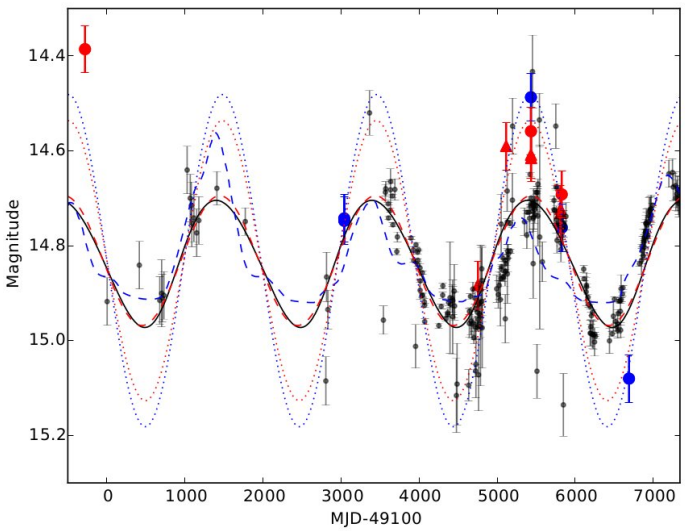


Figura 1.11: Optical variability of the quasar PG 1302-102. The black curve is the fit of D'Orazion, Haiman & Schiminovich (2015) using their model of a steadily accreting unequal-mass binary.

### 1.0.3. Evolution of SMBH binaries in galaxy mergers

As I discussed previously, the possibility that SMBHs interact between them is closely related to the fact that, in the context of hierarchical structure formation, their host galaxies frequently merge between them.

This picture of SMBHs interacting after a merger of galaxies was first considered by Begelman, Blandford & Rees (1980). They argue that in the early evolution of a galaxy merger the SMBHs will follow the center of each galactic core until they merge. Afterwards, the new core will experience violent relaxation in a characteristic galactic dynamical time $t_{\rm gal} \sim 10^8$ yr and the SMBHs will end coexisting inside a common spherical bulge. They noticed that the evolution of SMBHs inside this newly formed spherical stellar system can be divided in three dynamical phases:

- **Pairing phase:** First the SMBHs embedded in the distribution of stars exchange momentum with every single star that they encounter, deflecting the orbits of these stars that have a mass much smaller than the mass of the SMBHs. For each one of these encounters the SMBHs experience a loss of momentum. Summing over all the single interactions between the massive perturber of mass $M_{\rm BH}$ (in our case a SMBH) and the star of the background, Chandrasekar (1943) show that the massive perturber will experience a net gravitational drag or dynamical friction given by

$$\mathbf{F}_{\rm df} = -4\pi \ln(\Lambda) G^2 M_{\rm BH}^2 \rho_{\rm stars} \left[ \mathrm{erf}\left(\frac{V}{\sqrt{2}\sigma}\right) - \left(\sqrt{\frac{2}{\pi}}\frac{V}{\sigma}\right) exp\left(-\frac{V^2}{2\sigma^2}\right)\right] \frac{\mathbf{V}}{V^3},$$

  where $V$ and $M_{\rm BH}$ are the velocity and mass of the massive perturber, $\rho_{\rm stars}$ is the density of stars, $\sigma$ is the velocity dispersion of the background of stars, $G$ is the

gravitational constant and $\ln(\Lambda) \sim \ln(b_{\rm max}/b_{\rm min})$ is the Coulomb logarithm which express the non-locality of the drag as it comprises the whole range of impact parameters ($b$) relevant for the exchange of momentum in the interaction of the stars with the SMBH. Since gravity is a long-range force, $b_{max}$ is close to the size $L$ of the collissionless background, while $b_{\rm min} = V^2/GM_{\ rmBH}$ is the impact parameter for a large-scattering angle gravitational interaction.

This process drives the in-spiral of the two SMBHs into the center of the stellar system (Binney & Tremaine 1987) leading to the subsequent pairing of the SMBHs. The time that takes to two SMBHs, in an orbit of radius $r_{\rm circ}$ and velocity $V_{\rm circ}$, lose enough angular momentum to fall towards the center of the distribution of stars is given by

$$t_{\rm df} = 5 \times 10^8 \left(\frac{5}{\ln(M_{\rm stars}/M_{\rm BH})}\right) \left(\frac{r_{\rm cir}}{300\,{\rm pc}}\right)^2 \left(\frac{V_{\rm circ}}{\sqrt{2} \times 100\,{\rm km\,s^{-1}}}\right) \left(\frac{10^6\,M_\odot}{M_{\rm BH}}\right)\ {\rm yr}$$

where $M_{\rm stars}$ is the mass on stars enclosed by the orbit of the SMBHs. Therefore the SMBHs can sink to the center of the stellar system in a timescale comparable with $10^8$ years if they begin with a circular orbit of a few hundred parsecs.

- **Hardening phase:**

  The SMBHs that sink to the center of the stellar system, due to dynamical friction, will form a binary when their relative orbit enclose a mass on stars equal or smaller than the mass of the two SMBHs ($M_{\rm MBHs}$). This happens when the distance between the SMBHs reach a value comparable with

$$a_{\rm binary} \sim \frac{G\,M_{\rm MBHs}}{2\sigma^2} \sim 0.2 \left(\frac{M_{\rm MBHs}}{10^6 M_\odot}\right) \left(\frac{100km\,s^{-1}}{\sigma}\right)\ {\rm pc},$$

  separation at which the orbital velocity of the SMBHs is comparable with the dispersion velocity of the background stars (Dotti, Sesana & Decarli 2012).

  After reach this separation, the SMBHs will continue to get closer and closer due to dynamical friction, until their separation is

$$a_{\rm hard} \sim \frac{G\,\mu_{\rm MBHs}}{3\sigma^2} \sim 0.3 \frac{q}{(1+q)^2} \left(\frac{M_{\rm MBHs}}{10^6 M_\odot}\right) \left(\frac{100km\,s^{-1}}{\sigma}\right)\ {\rm pc},$$

  separation at which the binding energy per unit of mass of the binary exceeds $(3/2)\sigma^2$ (the average kinetic energy of a star in the stellar system).

  Then, the SMBH binary will begin to lose angular momentum by single star scatterings (3-body interaction). With each scattering the binary increase its binding energy ($E_{\rm binding}$) and therefore decrease its separation in a rate $\delta E_{\rm binding}/E_{\rm binding} = \delta a/a \sim m_{\rm star}/M_{MBHs}$, with $m_{\rm star}$ the mass of the star involved in the scattering. The total mass of stars that has to be ejected from the system by the binary in order to reach a separation $a_{\rm f}$ is

$$M_{\rm eject}(a_{\rm f}) \sim \frac{\mu_{MBHs}}{3} \ln\left(\frac{a_{\rm hard}}{a_{\rm f}}\right)$$

with $\mu_{MBHs}$ the reduced mass of the SMBH binary. If we set $a_{\rm f} = a_{\rm GW}$, where $a_{\rm GW}$ is the separation at which gravitational waves can drive the SMBH binary to coalescence within a Hubble time (a expression of this separation is presented below), then $M_{\rm eject}(a_{\rm GW}) \sim 10\,\mu_{MBHs}$.

If we assume that there is a constant flux of stars $F_{\rm stars} \sim n_{\rm stars}\sigma$ and that the binary cross section can be expressed as $A_{\rm bin} \sim \pi a G M_{\rm MBHs}/(2\sigma)$ we can compute the rate at which the separation of the binary decrease as $\delta a/a \sim (m_{\rm star}/M_{MBHs})\, F_{\rm stars}\, A_{\rm bin}\, \delta t$. Integrating this expression we obtain the hardening timescale

$$t_{\rm hard} = 7 \times 10^8 \left(\frac{\sigma}{100{\rm km\,s^{-1}}}\right)\left(\frac{10^4 M_\odot {\rm pc}^{-3}}{\rho_{stars}}\right)\left(\frac{10^{-3}{\rm pc}}{a_{\rm f}}\right) {\rm yr} \tag{1.1}$$

However, only stars which angular momentum and energy are such that their orbits are centrophilic, which means that they orbits pass closer enough to the binary in order to be scattered, can interact with the binary and drive its shrinking. The phase space that contains these selected stars is called loss-cone and typically has a mass much smaller than $M_{\rm eject}(a_{\rm GW})$, which means that the loss-cone will be depleted before the binary reach a separation comparable with $a_{\rm GW}$ (Makino & Funato 2004).

The further decay of the binary separation, after loss-cone depletion, will depend of two body star-star relaxation that will repopulate the loss-cone in a time $\sim$ (solid angle loss cone)$\times$(two-body relaxation time), where two-body relaxation time is the timescale in which, due to the gravitational deflection between stars, the orbits of the stars lose any memory of their initial configuration.

- **Gravitational wave emission phase:** The general relativity theory of Einstein predicts that the motion of masses trough the space-time generate a propagation of waves trough the space-time at the speed of light ($c$). In this context the SMBHs of a binary system will emit gravitational waves because they are rotating around each other. These waves will carry away mass-energy and angular momentum, and depending on the spin, also linear momentum. Therefore, the emission of gravitational waves will drive the shrinking of the SMBH binary. Peters & Mathew (1963) and Peters (1964) show that the timescale in which this shrinking leads to the coalescence of the SMBHs is

$$t_{\rm G} = \frac{5}{64}\frac{c^5}{G^3}\frac{(1+q)^2}{q\,F(e)}\frac{a^4}{M^3_{\rm MBHs}} \tag{1.2}$$

where $F(e)$ is a function with a strong dependence on the eccentricity $e$ of the binary. This expression for the shrinking timescale due to the emission of gravitational wave have a strong dependence on the binary separation ($\propto a^4$), meaning

that for large binary separations the emission of gravitational waves may not be efficient enough to drive the coalescence of the binary within the age of the Universe. Indeed, if we consider a SMBH binary of total mass $\sim 10^6$ $M_\odot$, initial separation $\sim 1$ pc and zero eccentricity, then $t_{\rm GW} \sim 10^{21}$ years which is much greater than the age of the Universe. Also, the hardening timescale ($t_{\rm hard}$, equation 1.1) is $t_{\rm hard} \propto a^{-1}$ which explains why for parsec scale and even hundredth parsec scale the scattering of stars dominates over the emission of gravitational waves as the main angular momentum extraction mechanism.

From equation 1.2 we can derive an expression to the scale $a_{\rm GW}$ at which gravitational waves drives the binary to coalescence on a timescale $t_{\rm GW} < 10^{10}$ years

$$a_{\rm GW} = 2 \times 10^{-3} \left( \frac{q\, F(e)}{(1+q)^2} \right)^{1/4} \left( \frac{M_{\rm MBHs}}{10^6 M_\odot} \right)^{3/4} \text{pc}, \tag{1.3}$$

length scale that is comparable to ten thousand Schwarzschild radius of a SMBH of mass $\sim 10^6$ $M_\odot$.

This path to coalescence of a pair of SMBHs has a bottleneck in the hardening phase, because if the refill of the loss-cone is not efficient enough then the shrinking of the binary separation will stall at parsec scale (last parsec problem). The solution of this last parsec problem is to refill this zone with new stars but, for spherical stellar system, the refilling time is of the order of the relaxation time which is greater than the age of the universe.

Some authors claim that in triaxial stellar systems the existence of centrophilic orbits (Merrit & Poon 2004; Berczik etal. 2006) can keep the loss-cone full (Khan etal 2011), making possible to the background of stars drive the shrinking of the binary to coalescence in a timescale of the order of one Gyr (Khan etal 2011) to ten Gyr (Berczik etal. 2006). However, recent studies show that the feeding of the loss-cone by cetrophilic orbits has a significant dependence in the number of particles used to model the distribution of stars (Vasiliev, Antonini & Merritt 2014) and that the binary hardening rate is always substantially lower than its maximum possible rate ("full-loss-cone" rate), besides it decreases with time (Vasiliev, Antonini & Merritt 2015, nevertheless they show that some degree of triaxiality may permit the binary coalescence on a timescale $\sim 1$ Gyr).

Even when the triaxiality is an expected characteristic of the merger remnant (Preto et al. 2012), the typical time scales that are obtained in this systems for the coalescence of the MBH binary are comparable or greater than the typical time that takes for a galaxy to be involve in two major mergers (see figure 1.3). This makes the conclusion of coalescence of the MBH binary, driven only by the action of the stars, a more delicate statement because we are not sure how another merger can change the outcome of the binary evolution, because it will change the environment of the binary.

In this picture of SMBHs inside stellar system, proposed by Begelman, Blandford & Rees 1980 (see figure 1.12), the effect of gas is only considered when it fuels the SMBHs. They propose that if the gas falls into the SMBHs, the increase of their mass will produce an orbital contraction, shrinking the binary separation. However, they do not consider

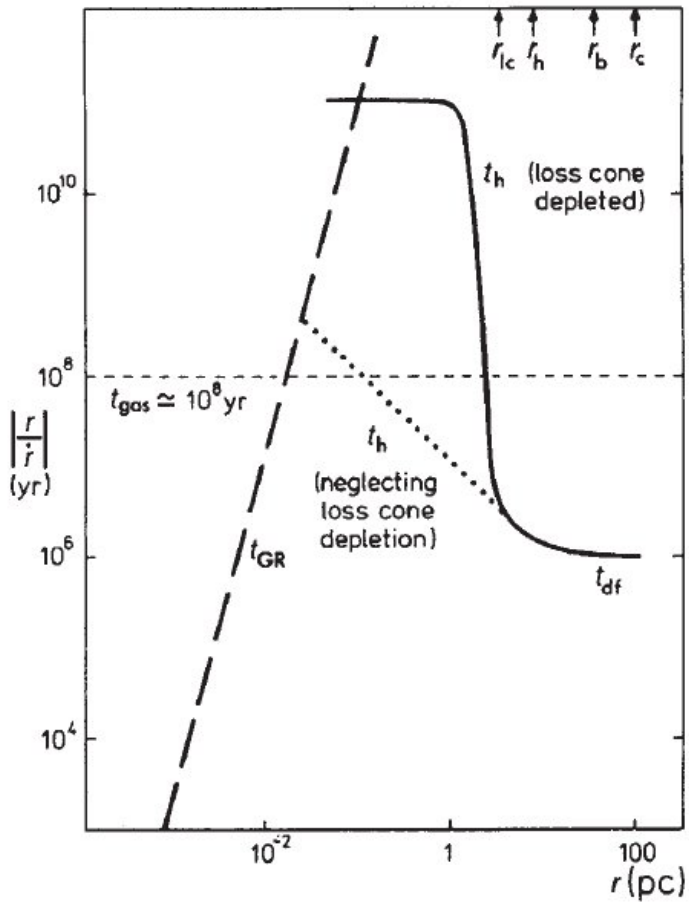


Figura 1.12: Diagram of the time scales involved in the approach and eventual coalescence of a SMBH binary (Begelman, Blandford & Rees 1980). The radius $r_{\rm b}$, $r_{\rm h}$, $r_{\rm lc}$ are the separation of the SMBHs when they form a binary, when they begin the hardening phase and when the loss-cone is depleted, respectively. The dashed line shows the evolution of the binary separation ignoring the depletion of the loss-cone.

any other dynamical effect of the gas on the path to coalescence.

If the galaxies that are involved in the merger are rich in gas, numerical simulations show that 60 to 90 % of this gas falls to the central kilo parsec of the remnant (Barnes & Hernquist 1996; Mihos & Hernquist 1996; Barnes 2002; Mayer et al. 2007, 2010). This is consistent with observations of gas-rich interacting galaxies, where it is often found that the amount of gas contained in their central regions is comparable with the total gas content of a large gas-rich galaxy (Sanders & Mirabel 1996; Downes & Solomon 1998; Medling et al. 2014; Ueda et al. 2014). Therefore, even in a relative dry merger, for example the merger of two **Sa** galaxies of $10^{12} M_{\odot}$ with a gas mass fraction of the order of 1 %∼5 % (Young et al. 1995), if the amount of gas that reach the central kilo parsec of the remnant is only 60 %,then the mass in gas of this central region will be of the order of 1 - 5 $\times 10^{10} M_{\odot}$, which is ten to hundred times greater than the mass of the SMBHs that lives at the center of these galaxies. For this reason, it is natural to expect that not only the stars but also the nuclear gas that surrounds the SMBH binary after a merger, will have an important influence in its dynamical evolution.

Although in principle the stars and the gas are good candidates to extract enough angular momentum of the MBH binary, in order to decrease its separation down to the scale where the emission of gravitational waves can drive its final coalescence ($a_{\rm GW} \sim 10^{-3}$ parsecs for a SMBH binary of mass $\sim 10^6$ $M_\odot$), the typical time scale in which this is achieved by the stars and the gas are very different.

When it is taken into account the effect of the gas over the evolution of a binary we found that, for simplified models of the typical environment on the nuclear region of strongly interacting galaxies, the coalescence of the SMBH binary is achieved on a timescale of the order of 2.5 Myr ( Escala etal 2004, 2005) or 16 Myr (Dotti etal 2006), which is between a hundred to thousand times shorter than the time scales found for triaxial stellar systems.

But the gas can also have problems to drive the binary to coalescence because the existence of gas inside the binary orbits is the result of the efficient dissipation of the angular momentum extracted from the binary. If this dissipation is not quick enough the tidal torque exerted by the binary will clear a cavity (Artymowicz & Lubow 1996; del Valle & Escala 2012, 2014) with a size of the order of 2 times the binary separation (Artymowicz & Lubow 1996; Farris etal 2014). Thus, to determine how efficiently the gas can shrink the SMBH binary separation we need a better understanding of the interaction between a binary and a gaseous background.

### 1.0.4. Binary-disk interaction

Both, numerical simulations of merging galaxies (Barnes & Hernquist 1996; Mihos & Hernquist 1996; Barnes 2002; Mayer et al. 2007, 2010) and observations of the molecular gas in the central kilo parsec of interacting galaxies (Downes & Solomon 1998; Medling et al. 2014; Ueda et al. 2014), suggest that the gas that is driven to the central region of the remnant of a galaxy merger often settles in a disk-like distribution or circum-nuclear disk (CND). Therefore, as a first approximation to study the effect of gas in the path to coalescence of a pair of SMBHs, it is crucial to get more insight of the dominant dynamical processes in binary-disk systems.

The binary-disk systems are repeatedly found in astrophysical contexts. Some examples are the interaction between planetary rings and satellites (Goldreich & Tremaine 1982), the formation of planets in protoplanetary disks and their migration (Goldreich & Tremaine 1980, Ward 1997, Armitage & Rice 2005, Baruteau & Masset 2013 ) and the evolution of stellar binaries (Shu et al. 1987, McKee & Ostriker 2007).

One of the most widely studied case is the one of a planet interacting with protoplanetary disk. In this case, the central star and the planet are the binary system which typically has an extreme mass ratio $q = M_{\rm planet}/M_* << 1$. In these disk-planet systems it is found that the planet experiences a migration to the center of the disk due to the gravitational torques produced by the disk onto the planet (Kley & Nelson 2012).

Usually, there are two main regimes of migration recognized: For low planet masses

($M_{\rm planet} \sim M_{\rm Earth}$) the disk is not strongly perturbed by the planet and the rate of migration of the planet is controlled by the sum of the torques arising from the inner and outer Lindblad resonances (resonances located in the disk where the local epicyclic frequency of the gas is equal to the orbital frequency of the planet) and corotation resonances (resonances located in the disk where the local orbital frequency of the gas is equal to the orbital frequency of the planet), which is generally non-zero (Armitage & Rice 2005). This type of migration is typically known as *Type I* migration. For more massive planets the deposition of angular momentum onto the disk is strong enough to repeal gas from an annular region surrounding the orbit of the planet, driving the formation of a gap in the disk. The size and location of this gap is controlled by the balance between the torque produced by the planet, that tends to open the gap, and the viscous dissipation of the gas, that tends to close the gap (Baruteau & Masset 2012). This process typically leads to a migration that is coupled with the viscous timescale of the disk and which is much slower than *Type I* migration. This type of migration is known as *Type II* migration (see figure 1.13 for a comparison of the gaseous disks in Type I and Type II migration).

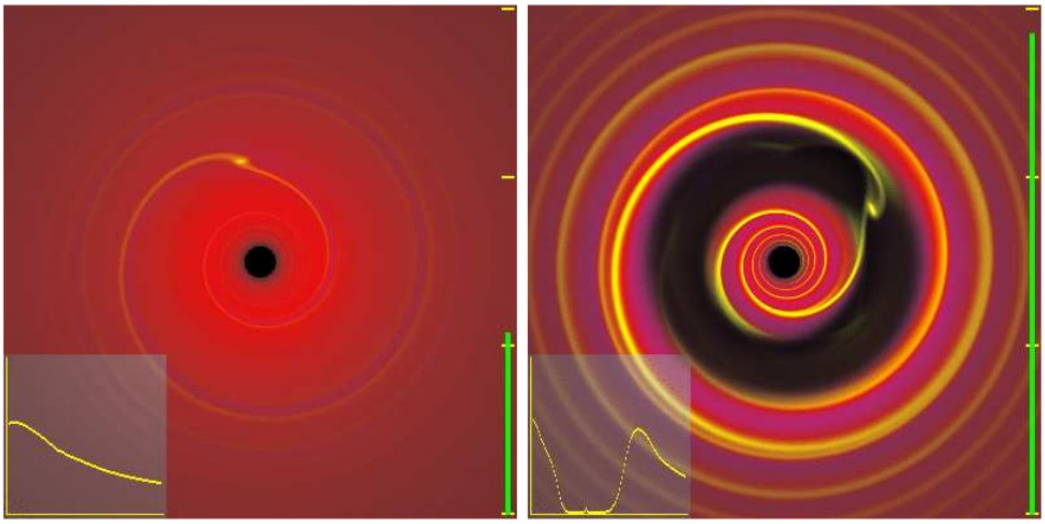

Figura 1.13: Type I migration regime (left panel) and Type II migration regime (right panel). In both cases the binary is a extreme mass binary with $q << 1$ (Armitage & Rice 2005).

Some authors use the same perturbative approach for systems where the mass ratio of the binary is comparable $q \sim 1$ (Artymowicz & Lubow 1994, 1996; MacFadyen & Milosavljevic 2008), even when for comparable mass binaries the secondary' gravitational potential can not be considered as a perturbation to the gravitational potential of the primary and therefore resonant torques does not drive the interaction between the binary and the disk (Shi et al. 2012). The studies that use this perturbative approach to study the interaction between a comparable mass binary and a gaseous disk typically found that the formation of a gap always occurs because they are mainly focused in the regime of low mass ($M_{\rm disk}/M_{\rm binary} << 1$) thin disks ($H_{\rm disk}/a_{\rm binary} << 1$) regime in which the dominant potential of the binary and the slow viscous diffusion of the gas leads inevitable to the formation of a gap (Artymowicz & Lubow 1994). Extending this result to SMBHs binaries many authors consider that after a major galaxy merger the SMBHs

binaries will inevitably excavate a gap on the gaseous disk in which they are embedded, and therefore, they will experience a slow *Type II* shrinking (Ivanov etal. 1999; Gould & Rix 2000; Roedig etal. 2011; Gold et al. 2013; Hayasaki, Saito & Mineshige 2013).

However, from observation of interacting galaxies such as ULIRGs, we found that the nuclear region of these galaxies often contains massive and highly turbulent gaseous disks, with masses of the order of $\sim 10^9$ $M_\odot$ and turbulent velocities of the order of $\sim 50-100$ km $s^{-1}$ (Downes & Solomon 1998; Medling et al. 2014). This is consistent with numerical simulations of merging galaxies where it is found that 60 % to 90 % of the gas of the galaxies involved in the merger end in the central kilo parsec of the merger remnant, resulting in a gaseous disk with a mass ten to hundred times greater than the mass of the SMBH binary ($M_{\rm disk}/M_{\rm binary} >> 1$). Therefore, we can not assume that the conditions that leads to gap formation in the study of Artymowicz & Lubow (1994) ($M_{\rm disk}/M_{\rm binary} << 1$ and $H_{\rm disk}/a_{\rm binary} << 1$) will be fulfilled in the nuclear region of merger remnants.

Therefore, in this thesis I argue that gap formation and the subsequent slow shrinking of a binary is not an inevitable outcome for SMBH binaries because in a major merger SMBH binaries will have a comparable mass ratio (for which the perturbative approach is not valid) and they will typically end embedded in a massive highly turbulent gaseous disk. Moreover, I argue that to determine if a SMBH will experience a slow or fast shrinking we need to derive a gap-opening criterion that allow us to determine which conditions of a SMBH binary/disk systems will lead to the formation of a gap.

### 1.0.5. Thesis outline

In this thesis I study the evolution of supermassive black holes (SMBH) in the nuclear region of the remnants of galaxy mergers. I focus my study in determine the different regimes of evolution of a SMBH binary that is embedded in a gaseous circum-nuclear disk (CND), that is expected to be formed in the central kilo parsec of a merger remnant. My aim is to derive a criterion to distinguish between two regimes of shrinking of the binary: a fast shrinking regime in which the binary separation shrinks in a time scale of the order of $10^7$ yr and a slow shrinking regime in which the binary shrinks slowly in a time scale typically longer than the age of the Universe. Determine which of these regimes is dominant in real galaxies will allow us to put constraints in the rate of SMBHs binary coalescence in the universe, which is a crucial ingredient to understand the evolution on mass of the cosmic population of SMBHs and determine the amount of gravitational waves sources that we expect to observe with the future European Laser Interferometer Space Antenna (eLISA, Amaro-Seoane et al. 2012). The organization of this thesis is as follow:

In **Chapter 2** I present a description of the numerical code that I use to test my analytical predictions. I discuss the basic principles of the smooth particle hydrodynamic technique (SPH) and of the computation of gravitational forces that is performed with a N-body technique. In these chapter I also show how I implement in the N-body/SPH code Gadget3 recipes for star formation, cooling and heating due to supernovae explosions to study the evolution of SMBHs binaries in more real systems. I also discuss how

I re-sample some of our simulations in order to increase their resolution so I will be able to follow the evolution of a SMBH binary to smaller scales.

In **Chapter 3** I present the derivation of a gap-opening criterion for comparable mass binaries ($0.1 \leq M_1/M_2 \leq 1.0$). This allow us to distinguish in what binary-disk systems the binary will experience a fast (systems without gap) or slow (systems with gap) shrinking. In this chapter I also test my gap-opening criterion against SPH simulations and I show that the prediction of my gap-opening criterion are consistent with these simulations and simulations of the literature.

In **Chapter 4** I use the star formation, cooling and supernova heating recipes that I implement in the code Gadget-3 to study the evolution of a pair of SMBHs embedded in a star forming cirum-nuclear disk down to a parsec scale. I show that for a one order of magnitude of variation on the star formation rate, the migration times scale of the pair of black holes only change in a factor three. I also show that the migration timescale in these simulation is only a factor 2 slower than in more idealized simulation where there is not star formation included.

In **Chapter 5** I simulate the merger of galaxy to follow the evolution SMBHs from galactic scale down to parsec scales. I evaluate our gap-opening criterion for the binary-disk system that are formed in situs in these simulations and I show that, for the four mergers that I simulate, the gap-opening criterion predicts that the binary will not be able to open a gap and therefore they will experience a fast shrinking, in concordance with the simulations. Also I show that in these mergers even if the mass of the SMBHs is of the order of $10^{10}$ $M_\odot$ the formation of a gap is difficult.

Finally in **Chapter 6** I summarize the more important results of my investigation and I discuss their implications on the evolution of SMBHs.

# Capítulo 2

# Method

In this chapter I present the method used in this thesis to study the evolution of SMBHs in dense gaseous environments. Although an important part of this thesis are analytical estimations of the gravitational interaction between SMBHs and circum-binary gaseous disks, I test all our analytical predictions against numerical simulations. All the simulations that I perform are run using the code Gadget-2 (or Gadget-3; Springel 2005) which follows the evolution of collisionless component (SMBHs, stars in galaxies and dark matter) and of an ideal gas, both subject to and coupled by gravity.

## 2.1. The N-body/SPH code Gadget

### 2.1.1. Gas dynamics and the SPH formulation

In the code Gadget-2 the gaseous medium (collisional component), such as the inter stellar medium (ISM) or the inter galactic medium (IGM), is modeled as an ideal, viscid gas which is governed by the continuity equation

$$\frac{dp}{dt} + \rho \nabla \cdot \mathbf{v} = 0, \tag{2.1}$$

the momentum equation

$$\frac{dv}{dt} = -\frac{\nabla P}{\rho} + a_{\rm visc} - \nabla \Phi, \tag{2.2}$$

and an energy per unit mass ($u$) equation

$$\frac{du}{dt} = -\frac{P}{\rho} \nabla \mathbf{v} + \left( \frac{du}{dt} \right)_{\rm visc}, \tag{2.3}$$

where $\rho$ is the density of a fluid element, $P$ the pressure onto the fluid element, $a_{\rm visc}$ the viscous acceleration, $\left(\frac{du}{dt}\right)_{\rm visc}$ is the viscous heating and $\Phi$ the gravitational potential onto the fluid element. In these equations is used the Lagrangian time derivative $d/dt = \partial/\partial t + \mathbf{v} \cdot \nabla$. To close the set of equations a simple polytropic equation of state is used for the gas

$$P = (\gamma - 1) \rho u, \tag{2.4}$$

where $\gamma$ is the adiabatic exponent, which for mono-atomic ideal gas is $\gamma = 5/3$.

To solve this set of equations the code Gadget-2 uses a SPH formulation. The SPH formulation uses a set of discrete particles to describe the state of a fluid, where the continuous fluid quantities are defined by a kernel interpolation technique (Lucy 1977; Gingold & Monahan 1977; Monahan 1992). Using this approach in Gadget-2 any quantity $\mathbf{A}$ in a point $\mathbf{r}$ of the fluid can be estimated as

$$\mathbf{A} = \sum_{j=1}^{N} m_j \frac{A_j}{\rho_j} W(|\mathbf{x_i} - \mathbf{x_j}|, h_i), \tag{2.5}$$

where $x_j$ is the position of the fluid tracer $j$, $\rho_j$ is the density associated to the fluid tracer j and $W(r_{ij}, h_i)$ is the SPH smoothing kernel defined as

$$W(r,h) = \frac{8}{\pi h^3} \begin{cases} 1 - 6\left(\frac{r}{h}\right)^2 + 6\left(\frac{r}{h}\right)^3 & 0 \leq \frac{r}{h} \leq \frac{1}{2} \\ 2\left(1 - \frac{r}{h}\right)^3 & \frac{1}{2} < \frac{r}{h} \leq 1 \\ 0 & \frac{r}{h} > 1 \end{cases}, \tag{2.6}$$

where $h_i$ is called the smoothing length of the particle $i$ and is defined such that the kernel volume around the particle $i$ contains a constant mass of neighbour particles.

From this formulation we found that the density estimate of a fluid tracer $i$ is

$$\rho_i = \sum_{j=1}^{N} m_j W(|\mathbf{x_i} - \mathbf{x_j}|, h_i). \tag{2.7}$$

We note that if $N_{sph}$ is the number of neighbours and $\bar{m}$ is the average mass per particle, $h_i$ follows the implicit equation

$$\bar{m}\, N_{\rm SPH} = \frac{4\pi}{3}\, h_i^3\, \rho_i\,. \tag{2.8}$$

Therefore, for a constant value of $N_{sph}$ the smoothing length $h_i$ is smaller in regions of high density.

The essential point of the SPH formulation is that allows us to construct a differentiable interpolant of a function from its values at the particles (interpolation points) by using the differentiable kernel. Therefore to obtain derivatives of any quantity of the fluid $\mathbf{A}$ there is no need to use finite differences and no need for a grid. For example if we need to compute the derivative of a fluid quantity $\mathbf{A}$ we obtain that

$$\nabla\, \mathbf{A} = \sum_{j=1}^{N} m_j \frac{A_j}{\rho_j} \nabla W(|\mathbf{x_i} - \mathbf{x_j}|, h_i) \tag{2.9}$$

With the estimation of any quantity for the $i$ particle tracer ($\mathbf{A_i}$) and starting from a discrete version of the fluid Lagrangian, the code Gadget-2 computes the equations of motion of the particle tracer and their energy evolution. However, to solve these equations we also need to know the gravitational force exerted onto the tracer particle by the other SPH particles and by the collisionless component. In the next subsection we explain how Gadget-2 computes these gravitational forces.

### 2.1.2. Collisionless dynamics and gravity

The continuum limit of a self-gravitating collisionless component (such as stars in a galaxy or dark matter) can be described by the collisionless Boltzmann equation

$$\frac{df}{dt} = \frac{\partial f}{\partial t} + \mathbf{v}\frac{\partial f}{\partial \mathbf{r}} - \frac{\partial \Phi}{\partial \mathbf{r}}\frac{\partial f}{\partial \mathbf{v}} = 0\,, \tag{2.10}$$

where $f(\mathbf{r}, \mathbf{v}, t)\, d\mathbf{v}\, d\mathbf{r}$ is the phase space density and $\Phi$ is the gravitational potential that satisfies the Poisson's equation (Binney & Tremaine 1987). As this set of coupled equations is too difficult to be solved directly, the code Gadget-2 uses a common N-body approach where the phase "fluid" is represented by a finite number of N tracer particles.

The dynamics of these N particles is described by the Hamiltonian

$$\mathbf{H} = \sum_i \frac{\mathbf{p}_i^2}{2m_i} + \frac{1}{2}\sum_{ij} m_i m_j \Phi(\mathbf{x_i} - \mathbf{x_j}) \tag{2.11}$$

here H is function of $\mathbf{p_1}$,$\mathbf{p_1}$,..., $\mathbf{p_N}$,$\mathbf{x_1}$,$\mathbf{x_2}$,...,$\mathbf{x_N}$ and t, where $\mathbf{x_i}$ are the coordinate vectors of the N particles particles with canonical momentum $\mathbf{p_i} = m_i \dot{\mathbf{x}}_\mathbf{i}$.

To derive the equations of motion of the N particles from this Hamiltonian we need the gravitational potential produced by each particle $j$ onto each particle $i$ ($\Phi(\mathbf{x_i} - \mathbf{x_j})$). In principle this potential has to be the potential of a point mass $\Phi(\mathbf{r}) = -Gm/r$, however this potential produces problems of integration when two particles get too close ($r$ to small). For this reason, the code Gadget-2 uses a normalised gravitational softening kernel of scale $\varepsilon$ to represent the particle gravitational potential, which is analog to assume that the mass of the particle is distributed in a sphere of radius $\sim \varepsilon$ with a density profile determined by the kernel. The exact form of the gravitational softening kernel is derived by taking the force from a point mass $m_i$ to be the one resulting from a density distribution $\rho_i(r) = m_i W(r; \varepsilon)$. This lead to a potential of the form

$$\phi(\mathbf{r}) = -G\frac{m}{\varepsilon} W_2(r, \varepsilon) \tag{2.12}$$

where

$$W_2(r,\varepsilon) = \begin{cases} -\frac{16}{3}\left(\frac{r}{\varepsilon}\right)^2 + \frac{48}{5}\left(\frac{r}{\varepsilon}\right)^4 - \frac{32}{5}\left(\frac{r}{\varepsilon}\right)^5 + \frac{14}{5} & 0 \le \frac{r}{\varepsilon} \le \frac{1}{2} \\ -\frac{1}{15}\left(\frac{r}{\varepsilon}\right)^{-1} - \frac{32}{3}\left(\frac{r}{\varepsilon}\right)^2 + 16\left(\frac{r}{\varepsilon}\right)^3 - \frac{48}{5}\left(\frac{r}{\varepsilon}\right)^4 + \frac{32}{15}\left(\frac{r}{\varepsilon}\right)^5 + \frac{16}{5} & \frac{1}{2} < \frac{r}{\varepsilon} \le 1 \\ \left(\frac{r}{\varepsilon}\right)^{-1} & \frac{r}{\varepsilon} > 1 \end{cases}, \tag{2.13}$$

Finally as a complete force computation of the gravitational force between the N particles particles (of the collisional and collisionless components) involves a double sum, its computation results in a $N^2$ scaling of the computational cost. This reflects the long range nature of gravity, where each particle interacts with every other particle, making high accuracy solutions for the gravitational force very expensive for large N. For this reason the code Gadget-2 uses a tree algorithm to compute the gravitational force between particles. This algorithm is a hierarchical multipole expansion for which distant

particles are grouped into larger cells, allowing their gravity to be accounted for means of a single multipole force.

With this algorithm the summation of the gravitational potential onto a particle can be computed with just $\mathcal{O}(\log N)$ interactions, instead of the N-1 interactions needed to compute the gravitational force in a direct summation scheme (Springel *et al* 2001). It should be noted that the final result of the tree algorithm will in general only represent an approximation to the true force. However, the error of this estimation in the code GADGET-2 is controlled by setting the size of the cells, for which a multipole expansion of the gravitational force will be used, such that the force accuracy is smaller than some tolerance. We set this tolerance as 0.005 which means that the gravitational force computed from this hierarchical multipole expansion has a maximum perceptual error of 0.5 %.

## 2.2. Implementation of star formation, cooling and feedback in Gadegt-3

In this section I will introduce the recipes for star formation, supernovae heating and cooling that I implement in the code GADGET3. For make easier the comparison of our recipes with some other recipes typically used in the literature we include in table 1 a summary of these recipes.

### 2.2.1. Cooling

The cooling due to radiative emission is typically modeled as a function of the metallicity, density, and temperature of the ISM ($\Lambda(\rho, T, z_m)$) and its action on the ISM can be described by the relation

$$\frac{du}{dt} = \rho\Lambda(\rho, T, z_m) \tag{2.14}$$

where $u$, $\rho$, $T$ and $z_m$ are the internal energy, density, temperature and metalicity of the ISM respectively.

For temperatures between $10^4$ K and $10^8$ K I estimate the cooling function $\Lambda$ in the same way described by Katz *etal* (1996), considering the radiative processes that are produced in an optically thin gas with solar metallicity. The abundance of the different ionized states of the different species are explicitly computed under the supposition of an collision-less equilibrium state.

As in my simulations I pretend to resolve the multiphase structure of the ISM and the high density of low temperature where the stars form, I extend the cooling functions down to 50 K using the parametrization of Gerritsen & Icke (1997). The extension of the cooling function down to 50 K it is essential to model the star formation without the necessity of a fine-tune of the controlling parameters of the star formation recipe (Saitoh et al. 2008 Gerritsen & Icke 1997, Ceverino & Klypin 2009).

Tabla 1: Recipes on the literature

| Reference | SF Criteria | Cooling | Resolution |
|---|---|---|---|
| Gerritsen & Icke 1997 | $M_{\rm J} < M_{\rm c} = 10 m_{\rm sph} \approx 10^5 M_\odot$<br>$t_{\rm criterio1} > t_c = \frac{f_{\rm c}}{\sqrt{4\pi G\rho}}$ | $10 < T < 10^6$ (Function)<br>Dalgarno & McGray 1972 | $N_{\rm sph} = 5000$<br>$h_{\rm gas} \approx 0.2[Kpc]$ $r_{\rm gas} \approx 5[Kpc]$ |
| Wada & Norman 2000 | $\Sigma_{gas} > 5 \times 10^4 M_\odot pc^{-2}$<br>$T_{gas} < 50[K]$<br>criteria 1 and 2 full-filled during $5 Myr$ | $10 < T < 10^8$ (Table)<br>Spaans & Norman 1997 | $\sim 1\,[pc]$ |
| Stinson *et al* 2006 | $n_H > 0.1 cm^{-3}$ y Virializado<br>$T_{gas} < 1.5 \times 10^4 [K]$<br>$\nabla \cdot v < 0$ | $10^4 < T < 10^9$<br>KWH | $N_{\rm sph} \approx 10.000 - 300.000$<br>$300 - 600\,[pc]$ |
| Tasker & Bryan 2006 | $n_H > 1000 cm^{-3}$<br>$M_{gas} > M_{jeans}$<br>$\nabla \cdot v < 0$<br>$\tau_{cool} < \tau_{dyn}$ | $300 < T < 10^9$<br>Sarazin & White 1987<br>Rosen & Bregman 1995 | $25 - 50\,[pc]$ |
| Saitho *et al* 2008 | $n_H > 100 cm^{-3}$<br>$T_{gas} < 5 \times 10^3 [K]$ (80 % SF at $100[K]$)<br>$\nabla \cdot v < 0$ | $10 < T < 10^8$ (Table)<br>Spaans & Norman 1997 | $m_{sph} \sim 10^{2-3} M_\odot$ |
| Ceverino & Klypin 2009 | $\rho_{gas} > 0.035 M_\odot pc^{-3}$ $(n_H = 1 cm^{-3})$<br>$T_{gas} < 10^4 K$ (50 % at $300[K]$) | $10^2 < T < 10^9$ (Table)<br>Kravstsov 2003<br>Ferland etal 1998 CLOUDY | $30 - 70\,[pc]$ |
| Governato *et al* 2009 | $n_H > 100 cm^{-3}$<br>$T_{gas} < 10^4 [K]$ | $10^4 < T < 10^8$ (Table)<br>Spaans & Norman 1997 | $m_{clumps} \sim 10^5 M_\odot$ |
| Hopkins *et al* 2011 | $n_H > 100 cm^{-3}$ | $1 < T < 10^9$ (Table)<br>Sánchez-Salcedo *et al* 2002<br>Ferland etal 1998 CLOUDY | $2.5 - 3.5\,[pc]$ |

### 2.2.2. Star Formation

To define the star formation recipes I rely in the theoretical (Bromm, Coppi & Larson 2002) and observational restrictions (Evans 1999) that suggest that the star forming region have temperatures between 100 to 200 K and densities between $10^3$ to $10^5\, cm^{-3}$, and also the expectation that the star forming regions have to be initially under collapse. From this simple restrictions for the star forming regions I consider that gas particles will be able to form stars only if their temperature are below some limit, their density are greater than some critical value and the velocity field around them is convergent,

$$n_{\rm H} \geq n_{\rm crit} \tag{2.15}$$
$$T_{gas} \leq T_{\rm crit} \tag{2.16}$$
$$\nabla \cdot \vec{v} < 0\,. \tag{2.17}$$

Ideally in any region where these three criteria are fulfilled I expect star formation, but as my simulations do not have the necessary mass resolutions to capture the formation of singles stars I use a stochastic description for the star formation process. For each gas particle of mass $m_{\rm gas}$ that satisfy these criteria I compute a star formation probability $p$ defined as

$$p = \frac{m_{\rm gas}}{m_\star}\left(1 - e^{c_\star \frac{\Delta t}{t_{\rm g}}}\right)\,, \tag{2.18}$$

where $m_\star$ is the mass of the star particle, $c_\star$ is the constant star formation efficiency factor and $t_{\rm dyn} = ({\rm G}\,\rho)^{-1/2}$ is the dynamical time. Here following Stinson et al. (2006) I choose the star formation timescale as the dynamical timescale without any consideration of the cooling timescale because we introduce the thermal star formation criterion (2.16) that constraints star formation to gas regions that are cool enough to collapse unimpeded by gas pressure. Finally for each star formation eligible gas particle I draw a random number $r$ between zero and one, and if $r < p$ a new star particle of mass $m_{\rm star}$ is spawned. If the mass of the forming stars results to be equal to the mass of the progenitor gas particle then I transform the gas particle into a star particle.

### 2.2.3. Feedback

Every newly formed "star" is assumed to be a Single Stellar Population (SSP) with a three piece power law IMF as defined in Miller & Scalo (1979, hereafter MS79). From this IMF and the same stellar lifetime calculations used by Stinson etal (2006), I compute for each SSP the number of type II supernovae (SNII) events in function of time ($N_{\rm snII}(t)$) as.

$$N_{\rm snII}(t) = \int_{M_{\rm low}(t-t_{\rm form})}^{M_{up}(t-t_{\rm form})} \phi(m)\,\frac{dm}{m} \tag{2.19}$$

Where $\phi(m)$ is the IMF of the SSP, $t_{\rm form}$ is the time in which the SSP was formed and $M_{\rm low}(t)$ ($M_{\rm up}(t)$ ) is the mass of the smaller (bigger) star that explode as a supernova in the time t. For this number of SNII events per unit time I compute the total energy that the SSP deposits in the ISM assuming a nominal energy per explosion EsnII = $10^{51}$ ergs.

I distribute all this energy in the closest 32 gas particles using the SPH kernel function of Gadget as weight function (for a region of density $\sim 100$ cm$^{-3}$ these 32 particles are contained inside a sphere of radius $\sim 1.3 \times (m_{\rm sph}/M_{\odot})^{1/3}$ pc, with $m_{\rm sph}$ the mass of the gas particles). I not include any heating by supernovae type Ia (SNIa) because the typical time of integration of our simulations is 30-100 Myr and the SNIa timescale is of the order of 1 Gyr.

In the same way that Stinson *etal* (2006), when a gas particle is heated by the supernova feedback of a closes star particle the cooling of the gas particle is turned off only for a time equal to the expected lifespan of the shock wave produced by the supernova; $t_{max} = 10^{6.85} E_{51}^{0.33} n_0 P_{04}^{-0.7} yr$ where $E_{51}$ is the energy per explosion in units of $10^{51}$ erg, $n_0$ is the density of hydrogen of the region where the shock wave expand and $P$ is the pressure in this region (Mckee & Ostriker 1977; Stinson et al. 2006).

## 2.3. Recipes test

In order to test the star formation, feedback and cooling recipes I analyze the influence of these recipes in two test simulations. The first test is the study of the shock expansion in the gas after the explosion of a star as supernova. The second test is the study of the relation between the density of the star formation rate and the density of the gas, to determine if they follow the Kenniccut-Shcmidt relation. I use these tests to ensure that I implement in a correct way the recipes. Although these are only two tests, the applicability of these recipes is supported by the large number of simulations that use these same recipes to study astrophysical systems of different sizes with different resolutions (e.g: Stinson et al. 2006; Tasker & Bryan 2006; Mashchenko, Wadsley & Couchman 2008; Christensen et al. 2010; Guedes et al. 2011; Van Wassenhove et al. 2012)

### 2.3.1. Shock expansion

When a stars explode as supernova delivers energy to the interstellar medium, which generates a shock expansion through it. I include this energy input in the stellar feedback recipe in our more realistic simulations, therefore we must analyse if the shock expansion is well reproduced in our simulations.

I simulate one SN explosion in an homogeneous and adiabatic gaseous medium, and I study the evolution of the shock expansion in the gas. This expansion in these conditions was analytically studied by L. I. Sedov in 1946 who determined that the time evolution of the shock radius was $R_F \propto t^{0.4}$.

In figure 2.1 I show the time evolution of the shock radius in the adiabatic and homogeneous gas. The time evolution of the shock radius observed in my test simulation is consistent with the relation derived by Seldov 1946 $R_F \propto t^{0.4}$ during the simulation.

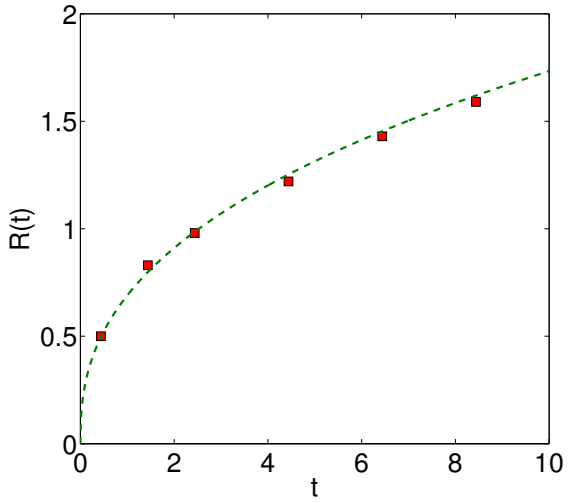


Figura 2.1: Time evolution of the shock radius generated by the energy injection in the adiabatic and homogeneous gas. The green dashed line shows the analytical solution from Seldov 1946. The red squares show the time evolution of the test simulation that includes the SN feedback.

In figure 2.2 I show the time evolution of the shock geometry generated by the SN explosion. Here we can see that the the shock geometry is spherical during the simulation. This shows that the energy injection delivered to 64 neighbors is good enough to keep all directions equally important for the SN explosion and the subsequent shock expansion. I also check that the energy delivered to the gas is actually the nominal supernova energy $10^{51}$ erg. This result is in concordance with my model which has no privileged direction at the moment of deliver the energy in the gaseous environment produced by the SN explosion.

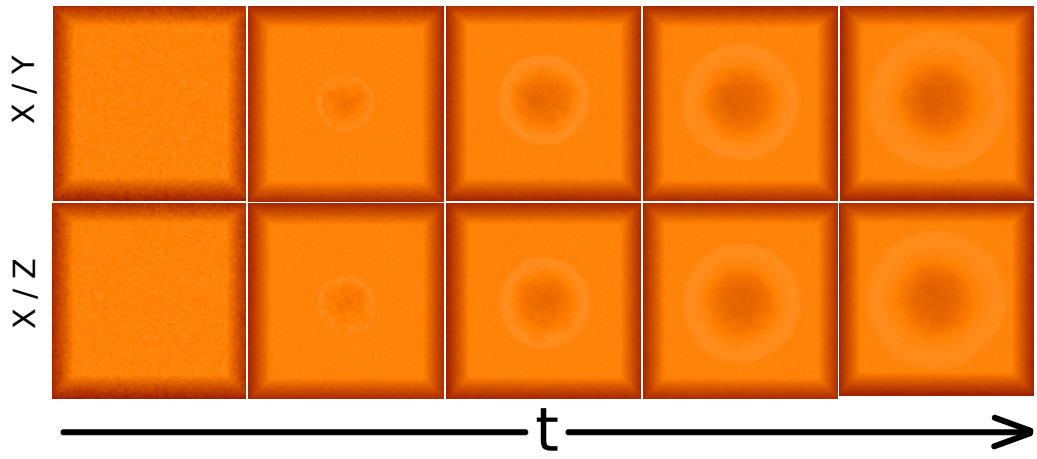


Figura 2.2: Time evolution of the protected density after the SN explosion. In the upper row we show the xy protection and in the lower row the xz protection. Here we can see that the shock geometry is spherical.

### 2.3.2. Relation of Kennicutt-Schmidt in an isolated galaxy

As an additional test for the recipes, I test if in a simulation of an isolated galaxy the Kenniccut-Schmidt relation is obeyed (Kennicutt 1998). In figure 2.3.2 I show with the values of $\Sigma_{\rm gas}$ and $\Sigma_{\rm SFR}$ for simulations of an isolated "Milky way" type galaxy using our recipes for star formation, cooling and heating. The green squares correspond to a simulation where $n_{\rm crit} = 100$ cm$^{-3}$, $T_{\rm crit} = 10^3$ K, $c_\star = 0.05$ and $E_{\rm SN} = 10^{51}$ erg and the red squares to a simulation where $n_{\rm crit} = 100$ cm$^{-3}$, $T_{\rm crit} = 10^3$ K, $c_\star = 0.05$ and $E_{\rm SN} = 10^{53}$ erg. We can see from this figure that for the typical values $c_\star = 0.05$ and $E_{\rm SN} = 10^{51}$ our simulation of an isolated galaxy using our recipes reproduce in a fairly good way the Kenniccut-Schmidt relation. Also I study the effect of increasing the energy released by the supernova explosions. I find that if we increase in two orders of magnitude the energy per supernova the star formation rate decreases from $\sim$30 M$_\odot$ yr$^{-1}$ kpc$^{-2}$ to $\sim$ 15 M$_\odot$ yr$^{-1}$ kpc$^{-2}$, which is only a factor two of difference. Therefore, in simulations running with these recipes the values of $\Sigma_{\rm gas}$ vs $\Sigma_{\rm SFR}$ does not depend strongly on the election of $E_{\rm SN}$. This is consistent with the work of Saitoh *et al.* (2006), where they find that for high star formation density thresholds $n_{\rm crit} > 10$ cm$^{-3}$ the star formation rate depends weakly on the exact values of the other parameters of the recipes of star formation and supernova feedback.

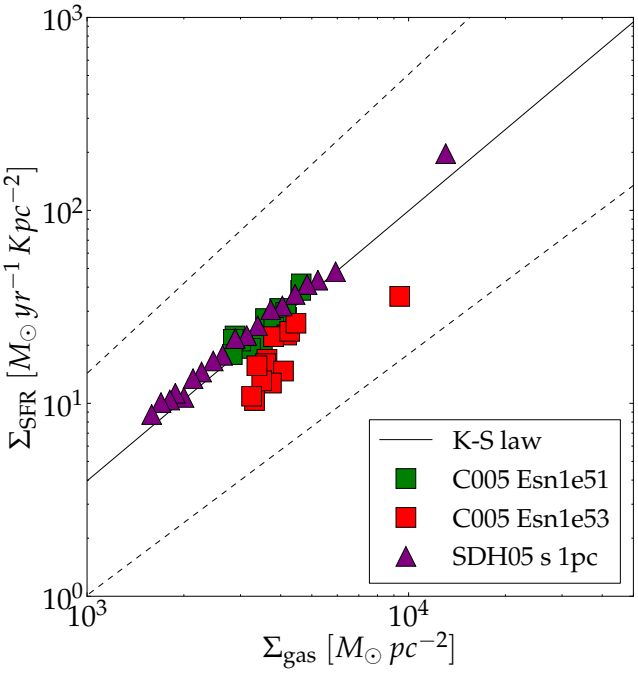


Figura 2.3: Relation of Kenniccut-Shmidt in a isolated galaxy for our recipes (C005) and the recipes included in the code Gadget-3 (SDH05). Points of the same color represent the value of $\Sigma_{\rm gas}$ v/s $\Sigma_{\rm SFR}$ in different times of the evolution of the same galaxy. The continuous line corresponds to the best fit of the correlation for 61 normal spiral galaxies and 36 infrared-selected star-bust galaxies obtained by (Kennicutt 1998). The dashed lines delimit the scatter of the observational relation obtained by (Kennicutt 1998).

I also compare the values of $\Sigma_{\rm gas}$ and $\Sigma_{\rm SFR}$ obtained with these recipes with the ones obtained with the recipes of star formation, cooling and heating included in the code Gadget-3. These recipes are define in such a way that the star formation is self regulated and it is only parametrized by one parameter; the star formation timescale $t_0^*$. We use $t_0^* = 2.1$ which is the same value used by Springel, Di Matteo and Hernquist (2005) (I name the runs using this recipe with a value of $t_0 = 2.1$ as SDH05). In figure 2.3 I plot with purple triangles the values of $\Sigma_{\rm gas}$ and $\Sigma_{\rm SFR}$ obtained for the simulation SDH05. I find that the values of $\Sigma_{\rm gas}$ and $\Sigma_{\rm SFR}$ from the isolated galaxy ran with our recipes are in concordance with the values obtained for the simulation SDH05.

## 2.4. Resampling

When we need to improve the resolution of a SPH simulations in some region of interest we can split each one of the particles in this region in many particles as we want in order to increase the mass resolution of our simulations (Kitsionas 2000;Bromm & Loeb 2003). This is particularly useful when we want to resolve the evolution of the separation between two SMBHs in a galaxy merger down to parsec scales because is too expensive to follow all the evolution of the galaxy merger with too many particles. Instead we can begin the simulation with a moderate number of particles $\sim 100000$ and when the SMBHs get closer we can increase the number of particles in the innermost part of the merger remnant where the SMBH binary is formed, in order to properly follow the evolution of the SMBHs binary.

When I split a particle in $N_{\rm split}$ more particles I randomly distribute these $N_{\rm split}$ particles by employing a standard Monte-Carlo comparison-rejection method, in such a way that the distribution of particles follows the SPH smoothing kernel function $W(r; h_{\rm parent})$ (where $h_{\rm parent}$ is the smoothing length of the parent particle) centered in the position of the "parent" particle. I set the velocity of these new particles equal to the velocity of the "parent" particle and the mass of each of these particles as $m_c = m_{\rm parent}/N_{\rm split}$, where $m_{\rm parent}$ is the mass of the parent particle. This procedure conserves linear and angular momentum well. Energy is also conserved well, although there arises a small artificial contribution to the gravitational potential energy due to the discreteness of the resampling.

# Capítulo 3

# Gap-Opening criteria for comparable mass binaries

Originally published by: del Valle & Escala, 2012, *The Astrophysical Journal*, **761**,33 and del Valle & Escala, 2014, *The Astrophysical Journal* **780**,84

We study the interaction between an unequal mass binary with an isothermal circumbinary disk, motivated by the theoretical and observational evidence that after a major merger of gas-rich galaxies, a massive gaseous disk with a SMBH binary will be formed in the nuclear region. We focus on the gravitational torques that the binary exerts onto the disk and how these torques can drive the formation of a gap in the disk. This exchange of angular momentum between the binary and the disk is mainly driven by the gravitational interaction between the binary and a strong non-axisymmetric density perturbation that is produced in the disk, as response to the presence of the binary. Using SPH numerical simulations we tested two gap-opening criterion, one that assumes that the geometry of the density perturbation is an ellipsoid/thick-spirals and another that assumes a geometry of flat-spirals for the density perturbation. We find that the flat-spirals gap opening criterion successfully predicts which simulations will have a gap on the disk and which simulations will not have a gap on the disk. We also study the limiting cases predicted by the gap-opening criteria. Since the viscosity in our simulations is considerably smaller than the expected value in the nuclear regions of gas-rich merging galaxies, we conclude that in such environments the formation of a circumbinary gap is unlikely.

## 3.1. Introduction

A binary embedded in a gaseous disk is a configuration that is repeatedly found in astrophysics at a variety of scales. Some examples are the interaction between planetary rings and satellites (Goldreich & Tremaine 1982), the formation of planets in protoplanetary disks and their migration (Goldreich & Tremaine 1980, Ward 1997, Armitage & Rice 2005, Baruteau & Masset 2013 ), the evolution of stellar binaries (Shu et al. 1987, McKee & Ostriker 2007), the interaction of stars and black holes in AGNs (Goodman & Tan 2004, Miralda-Escude & Kollmeier 2005, Levin 2007), and the expected interaction of massive black holes (MBHs) binaries at the center of merging galaxies. In all these cases, it is fundamental to have a proper understanding of the main dynamical processes

that drives the evolution of a binary-disk system.

The MBH binaries that interact with gaseous disks are expected to form in the context of hierarchical structure formation (White & Frenk 1991, Springel et al. 2005 ). In this scenario, the formation and evolution of galaxies is a complex process, where their final states will be sculpted by a sequence of mergers and accretion events. If the galaxies that are involved in this mergers are rich in gas, there is theoretical (Barnes & Hernquist 1992, 1996; Mihos & Hernquist 1996; Barnes 2002; Mayer et al. 2007, 2010) and observational (Sanders & Mirabel 1996; Downes & Solomon 1998) evidence that a large amount of the gas on these galaxies will reach the central kilo-parse (Kpc) of the newly formed system. Also, there is observational evidence for the existence of MBH at the center of practically all observed galaxies with a significant bulge (Richstone etal 1998, Magorrian etal 1998, Gultekin etal 2009). Therefore, it is expected that the MBH in the center of each galaxy follow the gas flow and form a MBH binary embedded in a gas environment at the central parsec of the newly formed galaxy, as is shown by a variety of numerical simulations (Kazantzidis et al. 2005, Mayer et al. 2007, Hopkins & Quataert 2010, Chapon et al. 2011).

Although numerical simulations suggests the formation of MBH binaries, the only conclusive evidence of pairs of black holes come from the observation of quasar pairs with separations of $\sim 100$ Kpc (Hennawi et al. 2006; Myers et al. 2007, 2008; Foreman et al. 2009; Shen et al. 2011, Liu et al. 2011) and some acreting black holes with separations of the order or smaller than one Kpc (Komosa et al. 2003, Fabbiano et al. 2011, Comerford et al. 2012). On the other hand, there is evidence of at least one MBH binary with a separation of a few parsecs (Rodriguez et al. 2006), but in general, the observational evidence of bound MBH binaries remains elusive, and most of the candidates have observational signatures that can be explained by other configuration and processes different from a MBH binary (Valtonen et al. 2008; Komossa et al. 2008; Boroson & Lauer 2009; Tsalmantza et al. 2011; Eracleous et al. 2011; Dotti, Sesana & Decarli 2012 and references therein).

Considering the lack of observational evidence, it is crucial to get more insight of the dynamical process of the binary-disk interaction to determine in what type of merger remnants it is more probable to find these binaries and how the binary separation of these systems depends on the characteristics of the central parsec of the mergers remnants.

A considerable amount of work and progress on the understanding of the interaction of a MBH binary with a gas environment has been made since Escala et al. (2004, 2005) showed, with numerical simulations, that "when the binary arrives at separations comparable to the gravitational influence radius of the black hole ($R_{\rm inf} = 2GM_{\rm BH}/(v^2 + c_{\rm s}^2)$)", localy the binary stars dominate the total gravitational field and the gas tends to follow the gravitational potential of the binary, forming a non-axisymmetric density perturbation that interacts gravitationally with the binary and drives a decrease on the binary separation. Due to the self-similar nature of the gravitational potential, in the regime where the gravitational potential is domianted by the MBH binary, the non-axisymmetric density perturbation is also self-similar in nature. This suggest that, although in the simulations of Escala et al. (2004, 2005) the shrinking of the binary stops at the gravitational resolution, the fast decay will continue down to scales where the gravitational wave emission is effective enough to bring the binary to coalescence.

For systems like the ones explored by Escala et al. (2004, 2005), where the gas mass of the disk is much greater than the binary mass, it is expected that the time the binary takes to merge will be on the order of a few initial orbital times (Escala et al. 2005, Dotti et al. 2006), unless a dramatic change happens in the nearby gas of the binary where the strong non-axisymmetric density perturbation forms (such as gap formation or gas ejection by the BH accretion luminosity). This contrasts with the results of simulations of disks with negligible masses, compared to the binary mass, where the coalescence time is found to be on the order of several thousands of local orbital times (Artymowicz & Lubow 1994; Ivanov, Papaloizou, & Polnarev 1999; Armitage & Natarajan 2002; Milosavljevic & Phinney 2005), which for $M_{BH} \geq 10^7 M_\odot$ is even longer than the Hubble time (Cuadra et al. 2009).

This fast/slow (few orbital times versus several thousand orbital times) migration duality can also be found in simulations of protoplanetary disks that harbour planets (eg. extreme mass ratios; Ward et al. 1989, Ward 1997, Bate et al. 2003, Armitage & Rice 2005; Baruteau & Masset 2012, Kocsis et al. 2012). In this type of simulations, the planet/star binary is an extreme mass ratio binary ($q \ll 1$) and the fast/slow migration regime is defined as TypeI/TypeII migration. In the Type I regime, the protoplanetary disk experiences a perturbation, due to the small gravitational potential of the planet. This allows a fast migration of the planet (in the order of a few $t_{\rm orb}$) with a characteristic time scale that scales as the inverse of the planet mass ($t_{\rm migration} \propto M_{\rm p}^{-1}$). The Type II migration (slow migration) is experienced by a planet when its Hill radius is greater than the local pressure scale height of the protoplanetary disk ($R_{\rm Hill} >> h$). In this case the perturbation in the protoplanetary disk due to the presence of the planet becomes important and the planet begins to excavate a gap on the disk. This leads to a coupled evolution of the planet and the disk on a viscous time scale, making the migration time much longer.

For the case of a comparable mass binary embedded in a disk, as in the extreme mass ratio case of a star-planet-disk system, the threshold between the fast and slow migrations is also determined by the formation of a gap or cavity in the disk. Therefore, if we can determine for which systems a gap is opened we can determine in what system a fast or slow migration will occur. For this reason, in this work we will derive a gap-opening criterion for comparable mass binaries($0.1 \leq q \leq 1$) which we will test against numerical simulations to prove its validity.

This work is organized as follows. In Section §3.2 we present the derivation of the analytic gap-opening criterion derived in the case of moderate mass ratio binaries ($0.1 \leq q \leq 1$) assuming that the non-axisymmetric density perturbation produced by the binary has an ellipsoidal geometry. In Section §3.3 we present the setup of the numerical simulations that we use to test our analytic gap-opening criterion. In Section §3.4 we describe how we identified the formation of a gap in our numerical simulations. In §3.5 we test the "ellipsoidal" analytic gap-opening criterion for the case of equal mass binaries against this numerical simulations. In Section §3.6 we extend our study for unequal, but comparable, mass ratio binaries and, in §3.7, we study why the formation of a gap in some simulations is not well predicted by the "ellipsoidal" gap-opening criterion and we derived a new gap-opening criterion that is consistent with all our numerical simulations.

In Section §3.8 we study the limits for the final evolution of a binary embedded in a gas disk that are predicted by this successful analytic gap-opening criterion. To improve the robustness of our study in section §3.9 we test our gap-opening criterion against numerical simulations from the literature. Finally, in Section §3.10 we discuss the implication of our results for real astrophysical systems and we present our conclusions.

## 3.2. Gap-opening criteria derivation

The most widely studied case for binary-disk interaction, is the case of a binary embedded in a gas disk with much smaller mass than the mass of the primary. This limiting case of low-mass disk ($M_{\rm disk}/M_{\rm primary} \ll 1$) is typically found in the late stages of star/planet formation (Lin & Papaloizou 1979; Goldreich& Tremaine 1982; Takeuchi et al. 1996; Armitage & Rice 2005; Baruteau & Masset 2012). In these studies, when the binary has an extreme-mass ratio ($q \ll 1$), the gravitational potential produced by the secondary is treated as a perturbation to the axisymmetric gravitational potential of the primary-disk system, allowing a linear approximation for the equations of motion of the secondary. From this approximation, studies find that the sum of the torques, arising from the inner and outer Lindblad and co-rotation resonances, drive the interaction between the secondary and the disk. This approach leads to predictions of the gap structure that are consistent with simulations within the same regime of validity of it ($q \ll 1$ and $M_{\rm disk}/M_{\rm primary} \ll 1$) (Ivanov et al. 1999; Armitage & Natarajan 2002; Nelson & Papaloizou 2003; Haiman et al. 2009; Baruteau & Masset 2012).

Motivated by the success of this approach in the planetary regime ($q \ll 1$), some authors extrapolate this analysis to other cases where $q \sim 1$ (Artymowicz & Lubow 1994, 1996; Gunther & Kley 2002; MacFadyen & Milosavljevic 2008) regardless of the strong nonlinear perturbation that is produced by the non-axisymmetric gravitational field of the binary, which breaks the validity of the linearization of the equations of motion in this regime ($q \sim 1$) (Shi et al. 2012).

In this paper we study the binary-disk interaction in the regime $q \sim 1$ without any assumption of linearity. For this purpose we explore if it's possible, due to the tidal nature of the binary-disk interaction, that the gap-opening process can be described by the interaction of the binary with a strong non-axisymmetric perturbation on the disk instead of a resonant process such as the one used in the linear approximation. This type of interaction between a strong non-axisymmetric perturbation and a binary was investigated in Escala et al. (2004, 2005). They show that, when the gravitational influence spheres (i.e. Hill spheres) of the two component of the binary overlap, a strong tidal non-axisymmetric perturbation is produced in the disk with an ellipsoidal geometry for an equal mass binary ($q = 1$). They also found that the symmetry axis of this strong non-axisymmetric perturbation is not coincident with the binary axis but lags behind it, producing a gravitational torque on the binary that is responsible for an angular momentum transport from the binary to the disk.

Motivated by the result of Escala *etal* 2005 we study the gravitational interaction bet-

ween the binary and an ellipsoid to derive analytically the exchange of angular momentum between the disk and the binary and then use this exchange of angular momentum to derive a gap-opening criterion. This binary-ellipsoid system can be treated as an equivalent one body problem subject to an external gravitational potential caused by the ellipsoidal perturbation. The gravitational potential of a uniform ellipsoid is given by

$$\Phi(x,y,z) = \pi\, G\, \rho\, (\, \alpha_0 x^2 + \beta_0 y^2 + \gamma_0 z^2 + \chi_0\, )\,, \tag{3.1}$$

with $\alpha_0$, $\beta_0$, $\gamma_0$ and $\chi_0$ constant given in Lamb (1879) which depend on the ratio between the principal axes of the ellipsoid. For the symmetry of the ellipsoidal perturbation observed in Escala et al. (2004, 2005) $\gamma_0 = \beta_0$ and $\chi_0 = 0$. Therefore, the Lagrangian of the binary-ellipsoid system in cylindrical coordinates has the form

$$\begin{aligned} \mathbf{L} &= \frac{1}{2}\mu\left[\left(\frac{dr}{dt}\right)^2 + r^2\left(\frac{d\phi}{dt}\right)^2 + \left(\frac{dz}{dt}\right)^2\right] + G\frac{\mu^2}{r} \\ &\quad -\frac{\pi}{2}G\mu\rho(\alpha_0 r^2\cos^2(\Delta\phi) + \beta_0 r^2\sin^2(\Delta\phi) + \gamma_0 z^2)\,, \end{aligned} \tag{3.2}$$

with $\mu = M_1 M_2/M_{\rm bin}$ being the reduced mass of the binary and $\Delta\phi$ the angle between the major axis of the ellipsoid and the binary axis which is approximately constant over the evolution of the system (Escala et al 2004, 2005). From this Lagrangian we derive the Euler-Lagrange equation for the coordinate $\phi$,

$$\begin{aligned} \frac{dl_{\rm bin}}{dt} &= \mu\frac{d}{dt}\left(r^2\frac{d\phi}{dt}\right) \\ &= -\pi r^2\,\mu\,\rho\,G\,(\beta_0 - \alpha_0)\cos(\Delta\phi)\sin(\Delta\phi)\,, \end{aligned} \tag{3.3}$$

This equation expresses the decrease of the angular momentum of the binary $l_{bin}$ and therefore, the injection of angular momentum (torque) from the binary to the disk.

To derive a criterion for the opening of a gap in the disk we compare the gap-opening time scale (determined by the torque that the binary exchange over the disk) with the gap-closing time scales (Goldreich & Tremaine 1980). The angular momentum $\Delta L$ that must be added to the gas to open a gap of radius $\Delta r$ in a disk with thickness h, is of the order of $\Delta L \approx \rho\,(\Delta r)^2\,h\,r\,v$. The torque that the binary exchange over the disk is $\tau = -{\rm dl_{bin}/dt} = {\rm r^2\rho\,\mu\,G\,\pi\,(\beta_0 - \alpha_0)\,\cos(\Delta\phi)\sin(\Delta\phi)}$. This torque injects an angular momentum $\Delta L$ on a time scale $\Delta t_{\rm open} = \Delta L/\tau$ and therefore, this is the characteristic time scale to open a gap. This tendency is opposed by viscous diffusion, which fills up a gap of with $\Delta r$ on a timescale $\Delta t_{\rm close} = (\Delta r)^2/\nu$ (Goldreich & Tremaine 1980) where $\nu$ is the turbulent viscosity of the gas that can be parametrised assuming the standard $\alpha$-prescription $\nu = \alpha_{\rm ss} c_{\rm s} h$ of Shakura & Sunyaev (1973) where $\alpha_{\rm ss}$ is the dimensionless viscosity parameter and $c_{\rm s}$ is the sound speed of the gas. Gap formation occurs when $\Delta t_{\rm open} \leq \Delta t_{\rm close}$, therefore, if we assume that $c_{\rm s}/v \approx h/r$, with $v$ the circular velocity of the binary-ellipsoid system, and, based on previous numerical results (Escala et al 2004, 2005), we assume that the binary and the ellipsoid (strong non-axisymmetric perturbation) co-rotate in a circular orbit it is straightforward to find that the binary will open a gap in the disk if

$$\frac{\Delta t_{\rm open}}{\Delta t_{\rm close}} = \frac{1}{f_q}\left(\frac{c_{\rm s}}{v}\right)^3\left(\frac{v}{v_{\rm bin}}\right)^2 \leq 1\,, \tag{3.4}$$

where we define $v_{\rm bin} = (G\mu/(2r))^{1/2}$ and where $f_q = f(\Delta\phi, \alpha_0, \beta_0, \alpha_{\rm ss}) = 2\pi(\beta_0 - \alpha_0)\cos(\Delta\phi)\sin(\Delta\phi)\alpha_{\rm ss}^{-1}$ is a dimensionless function of the geometric parameters of the ellipsoid $(\alpha_0, \beta_0)$, the offset angle $\Delta\phi$ and the viscosity parameter $\alpha_{\rm ss}$. The geometric parameters of the ellipsoid are approximately constant due to the self-similar behavior of the ellipsoid (Escala et al 2004, 2005). This formulation of the gap opening criterion contains information of the relative weight of the characteristic rotational speed of the binary-disk system ($v$), with the characteristic rotational speed of the isolated binary ($v_{\rm bin}$) and the thermal state of the disk ($c_{\rm s}$).

We note that regardless of the exact geometry of the strong non-axisymmetric density perturbation, the gravitational torque from the perturbed background medium onto the binary will have the form $\tau = r^2\rho G\mu K$, where $K$ is a parameter that depends on the geometry of the density perturbation. Therefore, the dimensionless function $f_q$ has in general the form $f_q = 2K/\alpha_{\rm ss}$ that represents the relative strength between the gravitational and viscous torque.

In addition, if we assume that the binary-disk system is in rotational support against the overall gravitational potential on a circular orbit, we can also express this same criterion in terms of the disk structural parameters and the mass of the binary-disk system:

$$\frac{\Delta t_{\rm open}}{\Delta t_{\rm close}} \;=\; \frac{1}{f_q}\left(\frac{h}{r}\right)^3\left[1+8\frac{M(<r)}{M_{\rm bin}}\right] \;\leq\; 1\,, \tag{3.5}$$

where $M(<r)$ is the total mass enclosed by the orbit of the binary.

## 3.3. Initial conditions and numerical method

In this section we present the SPH simulations that we ran to study the binary-disk interaction and test our gap-opening criterion. All our simulations consist of a unequal mass binary of mass ratio $q$, initial separation $a_0$, and mass $M_{\rm bin}$ embedded on an isothermal and stable ($Q > 1$) gas disk of radius $R_{\rm disk}$ and mass $M_{\rm disk}$. The orbit of the binary is coplanar with the gaseous disk. In these simulations we use a natural system of units where [mass] = 1, [distance] = 1, and $G = 1$. In these units, we set the initial radius of the disk as $R_{\rm disk} = 30$ and the mass of the disk as $M_{\rm disk} = 30$ for all the runs.

The density of the disk is given by

$$\rho(R,z) \;=\; \frac{\Sigma_0}{2\,h_{\rm c}}\,\frac{R_0}{R_{\rm c}}\cosh^{-2}\left(\frac{z}{h_{\rm c}}\right) \qquad R \leq R_c \tag{3.6}$$

$$\;=\; \frac{\Sigma_0}{2\,h_{\rm c}}\,\frac{R_0\,R_c}{R^2}\cosh^{-2}\left(\frac{z}{h_{\rm c}}\,\frac{R_{\rm c}}{R}\right) \qquad R_c \leq R \leq R_{\rm disk}\,, \tag{3.7}$$

where $R_{\rm c} = 3$, and $h_{\rm c}$ are the radius and thickness of the central zone of the disk where the surface density is constant. With this density we obtain a surface density $\Sigma(r) = constant$ for $R < R_{\rm c}$ and $\Sigma(r) \propto R^{-1}$ if $R > R_{\rm c}$. The vertical distribution of the disk changes over

the evolution of the system, but the initial vertical distribution chosen at least prevents an initial vertical collapse on the disk.

The parameter space that we explore with our numerical simulations is determined by the variation of four parameters $a_0$, $M_{\rm bin}$, $h_{\rm c}$ and $q$, in the ranges, $a_0 \in [2, 6]$, $M_{\rm bin} \in [1, 33]$, $h_{\rm c} \in [0.8, 3]$ and $q \in [0.1, 1]$. We run 41 simulations (see table 1) with different combinations of these parameters.

In addition to the disk and the binary we include a fixed Plummer potential (Plummer 1911) that helps to stabilize the disk and also, when we apply our result on the study of SMBH binaries in sections §3.8 and §3.10, will mimic the existence of an external stellar component. The total mass of the Plummer potential inside the initial orbit of the binary is $M_{\rm p} = 0.12\, M_{\rm disk}$ and its scale radius is $R_{\rm p} = 0.638\, R_{\rm disk}$. The applicability of the gap-opening criterion derived in §2, remains valid even in the presence of this Plummer potential because its mass can be included in the total mass enclosed by the orbit of the binary $M(< r)$.

We model the gaseous disk with a collection of $2 \times 10^5$ SPH particles of gravitational softening 0.1. We use a stable ($Q \geq 1$) isothermal disk to avoid fragmentation, to simplify the testing of our analytic criterion derived in the section §2. In table 1 we tabulate the minimum value of the parameter Q of Toomre of each simulation. Since the total potential of the system (Binary-Disk-Plummer) is non-axisymmetric and therefore lacks of a well defined circular velocity, we assume initially a symmetric representation of the binary potential to compute the circular velocity of the disk (see Appendix A for details). For the binary we use 2 collisionless particles with gravitational softening of 0.1. We run each simulation for 10-15 binary orbital times using the SPH code called GADGET2 (Springel 2005, Springel et al. 2001).

In addition, to test the numerical convergence of the results, we run simulations with 1 million SPH particles and find that the conclusions found in §3.10 for our analytic gap-opening criterion do not change (Appendix B).

Table 1: Run Parameters

| RUN | $q$ | $a_0/R_{disk}$ | $M(<r)/M_{bin}$ | $(c_s/v_{bin})^2$ | $Q_{min}$ |
|---|---|---|---|---|---|
| A1 | 0.1 | 0.100 | 0.0125 | 3.110 | 2.62 |
| A2 | 0.1 | 0.133 | 0.0222 | 1.780 | 2.20 |
| A3 | 0.1 | 0.133 | 0.0133 | 2.220 | 2.20 |
| A4 | 0.1 | 0.200 | 0.0500 | 4.650 | 2.19 |
| B1 | 0.3 | 0.100 | 0.0125 | 1.037 | 2.62 |
| B2 | 0.3 | 0.133 | 0.0222 | 0.593 | 2.20 |
| B3 | 0.3 | 0.133 | 0.0133 | 0.740 | 2.20 |
| B4 | 0.3 | 0.200 | 0.0500 | 1.550 | 2.19 |
| C1 | 0.5 | 0.100 | 0.0125 | 0.622 | 2.62 |
| C2 | 0.5 | 0.133 | 0.0222 | 0.365 | 2.20 |
| C3 | 0.5 | 0.133 | 0.0133 | 0.444 | 2.20 |
| C4 | 0.5 | 0.200 | 0.0500 | 0.930 | 2.19 |
| D1 | 1.0 | 0.100 | 0.0125 | 0.311 | 2.62 |
| D2 | 1.0 | 0.133 | 0.0222 | 0.178 | 2.20 |
| D3 | 1.0 | 0.133 | 0.0133 | 0.222 | 2.20 |
| D4 | 1.0 | 0.200 | 0.0500 | 0.465 | 2.19 |
| D5 | 1.0 | 0.133 | 0.05 | 0.088 | 2.62 |
| D6 | 1.0 | 0.1 | 0.06 | 0.080 | 2.50 |
| D7 | 1.0 | 0.1 | 0.06 | 0.159 | 2.50 |
| D8 | 1.0 | 0.1 | 0.06 | 0.199 | 2.49 |
| D9 | 1.0 | 0.1 | 0.06 | 0.279 | 2.48 |
| D10 | 1.0 | 0.067 | 0.06 | 0.053 | 2.50 |
| D11 | 1.0 | 0.1 | 0.1 | 0.133 | 2.22 |
| D13 | 1.0 | 0.067 | 0.1 | 0.089 | 2.20 |
| D14 | 1.0 | 0.1 | 0.1 | 0.199 | 2.20 |
| D15 | 1.0 | 0.067 | 0.1 | 0.178 | 2.20 |
| D16 | 1.0 | 0.067 | 0.1 | 0.222 | 2.20 |
| D17 | 1.0 | 0.1 | 0.1 | 0.465 | 2.19 |
| D18 | 1.0 | 0.067 | 0.1 | 0.311 | 2.19 |
| D19 | 1.0 | 0.1 | 0.12 | 0.159 | 2.14 |
| D20 | 1.0 | 0.05 | 0.12 | 0.080 | 2.15 |
| D21 | 1.0 | 0.05 | 0.12 | 0.199 | 2.14 |
| D21 | 1.0 | 0.067 | 0.2 | 0.178 | 2.01 |
| D22 | 1.0 | 0.033 | 0.2 | 0.088 | 2.01 |
| D23 | 1.0 | 0.033 | 0.2 | 0.219 | 1.99 |
| D24 | 1.0 | 0.067 | 0.2 | 0.623 | 1.98 |
| D25 | 1.0 | 0.017 | 0.4 | 0.090 | 1.85 |
| D26 | 1.0 | 0.033 | 0.4 | 0.175 | 1.85 |
| D27 | 1.0 | 0.067 | 0.4 | 0.356 | 1.85 |
| D28 | 1.0 | 0.017 | 2.0 | 0.452 | 1.70 |
| D29 | 1.0 | 0.067 | 2.0 | 1.779 | 1.70 |

## 3.4. How to identify the simulations with gap

In order to test our analytic gap opening criterion against SPH simulations, we first need a criterion that determines numerically in which of our simulations the binary opens a gap in the disk and in which ones it does not. To determine whether a gap is opened or not, we explore the radial density profile of each simulation and the evolution of the binary separation.

If the binary opens a gap in the disk, it must have a flow of gas from the central to the outer regions of the disk. This flow produces a "pile-up" of gas on the perimeter of the gap. This type of pile-up is also expected to form on the evolution of a circumbinary disk that interacts with an unequal mass binary but in this regime ($q \ll 1$) is associated to a drop in the density of the disk and not necessarily to the formation of a gap (Kocsis et al. 2012). The pile-up formed in the evolution of our simulations ($q = 1$) is represented by a peak in the density profile and its maximum is correlated to the existence of a gap in the disk. In the figure 3.1 we show that the density plot has a peak or pile-up if the disk has a gap. For the cases that the disk doesn't have a gap, this pile-up is less prominent or doesn't exist.

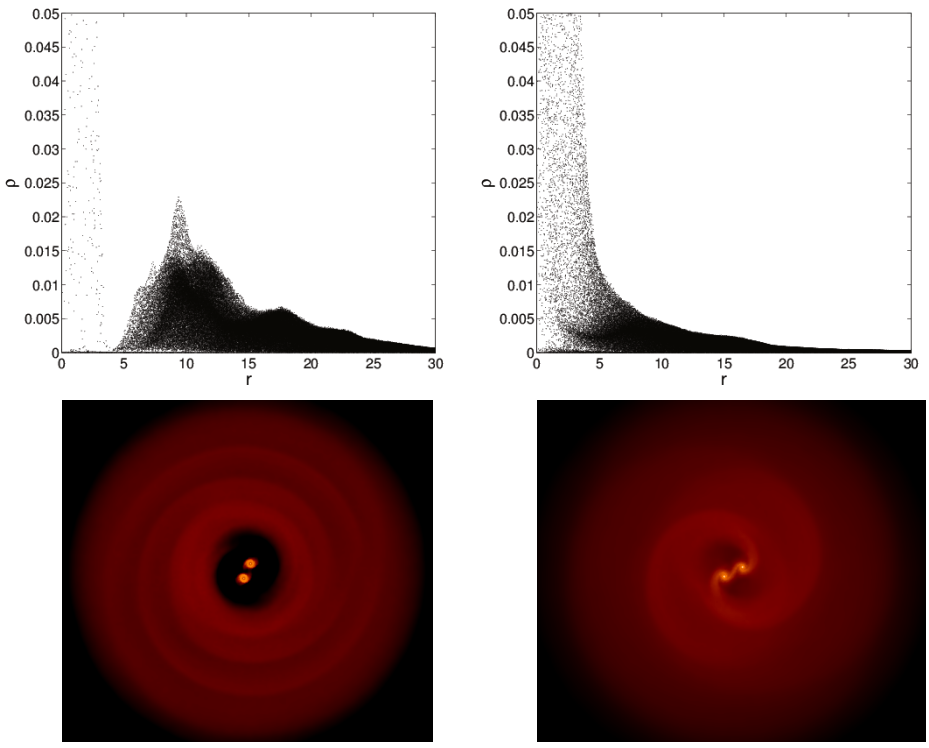


Figura 3.1: In the top: the density projection in the plane x-y of the simulation D12 (left) and D27 (right). In the bottom: The density profiles of the simulation D12 (left) and D27 (right). In this set of graphics is shown the correlation between the simulations with a gap (without a gap) and a density profile with a pile up of gas whose maximum value is $\rho_{\rm peak} > 0.015$ ($\rho_{\rm peak} < 0.015$) (see section §4)

We also explore if the gap can be identified as a drop in the azimuthal mean density.

Although in some cases the existence of a gap is correlated with a drop in the mean azimuthal density, in many other cases there are streams of gas or inner disks around individual components of the binary that hide the existence of a gap in an azimuthally averaged density plot. Therefore, we decided to use the peak in the density profile as our first indicator for the existence of a gap. In addition to this, we follow the evolution of the binary separation. The separation tell us whether the binary is migrating or not to the inner regions of the disk on a time scale comparable to its orbital time $t_{\rm orb}$, which is only possible if there is enough gas around the binary to extract efficiently the angular momentum of the binary in a orbital timescale. Therefore, a binary that is migrating to the center of the disk on a time scale $\sim$ $\rm t_{orb}$, is only consistent with a disk that does not have a gap (Type I migration).

Considering the density profile and the possible migration of the binary to the inner region of the disk, we called *opened* to a simulation in a given time $t$, if it has a peak or pill-up in density with $\rho_{\rm peak} \geq 0.015$ (in internal units) and if the binary separation do not decreases by more than 10 % in a orbit. If a simulation in a time $t$ have a maximum density of the pile up $\rho_{\rm peak} \leq 0.015$ and the binary separation decreases more than 10 % in a orbit, we called *closed*. Otherwise we called it *indefinite*.

We analyze our simulations at the times $t$ in which the binary complete 2, 3, 5, 7, 10 and 15 orbits. For all the simulations in each of these time intervals, we define it as *opened*, *closed* or *indefinite* if the gap in the disk is open, close or indefinite respectively.

## 3.5. Gap-opening criterion for equal mass binaries

### 3.5.1. Testing the gap-opening criterion

In order to test our analytic gap-opening criterion we plot the velocity parameters of the system $( \, ( \, v_{\rm bin} \, / \, v \, )^2 \, , \, ( \, c_{\rm s} \, / \, v \, )^3 \, )$. These parameters are present in one of the two equivalents gap-opening criteria (equation 3.4). In a first attempt we try to determine the values of the parameters $( \, 1 + M(< r) \, / \, M_{\rm bin} \, )^{-1}$ and $( h \, / \, r \, )^3$ that are present in the other gap-opening criterion (equation 3.5) but were poorly defined because the structural parameters of the disk (thick, radius and density profile) can vary strongly (variations on the order of 30-70 % ) in the vicinity of the binary, in time-scales shorter than the orbital time-scale of the binary, due to the local action of the gravitational potential of the components of the binary.

The velocity parameters are derived from the dynamical state of the binary which, unlike the structural parameters of the disk, have variations in times scales greater or at least comparable, to the time scale of the orbit of the binary. Therefore, to compute the structural parameters of the system we derive them from the velocity parameters. These structural and velocity parameters are related through the relations $8(M(< r)/M_{\rm bin}) + 1 = (v/v_{\rm bin})^2$ and $(h/r)^3 = (c_{\rm s}/v)^3$.

In figure 3.2, we plot two groups of simulations; the *opened* and the *closed* simulations

according to our definition. The *opened* simulations are represented by red open circles and the *closed* simulations are represented by blue filled circles. We find that the *opened* and *closed* simulations are distributed in two different regions. The interface that separates the set of simulations that are *opened* from the set of simulations that are *closed* can be modeled by a straight line (which slope is f as we will show in the next section). The linear nature of the interface indicates that the functional dependence of our gap-opening criterion on the parameters of the disk-binary system works fine, in the range of parameters that we explore. This encourages us to explore in more detail the significance of this linear interface.

An important consequence of Figure 2 is that the extension of the standard gap-opening criterion derived for the planetary regime ($q \ll 1$) to the regime $q \sim 1$ doesn't predicts the right shape of the interface line between the *opened* and *closed* simulations. For example the standard gap opening criterion in Lin & Papaloizou (1986) (Equation (4)) for the case $q = 1$ can be expressed as $(h/r)^3 \leq (1/40\alpha_{\rm ss})^{3/5}$ which corresponds to an horizontal line in Figure 2, which clearly cannot explain the distribution of *opened* and *closed* simulations in 3.2.

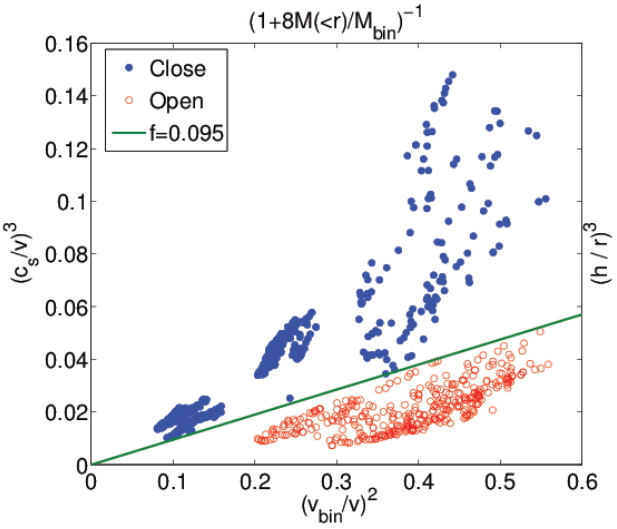


Figura 3.2: The figure shows the cubic ratio between the sound speed of the gas and the rotational velocity of the binary-disk system $(c_{\rm s}/v)^3$ plotted against the quadratic ratio between the rotational velocity of the isolated binary and the rotational velocity of the binary-disk system $(v_{\rm bin}/v)^2$. As $(v_{\rm bin}/v)^2 = (1 + 8M(< r)/M_{\rm bin})^{-1}$ and $(c_{\rm s}/v)^3 = (h/r)^3$ we also include this axis labels where $M(< r)/M_{\rm bin}$ is the enclosed to binary mass ration and $h/r$ is the ratio between the disk thickness and half the binary separation ($r = a/2$). The red circles are simulations where the binary has opened a gap in the disk (*opened* simulations) and the blue filled circles are simulations where the disk does not have a gap (*closed* simulations) (see section §4). The green line is the threshold between the *opened* simulations and the *closed* simulations that is predicted by our analytic gap-opening criterion. Below the green line are the *opened* simulations and above the line are the *closed* simulations. The slope of the interface is the function $f(\Delta\phi, \alpha_0, \beta_0, \alpha_{\rm ss})$.

### 3.5.2. Determining an average value for $f(\Delta\phi, \alpha_0, \beta_0, \alpha_{\rm ss})$

The interface-line that was shown in the previous section separates the parameter space, between the *opened* and *closed* simulations and can be interpreted as the critical case in which a simulation have equals opening and closing times (i.e $\Delta t_{open} = \Delta t_{close}$). The slope of the interface-line that separates the set of *opened* simulations from the set of *closed* simulations in the velocity variables graph (figure 3.2) is

$$m = \left(\frac{v}{v_{\rm bin}}\right)^2 \left(\frac{c_{\rm s}}{v}\right)^3 = \left(\frac{h}{r}\right)^3 \left[1 + 8\frac{M(<r)}{M_{\rm bin}}\right] . \tag{3.8}$$

We find a value for the slope of the interface-line approximately of $m = 0.095$.

From equation 3.4 for the case $\Delta t_{\rm open} = \Delta t_{\rm close}$ we can estimate that the dimensionless function $f$ that contains the information of the relative strength between the gravitational and viscous torques , is on average $f(\Delta\phi, \alpha_0, \beta_0, \alpha_{\rm ss}) = m$. Replacing this numerical value for $f$ in the equations 3.4 and 3.5 we can express the gap-opening criterion for an equal mass binary as

$$\left(\frac{v}{v_{bin}}\right)^2 \left(\frac{c_{\rm s}}{v}\right)^3 \;\leq\; 0.095\,. \tag{3.9}$$

or

$$\left(\frac{h}{r}\right)^3 \left[1 + 8\frac{M(<r)}{M_{\rm bin}}\right] \;\leq\; 0.095 \tag{3.10}$$

As $f \propto \alpha_{\rm ss}^{-1}$ any changes on the viscosity parameter $\alpha_{\rm ss}$ will change the slope of the interface-line of the figure 3.2. If we increase the value of $\alpha_{\rm ss}$ the slope will be less steep and the number of *closed* simulations will increase. This is consistent with the fact that with an increase of the viscosity it will be harder for the binary to open a gap on disk. In our simulations we can estimate $\alpha_{\rm ss}$ from the value of the SPH parameter of artificial viscosity $\alpha_{\rm sph}$ (Artymowicz & Lubow 1994, Murray 1996, Lodato & Price 2010, Taylor & Miller 2011). The value that we estimate ranges between $\alpha_{\rm ss} \approx 0.008 \sim 0.016$. However, independent to the exact value; the functional dependence of our gap-opening criterion remains unchanged.

### 3.5.3. Transition from *closed* regime to *opened* regime

Only one of our 29 simulations of equal mass binaries (simulation D15 in table 3.3) evolves from a state where the disk has no gap (*closed*) to a state where the disk has a gap (*opened*). The binary in this simulation initially migrates to the center of the disk driven by the action of the tidal torque. As the binary migrates to the center, eventually reaches a separation where the torque exerted into the disk is enough to open a gap. It is important to emphasize that this is only a particular case that already start near the *opened* region and doesn't mean that any binary as migrates to the center will be

able to open a gap. Moreover, in most cases studied, we have binaries that as migrate to the center never fulfil the condition to open a gap, because the mass ratio $M_{\rm bin}/M(<r)$ doesn't grows fast enough compared to the growth of the thickness $h/r$.

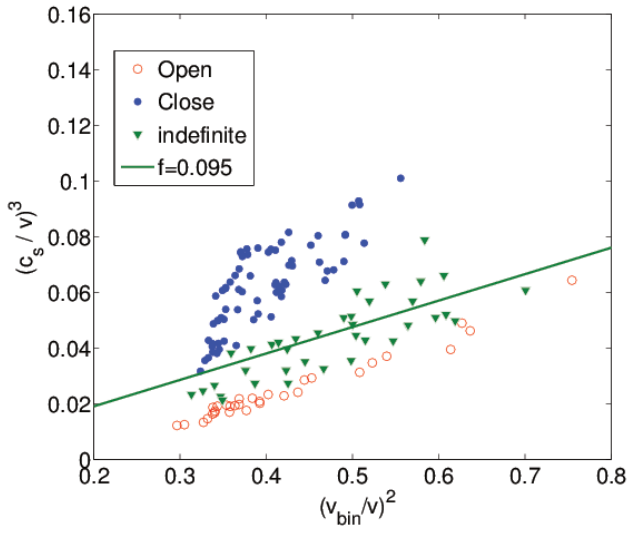


Figura 3.3: The figure shows the cubic ratio between the sound speed of the gas and the rotational velocity of the binary-disk system $(c_{\rm s}/v)^3$ plotted against the quadratic ratio between the rotational velocity of the isolated binary and the rotational velocity of the binary-disk system $(v_{\rm bin}/v)^2$. We plot three groups of points representing three groups of different regimes for a same simulation in different times (D15). The three regimes are *opened* (red open circles), *closed* (blue filled circles) and a transitory *indefinite* regime (green triangles) according to our definition (see section §4). The green line is the interface between the *opened* population of parameters (below the line) and the *closed* population of parameters (above the line). The slope of the interface is the function $f(\Delta\phi, \alpha_0, \beta_0, \alpha_{\rm ss})$. The three regimes are distributed in the plot consistently with the criterion.

It's interesting to visualize the transition of the simulation D15 between the *opened* and *closed* gap regions in the velocity parameters space $((v_{\rm bin}/v)^2, (c_{\rm s}/v)^3)$ (figure 3.3). In this plot we find that the three regimes of evolution in this simulation are distributed consistently with our criterion derived in §2, with the *closed* points above the threshold line ($f = 0.095$), the *opened* points below the threshold and the *indefinite* ones, oscillating around it.

## 3.6. Testing the gap-opening criterion for unequal mass binaries

In this section we include in our test of the gap-opening criterion the simulations of unequal mass binaries. We explore if all our *closed* and *opened* simulations of different $q$ can be well separated by the same gap-opening criterion with the same value of $f$.

In figure 3.4, we plot with open circles the simulations that we called *opened* simulations and with filled circles the *closed* simulations. In this plot, as in figure 3.2, the horizontal axis is $(v_{\rm bin}/v)^2$ and the vertical axis is $(c_{\rm s}/v)^3$. In the case of unequal mas binaries we use the secondary's orbital speed as the speed of the binary/density-perturbation system ($v$) because the strong non-axisymmetric density perturbation is formed by the gas that tends to follow the gravitational potential of the binary and therefore corotates with it.

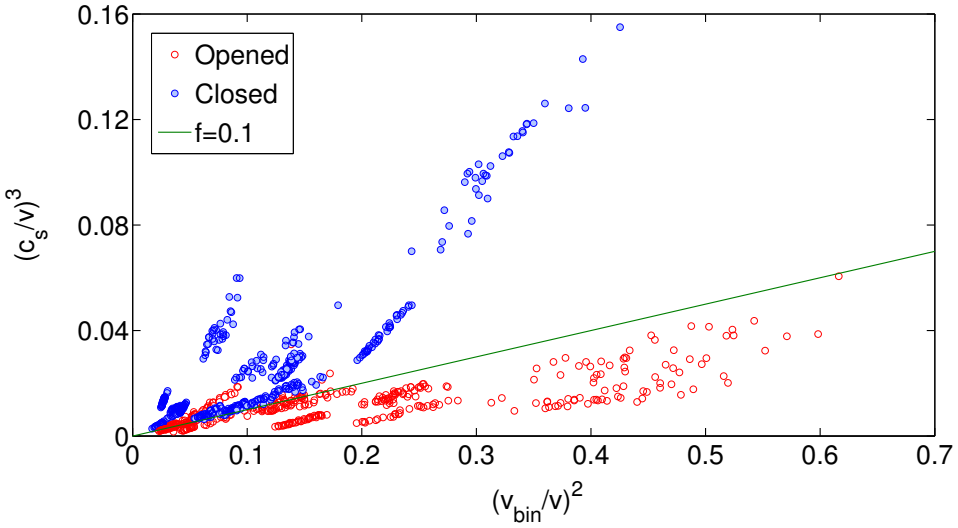


Figura 3.4: Cubic ratio between the sound speed of the gas and the rotational velocity of the binary-disk system $(c_{\rm s}/v)^3$ plotted against the quadratic ratio between the rotational velocity of the isolated binary and the rotational velocity of the binary-disk system $(v_{\rm bin}/v)^2$. The red circles are simulations where the binary has opened a gap in the disk (*opened* simulations) and the blue filled circles are simulations where the disk does not have a gap (*closed* simulations) (see section §4).We plot together all the simulations with different values of the mass ratio $q$ that we explore. The green line is the linear $q$-independent threshold between the *opened* simulations and the *closed* simulations that is predicted by our analytic gap-opening criterion. Below the green line are the *opened* simulations and above the line are the *closed* simulations. The slope of the interface is the function $f$.

We can see, from figure 3.4, that the average distribution of *opened* simulations and the average distribution of *closed* simulations populate two different regions of parameter space. As we explain in the previous section, the lower region that is populated by the *opened* simulations is the region, for which the opening time of a gap is shorter than the closing time ($\Delta t_{\rm open} < \Delta t_{\rm close}$) and the upper region, populated by the *closed* simulations, is the region for which the closing time of a gap is shorter than the opening time ($\Delta t_{\rm open} > \Delta t_{\rm close}$).

We first explore if the linear threshold can be assumed to be $q$-independent (i.e. $m_q = f$), even though the geometry of the density perturbation ($K_{\rm q}$) is expected to be $q$-dependent. This assumption implies that in figure 3.4 a line of slope $f$ will be sufficient

to model the threshold between the *opened* and *closed* simulations. We find that the slope of the line that better separate the *closed* simulations from the *opened* simulations is $m = f = 0.1$ (green line) which is very close to the value of $m$ that we found by only taking into account the simulations of equal mass binaries. Although from figure 3.4 we observe that the average distribution of *opened* simulations and the average distribution of *closed* simulation is correctly separated by one linear threshold, we find that are some simulations that are inconsistent with this threshold line. Indeed, the 17 % of the total number of simulations have positions in parameter space that are inconsistent with this $q$-independent threshold line. This discrepancy is even greater for the simulations of mass ratio $q = 0.1$ for which 40 % of the total number of them has a position in parameter space that can not be explained by this $q$-independent threshold line. This suggest that the value of $f_{\rm q}$ can not be assumed as a $q$-independent one.

As an alternative in figure 3.5 we test if a $q$-dependent slope for the threshold line is a better assumption. We separate the simulations with different values of $q$ in four different plots. In each of this four plots the axis are the same as those in figure 3.4 and we use a different slope $m_q = f_{\rm q}$ for the threshold line. We find that the values of the $q$-dependent slopes that better separates the *closed* simulations from the *opened* simulation are: $f_{q=1} = 0.095$, $f_{q=0.5} = 0.100$, $f_{q=0.3} = 0.110$ and $f_{q=0.1} = 0.180$. We found that the $q$-dependent threshold lines increases the number of simulations that are consistent with the gap-opening criterion, in comparison with the $q$-independent line.

For the case $q = 1$ (figure 3.5a), as we find in the previous section, all the simulations are well separated by this $q$-dependent linear threshold. For the other mass ratios, we find that the $q$-dependent linear threshold separates well almost all our simulations. However, there are still some simulations that are not consistent with this $q$-dependent threshold lines. These deviations are most important for the simulation with mass ratio $q = 0.1$ (figure 3.5d), but even for this extreme case, the number of simulations that deviates from the prediction of our $q$-dependent gap-opening criterion are less than 10 %. In the next section, we explore the possible causes for these deviations.

## 3.7. Deviation and their causes

In the previous section we test the analytic gap-opening criterion and found that, regardless of it simplicity, it successfully predict the distribution of *opened* and *closed* simulations in most cases. However, some simulations at certain times, have positions in the space of parameters (figure 3.5) that are inconsistent with this gap-opening criterion. For example, for $q = 0.3$ and $q = 0.1$ (3.5c and 3.5d respectively), it is clear that the linear shape of the threshold is not the best curve to explain the separation of *closed* and *opened* simulations, even if the slope of the linear threshold is not the same for all the values of $q$ that we explore. In order to explain these deviations, we focus on the approximations that we use to derive this gap-opening criterion.

In section §2, for the derivation of our analytic gap-opening criterion, we restrict the geometry of the non-axisymmetric density perturbation to an ellipsoid with a scale length

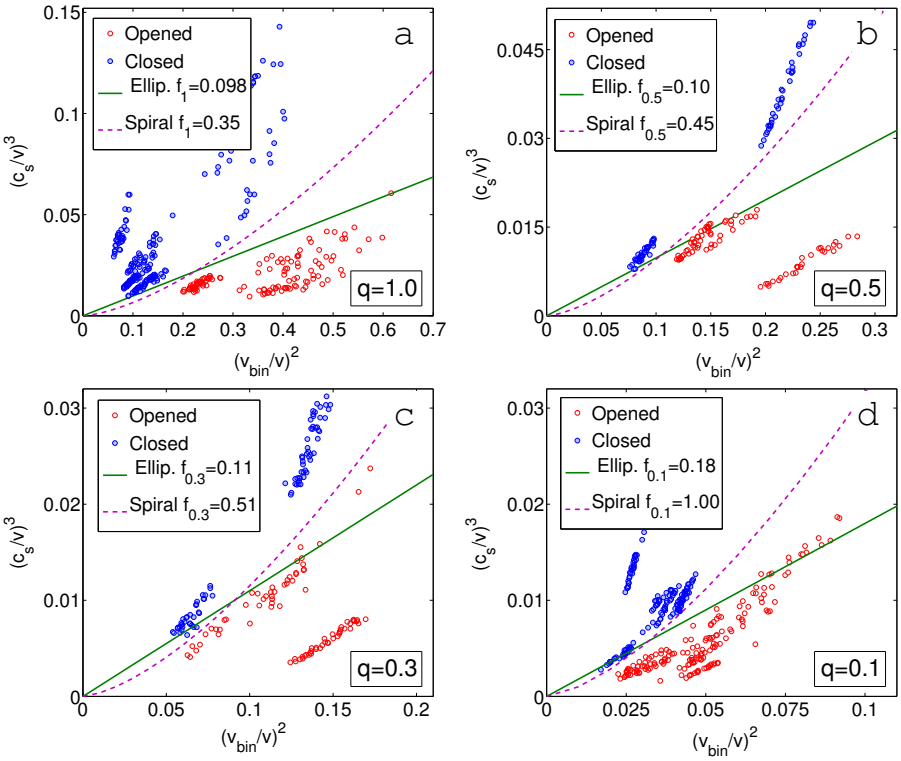


Figura 3.5: Cubic ratio between the sound speed of the gas and the rotational velocity of the binary-disk system $(c_s/v)^3$ plotted against the quadratic ratio between the rotational velocity of the isolated binary and the rotational velocity of the binary-disk system $(v_{\rm bin}/v)^2$. The red circles are simulations where the binary has opened a gap in the disk (*opened* simulations) and the blue filled circles are simulations where the disk does not have a gap (*closed* simulations) (see section §4). In all the figures the green line is the threshold between the *opened* simulations and the *closed* simulations that is predicted by our ellipsoidal gap-opening criterion. The purple dashed curve is the threshold between the *opened* simulations and the *closed* simulations that is predicted by our flat-spiral gap-opening criterion (see section §5). Below the purple dashed curve are the *opened* simulations and above the curve are the *closed* simulations. From top-left to bottom-right the figures are **2a**: Simulations with mass ratio $q = 1$. **2b**: Simulations with mass ration $q = 0.5$. **2c**: Simulations with mass ration $q = 0.3$. **2d**: Simulations with mass ration $q = 0.1$. For all figures the flat-spiral gap-opening criterion successfully separates the *closed* simulations from the *opened* simulations (purple dashed curve). In figure **2a**, for the equal mass binaries ($q = 1$), both the flat-spiral gap-opening criterion (purple dashed curve) and the ellipsoidal gap-opening criterion (green line) successfully separate the *closed* simulations from *opened* simulations.

equal to the binary separation $a$. For this ellipsoidal geometry the gravitational torque produced on the binary by the density perturbation has a quadratic dependence on the binary separation and can be expressed as $\tau = a^2 G\mu K_q$.

The assumption of an ellipsoidal geometry is based on the work of Escala et al. (2004, 2005). They found that, for the majority of the numerical simulations, the response of the gas to the gravitational potential of a binary has an ellipsoidal shape. However, the

numerical simulations of Escala et al. (2004, 2005) where the formation of such ellipsoidal density perturbation is present are far from the regime in which a gap can be formed.

In our numerical simulations, we explore the parameter space in the vicinity of the gap-forming regime and we find that the density perturbation has a spiral shape instead of an ellipsoidal one (figure 3.6). This spiral shaped density perturbations are also found by Escala et al. (2005) in two of their simulations (figure 10 and figure 12 of Escala et al. 2005), which are in the same gap-forming regime as our simulations.

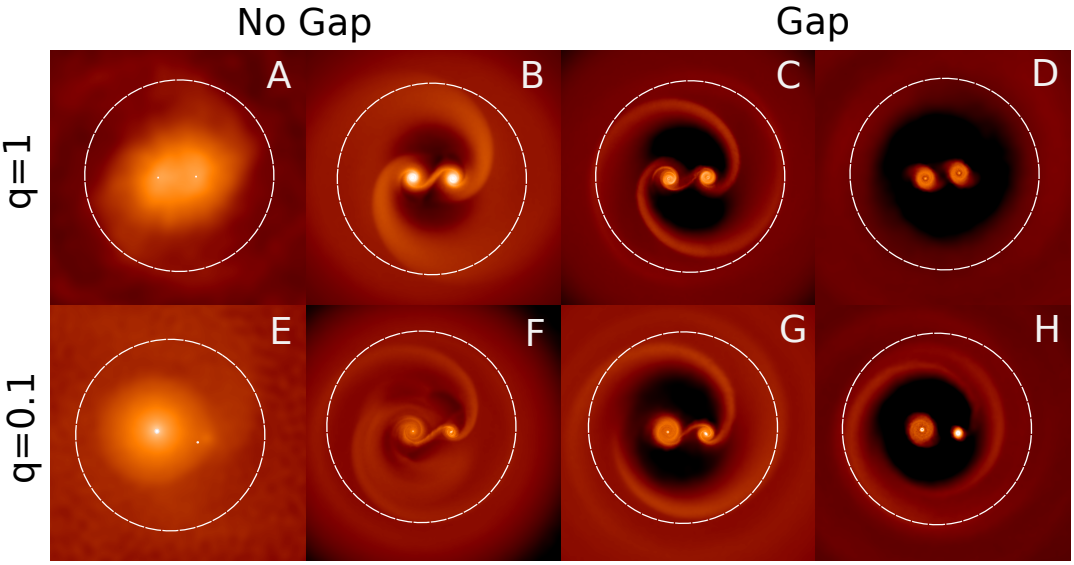


Figura 3.6: Surface density of eight simulations. The white dashed line enclose the region $r < 2a$ of the disk, with $a$ the binary separation. The figures from the top are simulations with $q = 1$. The bottom figures are simulatios with $q = 0.1$. From left to right the figures show **3.6A** and **3.6E**: binary that is far from the gap-forming regime, **3.6B** and **3.6F** binary with parameters in the vicinity of the gap-forming regime that does not form a gap on the disk, **3.6C** and **3.6G**: binary that begins to excavate a gap on the disk and, **3.6D** and **3.6H**: binary that excavate a gap on the disk. The geometry of the density perturbation is spiral for the simulations within the gap-forming regime (figures 3C, 3D, 3G and 3H ) and for the simulation in the vicinity of the gap-forming regime (figures 3B and 3F). In contrast we can see that for the simulation that is far from the gap-forming regime the density perturbation has an ellipsoidal geometry for $q = 1$ and a pear shape for $q = 0.1$ (figures 3A and 3E ).

The torque produced on the binary by such spiral shaped density perturbation will have the same quadratic dependence on the binary separation $a$, only if the vertical scale of the spiral is comparable to its radial scale (thick-spiral limit). Therefore, the torque given by $\tau \propto a^2$ that we use in the derivation of our analytic gap-opening criterion, will be valid only for the cases where the spiral density perturbation is in the thick-spiral limit.

The spiral density perturbations that are formed in our simulations tend to be more flat rather than thick, therefore the thick-spiral limit may not be valid for all simulations.

For a flat-spiral, the radial scale length of the perturbation is determined by the binary separation $a$ and, as the flat spiral pattern is embedded in the disk, its vertical scale height is truncated by the thickness of the disk ($h_{\rm spiral} \sim H_{\rm disk}$). Therefore the torque produced by this flat-spiral density perturbation can be written as $\tau_s = aH_{\rm disk}G\mu K_q$ where the product $aH_{\rm disk}$ is associated to the flat-spiral geometry.

From the torque produced by a flat-spiral geometry we derive a new gap-opening criterion following the same procedure of section §2:

$$\frac{\Delta t_{\rm open}}{\Delta t_{\rm close}} = \frac{1}{f_{\rm q}} \left(\frac{c_{\rm s}}{v}\right) \left(\frac{v}{v_{\rm bin}}\right)^2 \left(\frac{H_{\rm disk}}{a}\right) \leq 1\,. \tag{3.11}$$

To test if the assumption of a flat-spiral geometry for the density perturbation is a better approximation for our simulations, we compare the shape of the threshold between the group of *closed* and *opened* simulations that is predicted by the flat-spiral gap-opening criterion (equation 3.11 in the limit $\Delta t_{\rm open} = \Delta t_{\rm close}$) with the shape of the threshold that is predicted by the ellipsoidal criterion (equation 3.4 in the limit $\Delta t_{\rm open} = \Delta t_{\rm close}$).

Assuming for simplicity that $H_{\rm disk}/a = c_{\rm s}/v$ we compare the flat-spiral gap-opening criterion with the ellipsoidal criterion in the parameter space $(\,(v_{\rm bin}/v)^2\,,\,(c_{\rm s}/v)^3\,)$. In figure 3.5 the purple dashed lines represents the $q$-dependent thresholds between the *closed* and *opened* simulations, that is predicted by the flat-spiral gap-opening criterion. For this criterion the values of the $q$-dependent parameter $f_{\rm q}$ that better describe the threshold between the *closed* and the *opened* simulations are: $f_{q=1} = 0.35$, $f_{q=0.5} = 0.45$, $f_{q=0.3} = 0.51$ and $f_{q=0.1} = 1.00$.

This threshold has a shape that better separates the *closed* from the *opened* simulations, compared with the linear threshold predicted by the ellipsoidal gap-opening criterion. In fact, all the simulations that are not consistent with the linear threshold are consistent with the flat-spiral gap-opening criterion.

For the case of equal-mass binaries (figure 3.5a) the thresholds predicted by the flat-spiral and ellipsoidal gap opening criteria separated equally well the *closed* and *opened* simulation. In this case, the parameters of the systems that we explore are in the vicinity of the regime $a \sim H_{\rm disk}$, where the torque associated to the flat-spiral geometry ($\tau \propto aH_{\rm disk}$) and the torque associated to the ellipsoidal geometry ($\tau \propto a^2$) have comparable values making them indistinguishable. On the other hand, in our simulations, the unequal-mass binaries (figures 3.5b, 3.5c and 3.5d) are in systems where the thickness of the disk tends to be smaller than the binary separation, therefore the ellipsoidal torque and the flat-spiral torque have different values.

## 3.8. Limits for the final evolution of the binary

Now that we successfully tested our gap-opening criterion we explore the implications of this criterion for the final evolution of a shrinking binary.

The non-axisymmetric density perturbation that is formed in the disk by the presence of the binary is self-similar in nature and hence when the binary shrinks, the non-axisymmetric density perturbation also shrinks. Therefore, the gravitational interaction between the binary and the non-axisymmetric density perturbation will continue reducing the binary separation unless there is a dramatic change in the nearby gas of the binary such as the formation of a gap.

From the flat-spiral gap-opening criterion we can evaluate how likely it is that this decrease of the binary separation will lead, or not, to the formation of a gap. This is particularly important in the context of the evolution of SMBH binaries where the formation of a gap may stop the shrinking of the SMBH binary at separations where the emission of gravitational waves is not efficient enough to drive the final coalescence of the SMBH.

Assuming for simplicity a disk with a Mestel density profile we can write our flat-spiral gap opening criterion (equation 3.11) with its explicit dependence on the binary separation $a$ as

$$\left(\frac{c_{\rm s}^2 H_{\rm disk}}{G M_{\rm bin}}\right)\left(\frac{H_{\rm disk}}{q\,a}+\frac{H_{\rm disk}}{R_{\rm disk}}\frac{M_{\rm disk}}{M_{\rm bin}}\right)\;\leq\;\left(\frac{K_{\rm q}}{\alpha_{\rm ss}}\right)^2, \tag{3.12}$$

where we use the relations: $r_2 = (1+q)^{-1}a$, $\mu = qM_{\rm bin}/(1+q)^2$, $v_{\rm bin}^2 = G\mu/a$, $v^2 = G((M_{\rm gas}(r_2)/r_2) + v_{\rm bin}^2(a/r_2))$ and for a Mestel disk $M_{\rm gas}(r_2) = r_2\,M_{\rm disk}/R_{\rm disk}$.

From equation 3.12 we can see that the flat-spiral gap-opening criterion is a decreasing function of $a$ if the disk thickness $H_{\rm disk}$ is constant or does not depend strongly on $a$. In this case the decrease of the binary separation will not drive the system towards the formation of a gap. In fact, the decrease of the binary separation will drive away the binary from the regime where is possible to form a gap.

Although the assumption of a flat-spiral geometry for the density perturbation is more accurate to model the transition from *closed* to *opened* simulations, the density perturbation on a system where $a \ll H_{\rm disk}$ is expected to has an ellipsoidal geometry instead of flat-spiral geometry (for example this can be seen in the simulations of Escala et al. 2004, 2005). For this reason, we also studied the ellipsoidal gap-opening criterion. With the same relations that we used to derive the equation 3.12, we can write the ellipsoidal gap-opening criterion (equation 3.4) with its explicit dependence on $a$ as

$$\left(\frac{c_{\rm s}^2 H_{\rm disk}}{G M_{\rm bin}}\right)\left(\frac{1}{q}\left(\frac{H_{\rm disk}}{a}\right)^3+\frac{H_{\rm disk}^3}{a^2\,R_{\rm disk}}\frac{M_{\rm disk}}{M_{\rm bin}}\right)\;\leq\;\left(\frac{K_{\rm q}}{\alpha_{\rm ss}}\right)^2, \tag{3.13}$$

We can see from equation 3.13 that the ellipsoidal gap-opening criterion (like the flat-gap opening criterion) is a decreasing function of $a$ if the disk thickness is constant or does not depend strongly on $a$. Therefore, the decrease of the binary separation will not drive the system towards the formation of a gap.

In equations 3.12 and 3.13 we assume that the disk has a Mestel density profile for which the enclosed mass has the form $M_{\rm gas}(r) = M_{\rm disk}(r/R_{\rm disk})$. If we assume that the disk has a steeper density profile the enclosed mass will be a flatterfunction of $r$ or even a decreasing function of $r$. Accordingly, equations 3.12 and 3.13 will be more strongly decreasing functions of $a$. Hence, although the assumption of a Mestel density profile for the disk is not based in any expected condition of the density profile in real systems, the results and conclusions derived assuming a Mestel density profile are also valid for any other steeper profiles.

It is important to note that when $a \ll H_{\rm disk}$, we can assume that the disk thickness does not depend on the binary separation because at scales much greater than the binary separation, the binary gravitational potential looks like the gravitational potential of a single object of mass $M_{\rm bin}$. Moreover, the thickness of the disk will be determined by the total mass of the binary+disk and the thermal state of the disk. Therefore, we can conclude that for systems where a gap has never formed, the decrease of the binary separation to the limiting case $a \ll H_{\rm disk}$ will not lead to the formation of a gap.

From this analysis we can conclude that in a large variety of systems a gap will never be opend/formed unless some other process (other than the formation of a gap due to the binary/density-perturbation gravitational interaction) change the distribution of the nearby gas of the binary. This supports the idea that it is likely that the gas will drive the shrinking of the separation of SMBHs binaries down to scales where the gravitational wave emission is efficient enough to allow their subsequent coalescence.

## 3.9. Comparison with previous studies

To improve the robustness of our study in figure 3.7 we plot the parameters $M(< r)\,/\,M_{\rm bin}$ and $h\,/\,r$ (being $r = a/2$ with $a$ the binary separation) for our simulations with $q = 1$ and some *close* and *opened* simulations from the literature (Artymowicz & Lubow 1994; Artymowicz & Lubow 1996; Escala et al. 2005; MacFadyen & Milosavljevic 2008; Cuadra et al. 2009). In this figure we also plot the interface-curve ($\Delta t_{\rm open} = \Delta t_{\rm close}$) that for this space of parameters has an inverse-cubic form. For the cases of simulations with non-self gravitating disks (Artymowicz & Lubow 1994; Artymowicz & Lubow 1996; MacFadyen & Milosavljevic 2008) we assume $M(< r)/M_{\rm bin} = 0$. In all the *opened* simulations that we find in the literature the disk begins with a gap ($M(< r_0)/M_{\rm bin} = 0$) or have a much smaller mass than the binary, but we dont find any simulation where the formation of a gap is studied for a massive disks ($M(< r_0)/M_{\rm bin} > 1$). In figure 3.7 we can see that the simulations in which the disk begins with a gap, or it's open in the evolution of the simulation, (red open points I, II and III) are below the interface curve, consistent with the gap-opening criterion. The *closed* simulations (squares in figure 3.7) represent the final evolution of simulation that begins with initial condition as the used by Escala et al. 2005 and Dotti et al. 2006. These simulations are above the interface line and are also consistent with the gap opening criterion. Therefore all the simulations from papers that we refer from the literature are consistent with the gap-opening criterion independently of the different equations of state that are used for the disks.

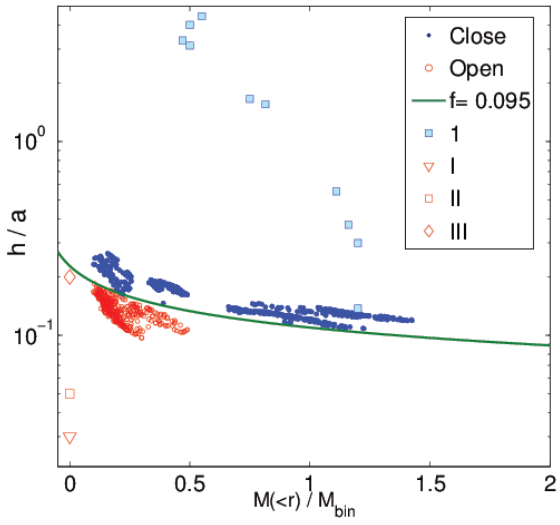


Figura 3.7: The ratio between disk thickness and binary separation ($h/a$) plotted against the enclosed to binary mass ratio ($M(< r)/M_{bin}$), for the simulations with a gap in the disk (open red circles) and without gap in the disk (blue filled circles). The continuous green curve represent the interface of this two populations of parameters (f = 0.095). The other points in the figure, are simulations already in the literature: Escala et al. 2005 (1), Artymowicz & Lubow 1994 (I), Artymowicz & Lubow 1994 and MacFadyen & Milosavljevic 2008 (II), Cuadra et al. 2009 (III). The points with arabic number labels, are simulations where the disk don't have a gap and the points with roman number labels are simulations where the disk have a gap. All the points are consistent with our analytic gap-opening criterion. The qualitative behavior predicted by the opening criterion is reproduced in this graph, as $h/a$ decreases, the binary-disk interaction tends to open a gap. Also if we decreases $M(< r)/M_{bin}$, the interaction tends to open a gap again.

## 3.10. Discussion and conclusions

In simulations of comparable mass binaries ($q \sim 1$) embedded in gas disks, the time scale for the shrinking of the binary separation can be of the order of a few orbital times (fast migration regime eg; Escala et al. 2004, 2005; Dotti et al. 2006) or of the order of a thousand orbital times (slow migration regime eg; Artymowicz & Lubow 1994; Ianov et al. 1999; Armitage & Natarajan 2002; Milosavljvic & Phinney 2005; Cuadra et al. 2009). The threshold between the fast and slow migration regime for comparable mass binaries, as in the planet migration case (extreme mass ratio binaries $q \ll 1$), is determined by the formation of a gap in the disk. Terefore, in this work, we test a gap-opening criterion that will enable us to estimate in what systems a fast or slow migration will proceed.

In the case of an equal mass binary Escala et al. (2004, 2005) found that, the exchange of angular momentum between the binary and a gaseous disk is driven by the gravitational interaction between the binary and a strong non-axysimmetric density perturbation with an ellipsoidal geometry. Considering this gravitational interaction we derived an

"ellipsoidal" gap-opening criterion and we successfully tested this criterion against 29 SPH simulations of equal mass binaries embedded in gaseous disks.

We study if this ellipsoidal gap-opening criterion is also valid for binaries with moderate mass ratio ($0.1 \leq q < 1$). For this purpose we ran 12 SPH simulations of binaries with moderate mass ratio embedded in gas disks and we tested the validity of the analytic ellipsoidal gap-opening criterion against these numerical simulations.

We find that the analytic ellipsoidal gap-opening criterion (equation 3.4), successfully predicts that the simulations where a gap is formed (*opened* simulations) and the simulations where there is no gap on the disk (*closed* simulations) are in average distributed in two separate regions in the parameter space ($(v_{\rm bin}/v)^2$ v/s $(c_{\rm s}/v)^3$) (see figure 3.4).

However, there are some simulations, at certain times, with positions in this parameter space that are inconsistent with the ellipsoidal gap-opening criterion (see figure 3.5). These deviations are most important for the case of binaries with mass ratio $q = 0.1$ where roughly the 9 % are inconsistent with the ellipsoidal gap-opening criterion.

In our simulations, we find that the strong non-axysimmetric density perturbation has a flat-spiral geometry, instead of the ellipsoidal geometry that we use to derive the ellipsoidal gap-opening criterion (see figure 3.6). Therefore, we derive a new gap-opening criterion using a flat-spiral geometry for the density perturbation. We find that, this flat-spiral gap-opening criterion (equation 3.11) is $q$-dependent and successfully separates the *closed* simulations from the *opened* simulation. In fact, all the simulations that we explore are consistent with this flat-spiral gap-opening criterion (see figure 3.5), including the roughly 9 % of simulations with mass ratio $q = 0.1$ that are inconsistent with the ellipsoidal gap-opening criterion.

The difference between the geometry of the density perturbation that we found in our simulations and the geometry of the density perturbation found in the simulations of Escala et al. (2004, 2005) is the result of the different regimes that these two types of simulations explore. In our simulations we explore the vicinity of the gap-forming regime while the simulations of Escala et al. (2004, 2005) are in general far from the gap-forming regime.

Far from the gap-forming regime the gravitational torque that the binary produces on the disk is efficiently absorbed and dissipated through the disk ($\Delta t_{\rm close} \ll \Delta t_{\rm open}$). Therefore, in such regime the gas corotates with the binary in a quasi equilibrium configuration and its structure follows the geometry of the gravitational equipotentials of the binary, which for $q = 1$ has an ellipsoidal shape. On the other hand, our simulations have parameters in the vicinity of the gap-forming regime ($\Delta t_{\rm open} \sim \Delta t_{\rm close}$) for which the angular momentum deposited in the gas, through the gravitational torque exerted by the binary, is not efficiently dissipated through the disk and a radial flow of gas is produced. In this non-equilibrium state the density perturbation takes a spiral shape, like the one observed in our simulations within the gap-forming regime (see figure 3.6) and in others simulations from the literature in the gap-forming regime (Hayasaki et al. 2008, Roedig et al. 2012 ,Shi et al. 2012).

Regardless of the exact geometry of the density perturbation, in the variety of simulations that study the interaction of a comparable mass binary with a gas disk, the torque produced over the binary comes from the same inner region of the disk. For example, for simulations where the density perturbation has an ellipsoidal shape the exchange of angular momentum between the disk and the binary comes from the gravitational interaction between the binary and the ellipsoidal density perturbation which is formed in the region of the disk $r \leq 2a$ (as shown in the figure 3.6A and by the simulations of Escala et al. 2004, 2005). In the simulations where the binary excavates a gap on the disk the gravitational torque also comes mainly from the inner region $r \leq 2a$ and is associated to the gravitational interaction between the binary and transitory streams of gas falling toward the gap region (Roedig et al. 2012, Shi et al. 2012). This can be seen directly from figure 5 of Shi et al. 2012 and figure 9 of Roedig et al. 2012 where they show the surface torque density on the disk associated to the transitory streams of gas. In our simulations the non-axisymetric density perturbation is also formed in the inner region $r \leq 2a$. This can be seen in figure 3.6 were we show for eight simulations the inner region $r \leq 2a$ enclosed by a white dashed circle.

From our successfully tested gap-opening criterion, we evaluate if the decrease of the binary separation will lead to the formation of a gap. We find that, for a binary embedded in a gas disk with a Mestel density profile (or any steeper density profile) as the binary separation decreases ($a \ll H_{\rm disk}$) the exchange of angular momentum between the binary and the non-axisymetric density perturbation will not lead to the formation of a gap. Then the fast decay of the binary will continue unless some other process changes the distribution of the nearby gas to the binary.

It is important to note that, in the flat-spiral gap-opening criterion (equation 3.11) and the ellipsoidal gap-opening criterion (equation 3.4), the difficulty that a binary has to open a gap in a disk increases with larger values of the dimensionless viscosity parameter $\alpha_{\rm ss}$ of Shakura & Sunyaev (1973). For our SPH simulations we estimate that $\alpha_{\rm ss} \approx 0.008 - 0.016$ from the value of the SPH parameter of artificial viscosity $\alpha_{\rm sph}$ (Artimowicz & Lubow 1994; Murray 1996; Lodato & Price 2012; Taylor & Miller 2012). In massive nuclear disks the gas will be globally unstable and therefore the torques will be larger, with an $\alpha_{\rm ss}$ of order unity (Krumholz et al. 2007, Escala et al. 2007). Moreover, from magnetohydrodynamic (MHD) simulations studies find that the presence of MHD stresses can significantly increase the torques, with an effective dimensionless viscosity parameter $\alpha \geq 0.2$ (Shi et al. 2012), a factor of $\geq 20$ greater than the estimate value of $\alpha_{\rm ss}$ in our SPH simulations.

From these estimates, we expect that the value of $\alpha_{\rm ss}$ in real gas-rich astrophysical systems, like the nuclear disk in ULRIGs (Downes & Solomon 1998) and Sub-millimeter Galaxies (Chapman et al. 2003, 2005; Takoni et al. 2006; Swinbank et al. 2010), will be one or two orders of magnitude greater than in our simulations. Therefore, in the nuclear region of the gas-rich merging galaxies, it is more likely that a SMBH binary will not be able to excavate a gap on the gas, allowing the gravitational torques from the gas to shrink the SMBH binary separation down to scales where gravitational wave emission can drive the final coalescence of the binary.

# Appendix A: Initial Conditions

In our set of simulations, the binary produces a strong non-axisymmetric component to the total gravitational field. Therefore, for the SPH particles near the binary there is not a well defined circular velocity $v(r)$. This is an inherent problem for the initialization of this type of simulations and we chose to solve this by approximating the binary potential by an spherical mass distribution with the same total mass, for computing the initial circular velocity. These spherical representations allow us to compute an initial circular velocity for all the particles of the disk, but the system will not start in a perfect equilibrium.

We probe different spherical mass distributions to study the effect of the initial velocity on the evolution of the system and then we select the mass distribution that produce the minor overestimation or underestimation of the equilibrium velocity. The spherical mass distributions that we study are: (1) spherical shell (2) point mass distribution and (3) sphere of constant density. The spherical shell (1) produces a discontinuity on the velocity that generates a ring-shaped gap due to an overestimation of the velocity in the region where the gap forms. The point mass distribution (2) overestimates the velocity for all the particles in the region $r < r_0$ because in this region the real enclosed mass is less than the mass that is assume by the point mass distribution. This overestimation opens an artificial gap in the center of the disk. The sphere of constant density (3) also generates an overestimation of the velocity in the region $r < r_0$ but this overestimation is less intense than the overestimation due to the point mass distribution, because, for the homogeneous sphere, the enclosed mass decreases with radius.

We select the sphere of constant density as the spherical mass distribution for computing the initial velocity, because approximates better the potential of the binary and the system starts closer to a rotationally supported equilibrium. The system is of course not in a perfect equilibrium and our approximation for the initial circular velocity leads to an initial readjustment of the density profile in about an orbital time. For that reason, we only analyze the simulations after 2 initial orbits of the binary, that is, after the system has relaxed into an quasi-equilibrium configuration.

We also include a static Plummer potential to increase the stability of the disk. This static potential decrease the overestimation of the rotational velocity in the inner region of the disk reducing the initial loses of gas in this region and the artificial formation of a gap. In the edges of the disk the cutoff of the disk produces a pressure gradient that drives the expansion of the disk edges. This flow of gas is also reduced due to the gravitational influence of this static potential. We use an static Plummer potential that have a total mass of 12 % the mass of the disk and its core radius is roughly at $0.6\,R_{\rm disk}$. With this selection of parameters the Plummer potential's mass initially enclosed by the orbit of the binary is %50 the total enclosed mass.

# Appendix B: Resolution Study

Our results are derived from the comparison of an analytic criterion for gap-opening against SPH numerical simulations. In the simulations presented in section §3, the disk is represented by a collection of $2 \times 10^5$ SPH particles. In order to check that we have the resolution required and that our results do not depend on that, we run four additional simulations with different numbers of SPH particles; $5 \times 10^5$, $8 \times 10^5$ and two with $10^6$.

Although, the evolution of the orbital parameters of the binary are not exactly the same for high and low resolution simulations, the global structure of the disk remain practically almost unchanged. The region of parameters that the low and high resolution simulations covers, in the velocity spaces of parameters, is very similar (figure 3.8) and the classification of these simulations (as *closed* or *opened*) remain the same. For the initial condition that we run with $2 \times 10^2$, $5 \times 10^5$, $8 \times 10^5$ and $10^6$ we find that the values of the velocity parameters converge with resolution (figure 3.9).

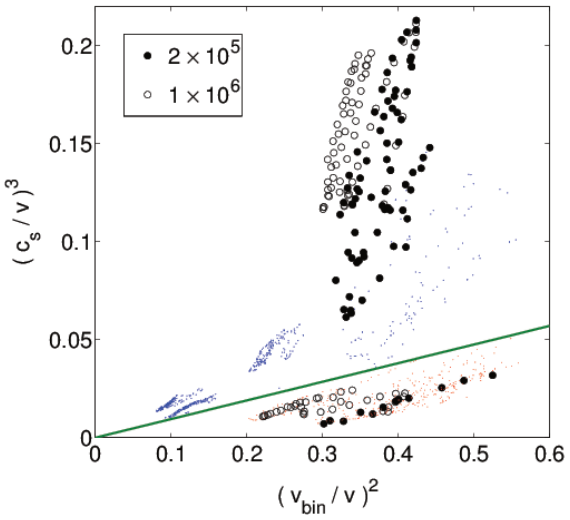


Figura 3.8: The cubic ratio between the sound speed of the gas and the rotational velocity of the binary-disk system, $(c_s/v)^2$ plotted against the quadratic ratio between the rotational velocity of the isolated binary and the rotational velocity of the binary-disk system $(v_{\rm bin}/v)^2$. The black dots are runs with $2 \times 10^5$ SPH particles and the black open circles are runs with $1 \times 10^6$ SPH particles. Also we plot all our others simulations with red (*opened* simulations) and blue (*closed* simulations) points for comparison. The green line is the interface between this two populations of parameters that is predicted by our analytic gap-opening criterion. The slope of the interface is the function $f(\Delta\phi, \alpha_0, \beta_0, \alpha_{\rm ss})$. The two simulations above (below) the green curve with $2 \times 10^5$ and $1 \times 10^6$ SPH particles are simulations with the same initial condition. Although, the evolution of the orbital parameters of the binary are not exactly the same for high and low resolution simulations, the global structure of the disk remain almost unchanged and the region of parameters that the low and high resolution simulations covers is very similar. The classification of these simulations (as *closed* or *opened*) remain the same for high and low resolution.

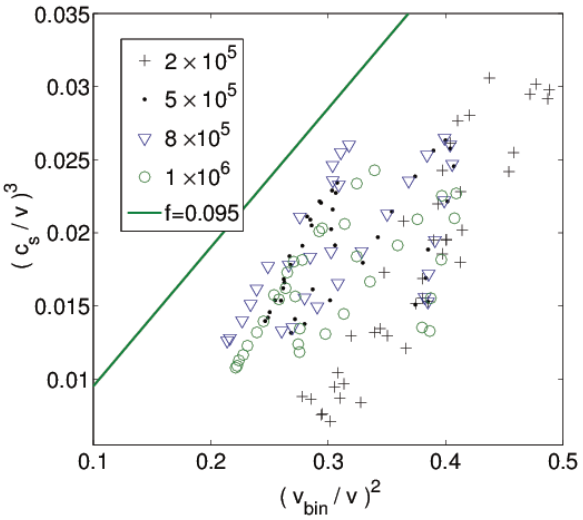


Figura 3.9: The cubic ratio between the sound speed of the gas and the rotational velocity of the binary-disk system, $(c_{\rm s}/v)^2$ plotted against the quadratic ratio between the rotational velocity of the isolated binary and the rotational velocity of the binary-disk system $(v_{\rm bin}/v)^2$. In this figure we plot four simulations with the same initial condition but different number of SPH particles: $2 \times 10^5$, $5 \times 10^5$, $8 \times 10^5$ and $1 \times 10^6$. The green line is the interface between the simulations where a gap is opened in the disk (*opened*) and the simulations where the disk dont have a gap (*closed*). Although, the evolution of the orbital parameters of the binary are not exactly the same for high and low resolution simulations, the global structure of the disk remain almost unchanged and the region of parameters that the low and high resolution simulations covers is very similar. The classification of these simulations *opened* remain the same for high and low resolution.

For the high resolution simulations we find a small shift to higher values of $(c_{\rm s}/v)^3$. This shift can change the value of the slope of the threshold between the *closed* and the *opened* simulations ($f$) in a $\%10$ or less. Therefore, the overall conclusions for the testing of our analytic gap-opening criterion against SPH simulations remain unchanged.

# Capítulo 4

# Super massive black holes in star forming gaseous circumnuclear discs

Originally published by del Valle, Escala, Maureira-Fredes, Molina, Cuadra & Amaro-Seoane, 2015, *The Astrophysical Journal*, **811**, 59

Using $N-$body/SPH simulations we study the evolution of the separation of a pair of SMBHs embedded in a star forming circumnuclear disk (CND[1]). This type of disk is expected to be formed in the central kilo parsec of the remnant of gas-rich galaxy mergers. Our simulations indicate that orbital decay of the SMBHs occurs more quickly when the mean density of the CND is higher, due to increased dynamical friction. However, in simulations where the CND is fragmented in high density gaseous clumps (clumpy CND), the orbits of the SMBHs are erratically perturbed by the gravitational interaction with these clumps, delaying, in some cases, the orbital decay of the SMBHs. The densities of these gaseous clumps in our simulations and in recent studies of clumpy CNDs are two orders of magnitude higher than the observed density of molecular clouds in isolated galaxies or ULIRGs, thus, we expect that SMBH orbits are perturbed less in real CNDs than in the simulated CNDs of this study and other recent studies. We also find that the migration timescale has a weak dependence on the star formation rate of the CND. Furthermore, the migration timescale of a SMBH pair in a star-forming clumpy CND is at most a factor three longer than the migration timescale of a pair of SMBHs in a CND modeled with more simple gas physics. Therefore, we estimate that the migration timescale of the SMBHs in a clumpy CND is on the order of $10^7$ yrs.

## 4.1. Introduction

In the context of hierarchical structure formation (White & Frenk 1991; Springel et al. 2005b) galaxies are sculpted by a sequence of mergers and accretion events. In the early evolution of these mergers, the cores of each galaxy will sink to the central region of the new system, until they coalesce forming a new virialized core. During the migration

[1]Here we use the terminology of gaseous circumnuclear discs (CND) to make reference to massive gaseous disks with sizes of the order of one kilo parsec and not to the collection of gas and dust clouds in the galactic centre of the milky way.

of the cores, the massive black holes (MBHs) that are expected to live at the central region of every galaxy (Richstone et al. 1998; Magorrian et al. 1998; Gultekin et al. 2009; Kormendy & Ho 2013) will follow the center of each core.

If the galaxies that are involved in this merger are rich in gas, numerical simulations show that 60 to 90 % of this gas can fall to the central kilo parsec of the remnant (Barnes & Hernquist 1996; Mihos & Hernquist 1996; Barnes 2002; Mayer et al. 2007, 2010). This is consistent with observations of gas-rich interacting galaxies, where it is often found that the amount of gas contained in their central regions is comparable with the total gas content of a large gas-rich galaxy (Sanders & Mirabel 1996; Downes & Solomon 1998; Medling et al. 2014; Ueda et al. 2014) Both numerical simulations and observations suggest that this gas often settles in a disk-like distribution, or circumnuclear disk (CND).

Several authors have performed numerical simulations studying the evolution of MBHs after a galaxy merger. In these simulations, a pair of MBHs is embedded in a gaseous CND. Most studies indicate that the pair of MBHs dissipate angular momentum into the ambient gas, which drives the formation of an MBH binary and the subsequent orbital decay of this binary down to separations on the order of $\sim 1 - 0.1$ pc. The timescale for this process is on the order of $10^7$ Myr (Escala et al. 2005; Dotti et al. 2006; Fiacconi et al. 2013) In some cases, the viscous torque of the gas is not strong enough to dissipate the angular momentum extracted from the MBH binary and the gas is forced to move away from the binary (del Valle & Escala 2012, 2014). In these cases, the MBH binary is left inside a cavity of low gas density, and dissipation of its angular momentum into its environment is less effective. As a result, the migration timescale of such systems can be longer than the Hubble time (Lodato et al. 2009; Cuadra et al. 2009). In each of these studies, it is assumed that the gas follows a simple polytropic equation of state and that the CND evolves without star formation.

More recent simulations of the evolution of MBH pairs in galaxy mergers include the effects of star formation, supernovae, and cooling (Hopkins & Quataert 2010; Callegariet al. 2011; Van Wassenhove et al. 2012; Roskar et al. 2014). These studies explore how the morphology of the galaxies, their gas fraction, and the geometry of the merger can affect the accretion and orbital evolution of the MBH pair. However, in these studies, the star formation rates and supernovae feedback are fixed in order to reproduce observed relations, such as the Kennicutt-Schmidt relation (Kennicutt 1998). Little attention has been given to how different efficiencies or intensities of these processes can affect the orbital evolution of an MBH pair after a galaxy merger.

In this work we investigate the evolution of two MBHs embedded in a CND and, for the first time, we explore how different star formation rates can result in different migration timescales of the MBH pair. In section §2 we describe the code used in our simulations, and how we model star formation, cooling, and supernovae heating. In section §3 we show how the MBHs' separation evolves for different star formation rates. In section §4 we compute the gravitational torque exerted by the gas on the SMBHs, and we show that high density gas, in the form of clumps, is the primary source of this torque. In section §5 we compare the mass and density of these gas clumps to observations. We also discuss some features missing from our simulations that are crucial to properly modeling

these clumps and obtaining densities in better agreement with observation. Finally, in section §6 we summarize the main results of our work and their implications on the orbital evolution of MBHs after a galaxy merger.

## 4.2. Code and simulation setup

### 4.2.1. Code

To compute the evolution of the SMBHs embedded in the CND, we use the code `Gadget-3` (Springel et al. 2001; Springel 2005). This code evolves the system by computing gravitational forces with a hierarchical tree algorithm, and it represents fluids by means of smoothed particle hydrodynamics (SPH; e.g.Monaghan1992).

The SPH technique have problems with resolving some hydrodynamical instabilities, such as Kelvin-Helmholtz or Rayleigh-Taylor instability, due to the generation of spurious forces on particles that are in regions with steep gradients of density (Agertz et al.2007; MckNally, Lyra & Passy 2012). Resolve these instabilities is important to model processes such as star formation and the generation of turbulence in the ISM. These instabilities are better resolved by codes that use an Eulerian grid based technique such as AMR. However, in these codes the orbit of massive particles experiences strong, spurious perturbations making massive particles to follow unphysical orbits. For this reason, Eulerian grid based codes are not suitable to study the orbital evolution of SMBHs embedded in a gaseous CND (Lupi, Haardt & Dotti 2014 and reference therein) and we choose to use SPH rather than a Eulerian grid based code.

To study how the formation of stars in a gaseous circumnuclear disk (CND) can affect the orbital evolution of a pair of SMBHs embedded in the CND, we created recipes for star formation, gas cooling, and heating due to supernovae and implemented these recipes in the `Gadget-3` code. Our recipes have certain key differences from those included in `Gadget-3`. In particular, in our recipes the gas can reach lower temperatures, star formation does not depend exclusively on gas density, and we do not assume the stellar feedback to be instantaneous. The recipes we implement resemble those of Stinson et al. (2006) used in the SPH code Gasoline (Wadsley et al. 2004), and those of Saitoh et al. (2008, 2010) used in simulations of isolated galaxies and galaxy mergers.

In our implementation, the cooling function is computed for an optically thin gas with solar metallicity. For temperatures between $10^{4.8}$ and $10^{8}$ K we compute the cooling essentially as described by Katz et al. (1996), and for temperature below $10^{4.8}$ K we extend the cooling functions down to 10 K using the parametrization of (Gerritsen & Icke 1997).

To model star formation, we examine every SPH gas particle and select those that, for some time step $\Delta t$, satisfy the following three criteria:

$$n_{\rm H} > n_{\rm min} \tag{4.1}$$

$$\vec{\nabla} \cdot \vec{v} < 0 \tag{4.2}$$

$$T < T_{\rm max}, \tag{4.3}$$

where is $n_{\rm H}$ the number density, $T$ the temperature, and $\vec{v}$ the velocity. $n_{\rm min}$ and $T_{\rm max}$ are parameters fixed before each simulation (they are described in section §2.2.). The gas particles selected in this way are treat as candidates for star formation.

For each gas particle that satisfies these criteria, we compute the probability $p$ of giving birth to a star of mass $m_\star$ (this mass is fixed throughout the simulation) as

$$p = \frac{m_{\rm gas}}{m_\star} \left(1 - e^{-\frac{C_\star \Delta t}{t_{\rm form}}}\right), \tag{4.4}$$

where $m_{\rm gas}$ is the mass of the gas particle, $C_\star$ is the constant that controls the star formation efficiency, and $t_{\rm form}$ is the star formation timescale, computed as the maximum of the cooling time $t_{\rm cool} = \rho\,\epsilon\,/n_H\,\Lambda(T)$ and the dynamical time $t_{\rm dyn} = (\mathrm{G}\,\rho)^{-1/2}$. Finally, for each star-formation-eligible gas particle, we draw a random number $r$ between zero and one. If $r < p$ a new star particle of mass $m_\star$ is spawned and the new mass of the parent gas particle is computed as: $m_{\rm gas,old} - m_\star$.

We assume that every newly formed star particle is a Single Stellar Population (SSP) with a three piece power law initial mass function (IMF) as defined in Miller & Scalo (1979). From this IMF, and the parametrization of Raiteri et al. (1996) for stellar lifetimes, we compute the number of type II supernovae (SNII) events that occur in each SSP as a function of time. Then we assume that for each of these SNII events the star particle deposits $10^{51}$ ergs of energy into the closest 32 gas particles. We do not include any heating by supernovae type Ia, because the typical time of integration of our simulations is 30 Myr and the SNIa timescale is on the order of 1 Gyr.

### 4.2.2. Simulation Setup

In order to model the pair of SMBHs embedded in a CND, we use the same initial conditions as Escala et al. (2005). In these initial conditions, the ratio between the mass of gas and the mass of stars in the CND is consistent with the mean value obtained from observations of the nuclear region of ULIRGs (Downes & Solomon 1998; Medling et al. 2014; Ueda et al. 2014). However, the radial extent of the CND is comparable to the radial extent of the smallest and more concentrated observed nuclear disks.

Initially, the CND follows a Mestel superficial density profile and has a mass $M_{\rm disk} = 5 \times 10^9\,M_\odot$. The radius of the CND is $R_{\rm disc} = 400$ pc and its thickness is $H_{\rm disk} = 40$ pc. The CND is modeled with 235331 SPH particles, each with a gravitational softening of 4 pc and a mass of $2.13 \times 10^4\,M_\odot$.

The stellar component is initially distributed in a spherical bulge. It follows a Plummer density profile having core radius 200 pc and mass within $r = 400$ pc $M_{\rm bulge}(r <$

$400\,\mathrm{pc}) = 5\,M_{\mathrm{disc}}$. This stellar bulge is modeled with $10^5$ collisionless particles with a gravitational softening of 4 pc and a mass of $2.45 \times 10^5\,M_\odot$.

The black hole pair is modeled by two collisionless particles of mass $M_{\mathrm{BH}} = 5{\times}10^7 M_\odot$. These particles are initially symmetric about the center of the disk, in circular orbits of radius 200 pc. The orbital plane is the plane of the disk.

For our recipe of star formation we need to set four free parameters: (1) the star formation efficiency $C_\star$, (2) the minimum density of gas required for star formation to occur $n_{\mathrm{min}}$, (3) the maximum temperature a gas particle that can give birth to a star may have $T_{\mathrm{max}}$, and (4) the mass of the newly formed star $m_\star$.

In order to resolve the formation of a clumpy multiphase medium, we assume a high star formation density threshold $n_{\mathrm{min}} = 10^4\,\mathrm{cm}^{-3}$, and a low star formation temperature threshold $T_{\mathrm{max}} = 10^3$ K (Stinson et al. 2006; Ceverino & Klypin 2009). We set the mass of the star particles as half of the original mass of the gas particles. Only the parameter $C_\star$ is varied from between simulations to obtain different star formations rates. However, we restrict our selection of $C_\star$ to values that reproduce an average star formation rate that is consistent with the empirical Kennicutt-Schmidt relation (Kennicutt 1998). In figure 4.1, we show the surface gas density and star formation rate (SFR) obtained for different values of $C_\star$, and compare this to the observed relation. The values of the parameter $C_\star$ that we use are 0.005, 0.015, 0.05, 0.15, and 0.5 (in table 5.1 these are the runs C0005, C0015, C005, C015 and C05 respectively). We also plot 4.1B the time evolution of the gas mass of the disk and the mass on new stars for the five different values of $C_\star$.

In order to see how the resolution of the gravitational forces affects the simulations, we ran ten simulations using lower gravitational softening for the black holes. In five of these simulations we set $\epsilon_{\mathrm{BH}} = 0.04$ pc and in the other five we set $\epsilon_{\mathrm{BH}} = 0.004$ pc. We label these runs with the suffixes "_$\epsilon$.04" and "_$\epsilon$.004", respectively.

We also ran two additional simulations to compare orbital evolution using our star formation recipe to orbital evolution with different recipes. In the first additional simulation, we used the hybrid multiphase model for star formation implemented in `Gadget-3` (Springel & Hernquist 2003; Springel et al. 2005a). This model assumes that the star formation is self-regulated and is parameterized only by the star formation timescale $t_0^*$. We use the typical value for this parameter, $t_0^* = 2.1$, which provides a good fit to the Kennicutt law (see figure 4.1). The other simulation (run E05) uses more idealized gas physics. There is no star formation and the gas follows an adiabatic equation of state. This simulation corresponds to the `run A` of (Escala et al. 2005).

All the simulations that we run are summarized in table 5.1.

Tabla 4.1: List of simulations and their parameters

| **Label** | **Code** | **SF** | $T_{\rm f}$ **[K]** | $C_\star$ | $\epsilon_{\rm BH}$ **[pc]** |
|---|---|---|---|---|---|
| C05 | G3 Mod. | yes | 25 | 0.5 | 4 |
| C015 | G3 Mod. | yes | 25 | 0.15 | 4 |
| C005 | G3 Mod. | yes | 25 | 0.05 | 4 |
| C0015 | G3 Mod. | yes | 25 | 0.015 | 4 |
| C0005 | G3 Mod. | yes | 25 | 0.005 | 4 |
| C05_$\epsilon$.04 | G3 Mod. | yes | 25 | 0.5 | 0.04 |
| C015_$\epsilon$.04 | G3 Mod. | yes | 25 | 0.15 | 0.04 |
| C005_$\epsilon$.04 | G3 Mod. | yes | 25 | 0.05 | 0.04 |
| C0015_$\epsilon$.04 | G3 Mod. | yes | 25 | 0.015 | 0.04 |
| C0005_$\epsilon$.04 | G3 Mod. | yes | 25 | 0.005 | 0.04 |
| C05_$\epsilon$.004 | G3 Mod. | yes | 25 | 0.5 | 0.004 |
| C015_$\epsilon$.004 | G3 Mod. | yes | 25 | 0.15 | 0.004 |
| C005_$\epsilon$.004 | G3 Mod. | yes | 25 | 0.05 | 0.004 |
| C0015_$\epsilon$.004 | G3 Mod. | yes | 25 | 0.015 | 0.004 |
| C0005_$\epsilon$.004 | G3 Mod. | yes | 25 | 0.005 | 0.004 |
| SDH05 | G3 | yes | $10^4$ | 0.05 | 4 |
| E05 | G1 | no | - | - | 4 |

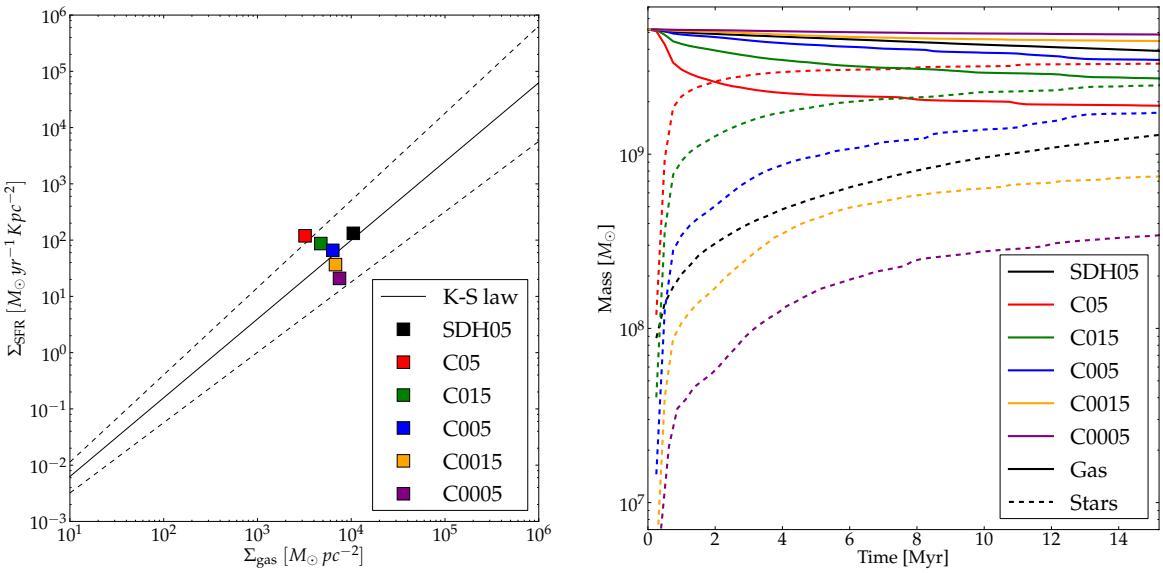


Figura 4.1: Left Panel: Correlation between disk-averaged SFR per unit area and average gas surface density. The continuous line corresponds to the best fit of the correlation for 61 normal spiral galaxies and 36 infrared-selected star-bust galaxies obtained by (Kennicutt 1998). The dashed lines delimit the scatter of the observational relation obtained by (Kennicutt 1998). Right Panel: Time evolution of the mass of gas (continuous curves) and stars (dashed curves) for six simulations. The black lines corresponds to a simulation using `Gadget-3`'s hybrid multiphase model for star formation. The colored continuous lines correspond to simulations using our implementation of star formation, feedback and cooling for five different values of the star formation efficiency $C_\star$ that appears in equation 4.4.

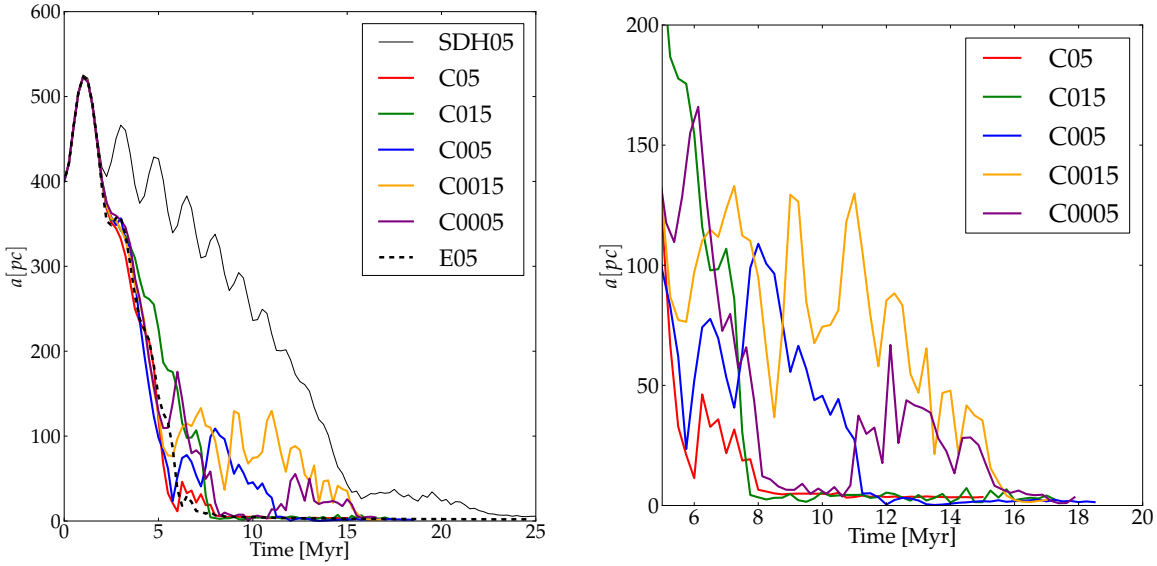


Figura 4.2: Left panel: Time evolution of the SMBHs' separation for seven different simulations. The black continuous line corresponds to a simulation using `Gadget-3`'s hybrid multiphase model for star formation. The black dashed line corresponds to the `run A` of the idealized simulations of Escala et al. (2005). The colored continuous lines correspond to simulations using our implementation of star formation, feedback and cooling for five different values of the star formation efficiency $C_\star$ that appears in equation 4.4. Right Panel: Zoom of figure left panel. In this figure it can be seen that the time it takes for the SMBHs to stabilize at a separation comparable to the gravitational softening is shorter for higher values of $C_\star$.

## 4.3. Evolution of the SMBHs separation

### 4.3.1. The evolution in our simulations

In figure 4.2 we show the time evolution of the SMBHs' separation $a$ for seven simulations. Five of these runs use our prescription for star formation, feedback and cooling. The values of the star formation efficiency $C_\star$ (see equation 4.4) used in these runs are 0.005, 0.015, 0.05, 0.15 and 0.5, which in figure 4.2 correspond to the purple, yellow, blue, green, and red continuous lines respectively. The black continuous line corresponds to a simulation using `Gadget-3`'s hybrid multiphase model for star formation (SDH05). The black dashed line corresponds to `run A` of Escala et al. (2005) (E05), which uses idealized gas physics and does not consider star formation.

From figure 4.2 we see that the time it takes for the SMBHs to reach a separation comparable to the gravitational softening is in the range of 7 to 25 Myr. The fastest migration time corresponds to the SMBHs in the E05 run (black dashed line) and the slowest migration corresponds to the SMBHs in the SDH05 run (black continuous line). In the simulations with our prescriptions, the SMBHs reach this separation at a time between these two limits.

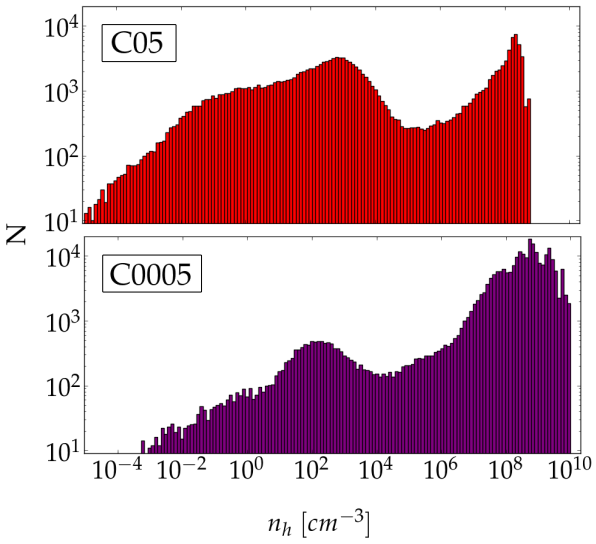


Figura 4.3: Gas density histogram at $t = 10$ Myr for two different values of $C_\star$. Note that for higher values of $C_\star$ the gas shows a more prominent low density phase. Also note that the maximum density of the gas is lower for higher values of $C_\star$.

In figure 4.2B we show a zoom of figure 4.2 for times larger than 5 Myr. Here we see that the time it takes for the SMBHs to stabilize at a separation comparable with the gravitational softening is shorter for higher values of $C_\star$. These times are 8, 7.9, 11.6, 16, and 17.2 Myr for runs C0005, C0015, C005, C015, and C05 respectively (see table 5.1). Also we found that in the two simulations with highest star formation efficiency, there are no large fluctuations in the SMBHs separation after $t = 8$ Myr.

From figures 4.2 and 4.2B, we concluded that orbital decay of the SMBH pair occurs over a timescale at most $\sim 2.4$ times longer in simulations using our recipes than in simulations using more idealized gas physics (E05).

It is important to note that in our simulations the orbital decay timescale varies by a factor of $\sim 2.1$ while the star formation efficiency extends over two orders of magnitude. So the orbital decay timescale in our simulations has a weak dependence on star formation efficiency.

The effect produced by $C_\star$ on the orbital decay of the SMBH pair should be expected because the orbital evolution of the pair depends on the torques produced by the gas, and the structure of the gas is sculpted by the star formation, cooling, and SNII heating. In the next section we explore this issue, computing the gas distribution of the CND for different star formation efficiencies.

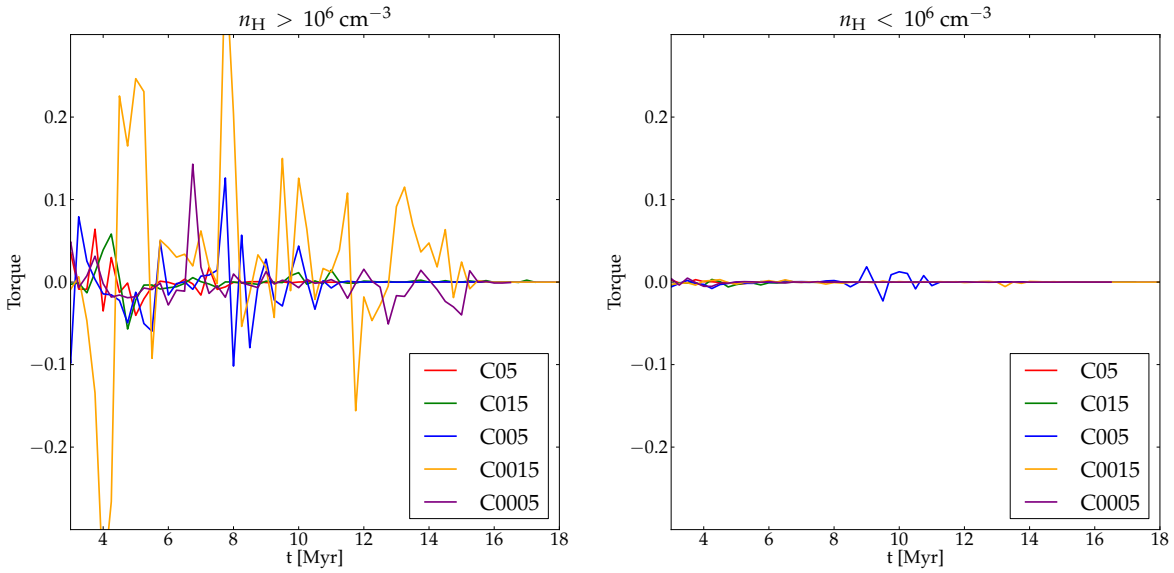


Figura 4.4: Torque experienced by the SMBHs due to gas with density above $10^6$ cm$^{-3}$ (left panel) a below $10^6$ cm$^{-3}$ (right panel). The lines of different colours represent simulations with for different values of $C_\star$. From this figure we see that practically all the gravitational torque is produced by gas with density higher than $10^6$ cm$^{-3}$.

### 4.3.2. Effect of the gas distribution on the orbital decay

In figure 4.3 we show the density distribution of the gas at $t = 10$ Myr for two different values of $C_\star$. From this figure, we find that for higher values of $C_\star$ a greater proportion of the gas has a low density and the maximum gas density is lower. This is because with more vigorous star formation, high density gas is more efficiently converted into stars. With a greater number of stars, there is a greater number of supernovae explosions, which heat the cold dense gas around the stars and drive the formation of a hot diffuse medium.

The torques the gas exerts on the SMBHs are density dependent, and we expect that most of the torque experienced by the SMBHs is due to high density gas. From figure 4.3, we would expect that in simulations with smaller values of $C_\star$, where the portion of high density gas is greater, the torque of the gas on the SMBHs is more intense and the in-spiral of the SMBHs faster. However, left panel of figure 4.4 shows that the torque produced by gas with a density greater than $10^6$ cm$^{-3}$ fluctuates repeatedly about zero, indicating that the high density gas does not always extract angular momentum from the SMBHs, but also deposits angular momentum into the SMBHs. This is consistent with the large fluctuations that we observe on the separation of the SMBHs in figure 4.2. For completeness, we plot in right panel of figure 4.4 the torque produced by gas less dense than $10^6$ cm$^{-3}$. It is clear from this figure that the effect of the low density gas on the orbits of the SMBHs is negligible.

The fluctuations of the torque exerted by the high density gas on the SMBHs may be the result of the spatial distribution of this gas in the disk. To explore this, we show the distribution of gas with densities greater than $10^6$ cm$^{-3}$ in the plane of the disk at $t =$

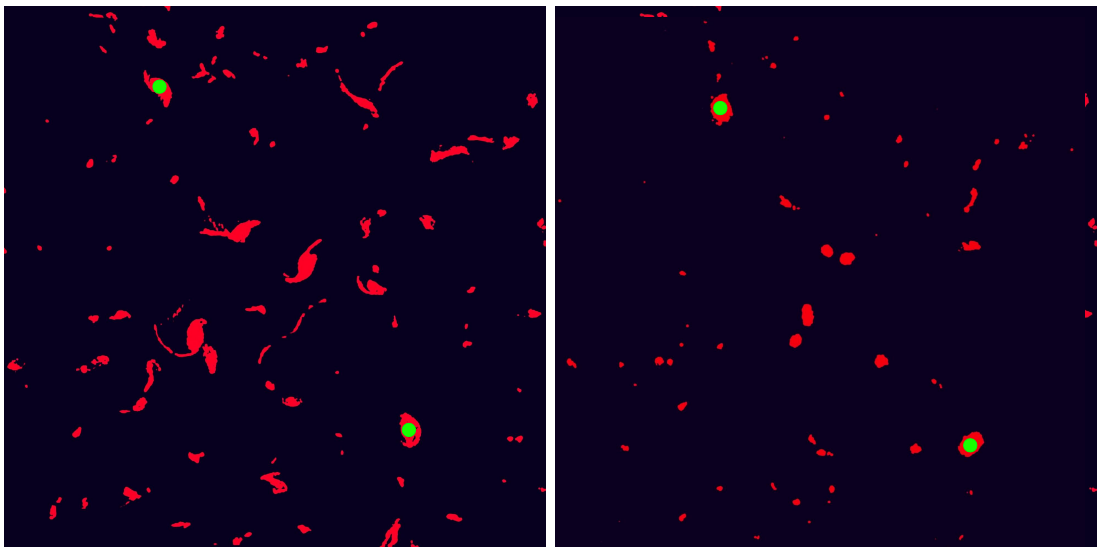

Figura 4.5: Distribution of gas in the plane of the disk at $t =$ 10 Myr for C0005 (left panel) and C05 (right panel). We only show the gas with density greater than $10^6$ cm$^{-3}$. The green circles are the two black holes.

Tabla 4.2: Gas clumps number and densities.

| $C_\star$ | $N_{\rm cl,t1}$ | $N_{\rm cl,t2}$ | $N_{\rm cl,t3}$ | $\Delta n_{\rm cl}$ [cm$^{-3}$] | $\bar{n_{\rm cl}}$ [cm$^{-3}$] |
|---|---|---|---|---|---|
| 0.005 | 86 | 44 | 38 | $10^6 - 10^{8.7}$ | $10^{7.6}$ |
| 0.015 | 84 | 39 | 25 | $10^6 - 10^{9.3}$ | $10^{7.9}$ |
| 0.05 | 87 | 32 | 19 | $10^6 - 10^{8.6}$ | $10^{7.7}$ |
| 0.15 | 70 | 27 | 15 | $10^6 - 10^{8.8}$ | $10^{7.9}$ |
| 0.5 | 37 | 16 | 9 | $10^6 - 10^{8.0}$ | $10^{7.1}$ |

$N_{\rm cl,t1}$ corresponds to the number of clumps at $t1$ =5 Myr, $N_{\rm cl,t2}$ corresponds to the number of clumps at $t2$ =10 Myr, and $N_{\rm cl,t3}$ corresponds to the number of clumps at $t3$ =15 Myr. $\Delta n_{\rm cl}$ corresponds to the range of densities of the clumps and $\bar{n_{\rm cl}}$ to the mean density of the clumps.

10 Myr for run C0005 in figure 4.5 and for run C05 in figure 4.5B. From these figures, we find that gas with density greater than $10^6$ cm$^{-3}$ is mainly concentrated in clumps, two of which surround the two black holes. In this clumpy CND, the SMBHs have encounters with these high density gaseous clumps, and depending on the characteristics of the encounter, they gain or lose angular momentum. This is reflected in the fluctuations of the gravitational torque produced by the high density gas on the SMBHs (figure 4.4).

From figures 4.5 and 4.5B, it seems that the main difference between run C0005 and run C05 is the number of clumps formed. This difference may be the cause of the different numbers of fluctuations in the SMBHs' separation seen in these runs, and the slightly different migration timescale of the SMBHs. Simulations with lower SFR yield a greater number of gaseous clumps, so it is more probable for the SMBHs to closely interact with one or more clumps in these simulations.

In order to determine if the number of clumps depends on and $C_\star$, we compute the number of clumps ($N_{\rm cl}$) as the number of groups of gas particles that are gravitational bound with central density greater than $10^6$ cm$^{-3}$. We compute $N_{\rm cl}$ at three different times– 5, 10, and 15 Myr– for each value of $C_\star$ explored. We also compute the mean density and the range of densities of these clumps. We summarize this information in table 2.

From table 2 we found that the number of clumps decreases as $C_\star$ increases. This is consistent with figure 4.3, where we found that higher SFR correspond to a lower proportion of high density gas. Therefore, in simulations with lower $C_\star$, the SMBHs are prone to interact with a higher number of gaseous clumps. This is reflected in the slight increase in fluctuations of both the separation and the gravitational torque experienced by the SMBHs that we observe in simulations with higher SFR.

Having explained in this section why the orbital decay timescale changes with $C_\star$ in simulations using our recipe, in the next section we analyze why the orbital decay of the SMBHs in these simulations is faster than in simulation SDH05 and typically slower than in simulation E05.

## 4.4. Gas physics and its effect on orbital decay

Before the SMBHs form a binary, the gas extracts angular momentum from the SMBHs through dynamical friction, which leads to the in-spiral of the SMBHs toward the center of the disk. As the intensity of the dynamical friction is proportional to the density of the gas, in a disk where the gas density is higher, the orbital decay of the SMBHs is faster (Chandrasekhar 1943; Ostriker 1999; Kim & Kim 2007).

In figure 4.6 we show the mean density of the gas around the SMBHs for the simulations E05, SDH05, and C005. The mean is taken over all gas particles within twice the gravitational influence radius (bound radius) of the SMBH: $R_{\rm bound} = 2GM_{\rm BH}/(c_{\rm s}^2 + v_{\rm rel}^2)$, where $c_{\rm s}$ is the sounds speed of the gas and $v_{\rm rel}$ is its velocity relative to the SMBH. We choose this region around each SMBH because most of the torque experienced by the SMBH comes from gas particles in this region.

As seen in figure 4.6, our recipes yield far greater gas density than the recipes used in simulation SDH05. This is because our recipes produce a greater density threshold for star formation than the threshold of simulation SDH05. Additionally, the temperature floor for star formation is much lower using our recipes (25 K in ours, as compared to $10^4$ K in SDH05). As a result, the orbital decay of the SMBHs in simulations using our recipes is faster than in simulation SDH05.

Figure 4.6 also shows that the density of the gas in simulations with our recipes is much greater than in simulation E05. However, after $t \sim 6$ Myr, in some of the simulations with our recipes, the migration of the SMBHs slows. This is because in the simulations with our recipes, the CND is fragmented in a few tens of high density gaseous clumps and these gaseous clumps erratically perturb the orbits of the SMBHs. So even though in these simulations the density is higher than in simulation E05, the orbital decay of the

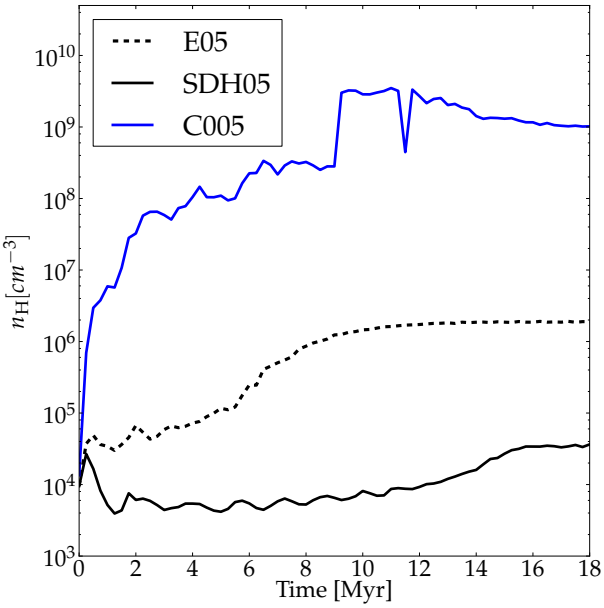


Figura 4.6: Mean density of the gas around the SMBHs as a function of time for simulations E05, SDH05, and C0005. The mean is taken over all gas particles within twice the gravitational influence radius of the SMBH.

SMBHs is, in some cases, delayed due to the interaction of the SMBHs with these gaseous clumps. The CND of simulation E05 is smoother than the CND in simulations with our recipes, and there are no high density gaseous clumps in it to perturb the SMBHs orbits.

In the next section we investigate whether these perturbations are likely to affect the evolution of SMBHs in real CNDs by comparing properties of the clumps in our simulations to observations.

## 4.5. Gaseous clumps

### 4.5.1. Density of the gaseous clumps.

As seen in section §3.2, the stochastic fluctuations of the SMBHs' separation comes from gravitational interaction between the black holes and high density gas clumps ($n_{\rm h} > 10^6 {\rm cm}^{-3}$). However, these fluctuations are unlikely to occur in real CNDs because intensity of the gravitational torques is density dependent, and the densities of the gas clumps in our simulations are higher than the densities of gas clumps in observed CNDs. For example, if we compare our clumps' densities with the density of molecular clouds in isolated galaxies (Mathis 1990; Oka et al. 2001; Struve & Conway 2010) or ultra luminous infrared galaxies (Downes & Solomon 1998; Schulz et al. 2007), which are typically $\sim 10^2 - 10^5 {\rm cm}^{-3}$, we find that the density of the clumps in our simulations is at least two orders of magnitude greater. Inside the molecular clouds, there are star forming regions (cold or hot cores) with densities comparable to the mean density of the clumps in our

simulations ($< n_{\rm h} > \sim 10^7 {\rm cm}^{-3}$). However, they are one or two orders of magnitude less dense than roughly half of the gas clumps in our simulations ($n_{\rm h} \sim 10^6 - 10^{9.3} {\rm cm}^{-3}$). Even though one of the gas clumps that perturbs the SMBH orbits may have a density comparable with the density of these cores, the mass of these cores is on the order of $\sim 10^3\, M_\odot$ (Garay et al. 2004; Muñoz et al. 2007), which is at least two orders of magnitude smaller than the mass of any of the clumps in our simulations.

The clumps in our simulations have these extremely high densities because our recipes do not account for all of the physical processes that sculpt the clumps. For example, in our simulations we use a cooling that assumes that the gas is optically thin while the clumps in our simulations are optically thick ($\tau >> 1$). Also, there is a large amount of energy that we are not considering in our simulations, such as the energy of photons emitted by the stars and by the black hole's accretion disk. The effects of turbulence, which is typically damped in SPH codes, are also omitted. All these physical processes will prevent the further collapse of the clumps, promoting the formation of clumps with lower (and hence more realistic) densities.

### 4.5.2. Force resolution and the SMBH-clump interaction.

The high densities of the gaseous clumps can affect the orbits of the SMBHs in a spurious way. The gravitational pull at the edge of these clumps can be greater than the gravitational pull at the "edge" of the SMBHs in our simulations, where we define the edge of an SMBH to be its gravitational softening. We define the effective mass density of our black holes ($\rho_{\rm BH}$) to be the mass of the black hole ($M_{\rm BH}$) enclosed within a sphere of radius equal to the gravitational softening of the black holes ($\epsilon_{\rm BH}$), i.e. $\rho_{\rm BH} = 3\, M_{\rm BH}/(4\pi\epsilon_{\rm BH}^3)$. We can compare $\rho_{\rm BH}$ with the mass density of the gaseous clumps ($\rho_{\rm cl} = m_{\rm H}\, n_{\rm cl}$) to determine if, in our simulations, the clumps are more compact than the black holes. For a gravitational softening of 4 pc, we find that $\rho_{\rm BH} = 3.8 m_{\rm H} \times 10^6 {\rm cm}^{-3}$. Hence, in our simulations the density of the gaseous clumps is greater than the effective mass density of the black holes. This implies that the gravitational pull at the edge of the black holes ($F_{\rm BH}(\epsilon) \propto \epsilon\rho_{\rm BH}$) is typically smaller than the gravitational pull at the edge of the clumps ($F_{\rm cl}(R_{\rm cl}) \propto R_{\rm cl}\,\rho_{\rm cl} = 4 - 5\,\epsilon\,\rho_{\rm cl}$). Indeed, considering a gravitational softening of 4 pc, and the minimum and maximum densities of the gaseous clumps in our simulations, $F_{\rm BH}(\epsilon)/F_{\rm cl}(R_{\rm cl}) \sim 0.04$ - 10. Therefore, a black hole sees the clumps as point masses, and it is not able to disrupt them when it has a close encounter with one of them, within a distance $\lesssim 4$ pc. Instead, in our simulations a close encounter within this distance will result in the scattering of the black hole.

If we decrease $\epsilon_{\rm BH}$, we would expect the higher resolution of the black hole's gravitational force to allow the black hole to disrupt a clump in a close encounter, where the minimum distance is $\lesssim 4$ pc. To illustrate how decreasing $\epsilon_{\rm BH}$ affects the outcome of close encounters, we show how an encounter proceeds for different values of $\epsilon_{\rm BH}$ in the bottom two rows of figure 4.8. Snapshots farther right in this figure correspond to later times. The first row of this figure shows a different encounter– one that illustrates scattering of the SMBH. In the middle row (run C0015_$\epsilon$.004), we see that the SMBH's gravitational potential disrupts the clump, and the SMBH does not scatter significantly. On the other hand, in the lower row (run C0015) where $\epsilon_{\rm BH}$ is larger, the black hole is not

able to disrupt the clump. The orbit of the SMBH is perturbed and the gaseous clump is scattered.

If these close encounters, where the minimum distance between the black hole and the clump is $\lesssim 4$ pc, are the primary source of large fluctuations in the separation of the black holes, then we expect decreasing $\epsilon_{\rm BH}$ sufficiently would cause these fluctuations to disappear. More precisely, we expect the large fluctuations to disappear once $F_{\rm BH}(\epsilon)/F_{\rm cl}(\epsilon) > 1$ for all clumps in the simulation.

In figures 4.8 we show the evolution of the SMBHs' separation for different values of $\epsilon_{\rm BH}$. The smallest value that we choose for $\epsilon_{\rm BH}$ is still much greater than the Schwarzschild radius of the black holes in our simulations ($R_{\rm sch} = 4.78 \times 10^{-6}$ pc). We note that, as we change $\epsilon_{\rm BH}$, the orbits of the black holes change. So, in simulations with the same SFR but different $\epsilon_{\rm BH}$, the black holes don't have close encounters with the same gaseous clumps. We found that in three of our simulations (runs C0015_$\epsilon$.004, C005_$\epsilon$.004, and C05_$\epsilon$.004), making $\epsilon_{\rm BH}$ smaller causes the large fluctuations to disappear. As expected, the better resolution of the gravitational force of the black holes in these simulations allows them to disrupt the clumps in all close encounters. In contrast, we found that in the runs C0005_$\epsilon$.004 and C015_$\epsilon$.004, some large fluctuations in the separation of the pair occurred (see peaks enclosed by red circles in figures 4.8 and 4.8D) that are even larger than the fluctuations observed in the simulations with the same SFR, but larger $\epsilon_{\rm BH}$ (runs C0005 and C015). We analyzed each of these large fluctuations to determine why they are present even when the black hole's gravitational force is resolved down to scales of 0.004 pc, where $F_{\rm BH}(\epsilon_{\rm BH})$ is larger.

In the case of run C0005_$\epsilon$.004, we identify two large fluctuations (enclosed by red circles in figure 4.8). In figure 4.9, we show the evolution of the orbits of the black holes during these two large fluctuations. The upper row of figure 4.9 shows the orbits of the black holes during the first of these large fluctuations, and the lower row of figure4.9 shows the second of these large fluctuations. We found that these two large fluctuations occurred because the black holes follow orbits of different radius and eccentricity, but with respect to nearly the same center, which is located close to the densest and most massive gas clump of the simulation ($n_{\rm cl} = 7.4 \times 10^8 {\rm cm}^{-3}$ and $M_{\rm cl} = 8.8 \times 10^8\ M_\odot$). Therefore, the large fluctuations in run C0005_$\epsilon$.004 are not the result of close encounters with high density clumps. Instead they are the result of the movement of the black holes which, at the moment of these fluctuations, are not bound together.

Run C015_$\epsilon$.004 also has two large fluctuations in the separation of the black holes (enclosed by red circles in figure 4.8D). We show the evolution of the orbit of the black holes during these two large fluctuations in figure 4.10. From the upper row of figure 4.10, we found that the first large fluctuation is the result of scattering of one of the black holes due to gravitational interaction with a high density gas clump. This gas clump had in turn been ejected from a past scattering with another high density gas clump. In the lower row of figure 4.10, we see that the second large fluctuation is the result of scattering with the same gas clump responsible of the first large fluctuation. Both of these close encounters have a minimum distance which is greater than 10 pc, and therefore they are not artificially produced by low resolution of the gravitational force of the black holes.

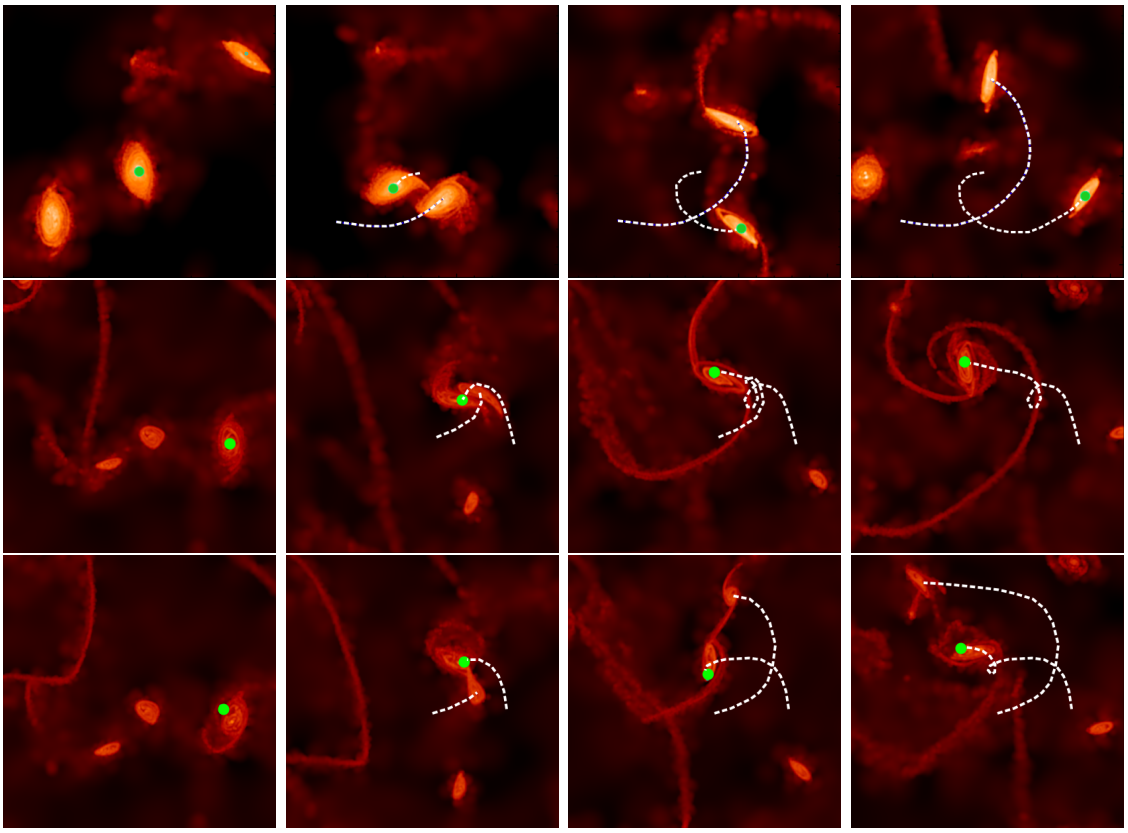

Figura 4.7: Distribution of gas in the plane of the disk. Time of the snapshots increases from left to right. The figures show the interaction between one black hole and a clump for three different simulations (upper, middle, and lower rows). The upper row corresponds to the run C0015, where $\epsilon_{\rm BH} = 4$ pc; the middle row correspond to the run C0015_$\epsilon$.004, where $\epsilon_{\rm BH} = 0.004$ pc; and the lower row correspond to a run with $\epsilon_{\rm BH} = 4$ pc restarted from simulation C0015_$\epsilon$.004 in order to follow the same close encounter that we show in the middle row but with a higher gravitational softening. In all the panels the SMBH is represented as a green filled circle. In the upper and lower row we see that, where $\epsilon_{\rm BH} = 4$ and thus the density of the black hole is comparable with the density of the gas, the close encounter produces a slingshot effect on the black hole. In contrast, we see in the middle row that, when $\epsilon_{\rm BH} = 0.004$, as the effective density of the black hole is greater than the density of the clumps, the clump is disrupted in the close encounter with the black hole.

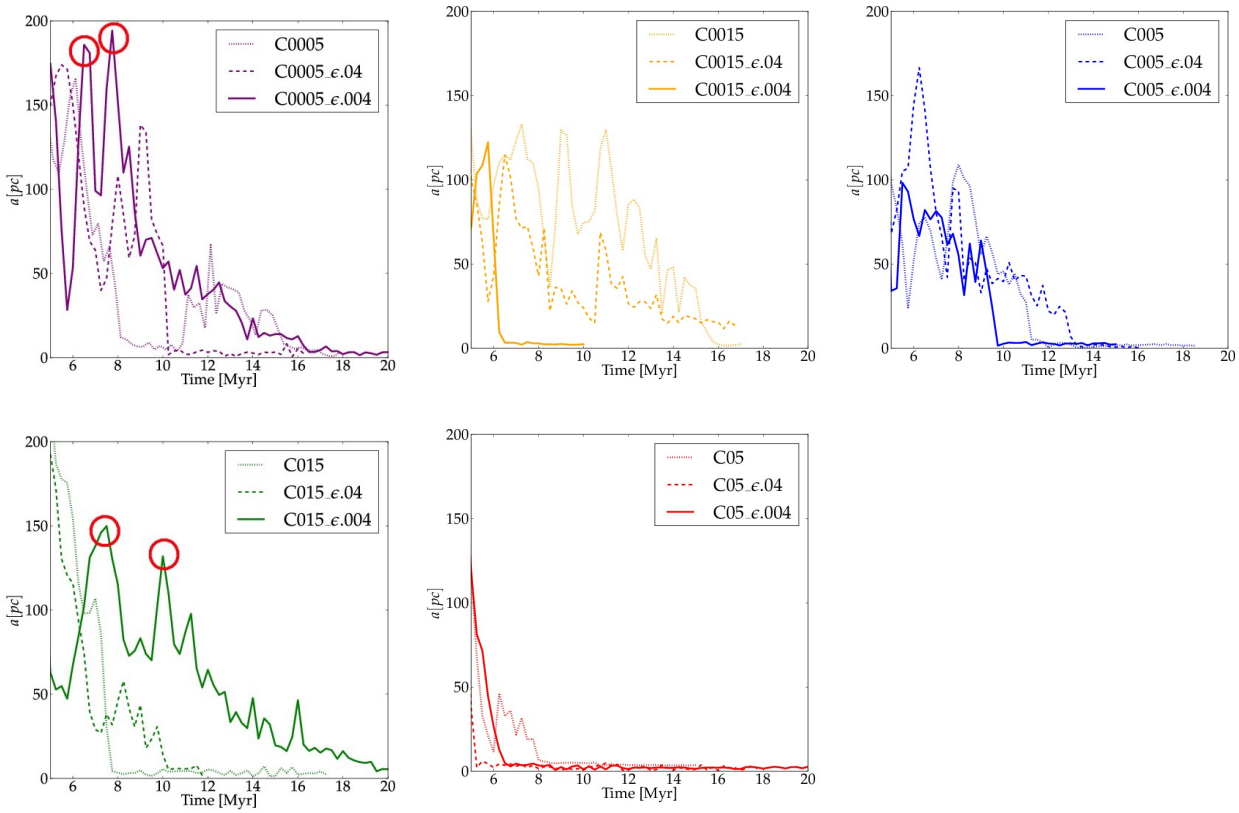


Figura 4.8: Evolution of the SMBHs' separation for simulations with different values of the gravitational softening of the black holes and different values of $C_*$. The continuous line correspond to simulations where $\epsilon$ 4 pc, the doted line to simulations where $\epsilon$ 0.04 pc and the dashed line to simulations where $\epsilon$ 0.004 pc. Each panel correspond to a different values of the star formation efficiency: $C_\star = 0.005$ (left upper panel), $C_\star = 0.015$ (middle upper panel), $C_\star = 0.05$ (right upper panel), $C_\star = 0.15$ (left lower panel) and $C_\star = 0.5$ (left middle panel).

However, the clump that produces these two large fluctuations in the separation of the black holes is the most dense and massive clump in run C015_$\epsilon$.004 ($3.5 \times 10^8 \mathrm{cm}^{-3}$ and $4 \times 10^8\ M_\odot$). So this clump is the most extreme clump in our simulation and hence, the two scatterings produced by it are highly unlikely to happen in a real CND. We note that shortly after the last scattering ($\sim$ 2 Myr), this clump is disrupted by one of the black holes, and after this disruption the orbital decay of the SMBH pair continues relatively smoothly.

Intense, fluctuating gravitational torques experienced by SMBH pairs in a clumpy medium have also been observed in numerical simulations by other authors (Escala et al. 2004; Fiacconi et al. 2013; Roskar et al. 2014). To compare our results with the ones obtained by Fiacconi et al. (2013), we estimate the effective density of the black holes and the clumps of their simulations. Using figure 3 of Fiacconi et al. (2013), we estimate that the density of their clumps range between $0.8 \times 10^6 \mathrm{cm}^{-3}$ and $13 \times 10^6 \mathrm{cm}^{-3}$. This estimate is a lower bound for the density, because we assume that the vertical size of their clumps is comparable to the thickness of their disk. If we compare this density range with the effective density of their black holes (which is $\rho_{\mathrm{BH}} = 7.9\, m_{\mathrm{H}} \times 10^7 \mathrm{cm}^{-3}$), we find that $\rho_{\mathrm{BH}}$ is typically greater than the density of their clumps and therefore their simulations don't suffer of a bad resolved black holes force. However, from our estimation, we found that the density of these gas clumps is greater, or equal, than the density of the densest, observed molecular clouds. This means that in these simulations the stochastic gravitational torques experienced by the black holes due to the gravitational interaction with the densest gas clumps can be overestimated.

## 4.6. Conclusions

We studied the evolution of a pair of SMBHs embedded in a star forming CND to explore how different SFR and gas physics can result in different timescales for the orbital decay of the pair. For this purpose, we ran twenty three N-body/SPH simulations. In eighteen of these simulations we used a modified version of the code `Gadget-3` in which we implemented recipes for star formation, cooling and supernovae explosions that resemble the ones used by other authors in the study of SMBH pairs (Callegari et al. 2011; Van Wassenhove et al. 2012; Roskar et al. 2014). The other two simulations used different gas physics. In one of these simulations we used the hybrid multiphase model for star formation implemented in `Gadget-3` Springel & Hernquist 2003; Springel et al. 2005a), where it is assumed that star formation is self regulated (simulation SDH05). In the other one, the gas thermodynamics is simpler and there is no star formation (simulation E05).

Before the SMBH pair forms a binary, their orbital decay is driven by dynamical friction coming from their gaseous environment. As this dynamical friction is density dependent, we expect the orbital decay of the SMBHs to occur more quickly in simulations where the gas density of the CND is higher. The simulations we ran with our recipes resulted in a higher mean gas density around the SMBHs than simulation SDH05, and accordingly we found the SMBHs' orbital decay to be faster using our recipes. However,

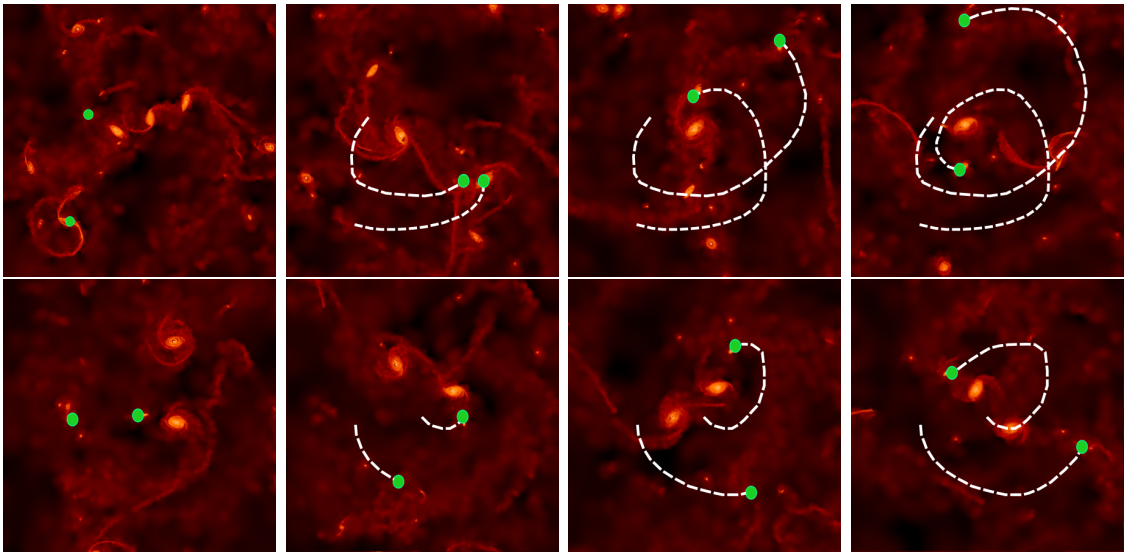

Figura 4.9: Distribution of gas in the plane of the disk, from left to right the time of the snapshots increases. The figures show the orbit of the black holes in the run C0005_$\epsilon$.004. The upper row shows the evolution during the first large fluctuation in the SMBHs' separation (first red circle in figure 4.8). The lower row shows the evolution during the second large fluctuation on the SMBHs' separation (second red circle in figure 4.8). Here we can see that the two large fluctuations are the result of the changing separation of the black holes as they orbit a common center, near the center of very dense and massive gas clump, with different orbital radii. The fluctuations are not the result of close encounters with high density gas clumps.

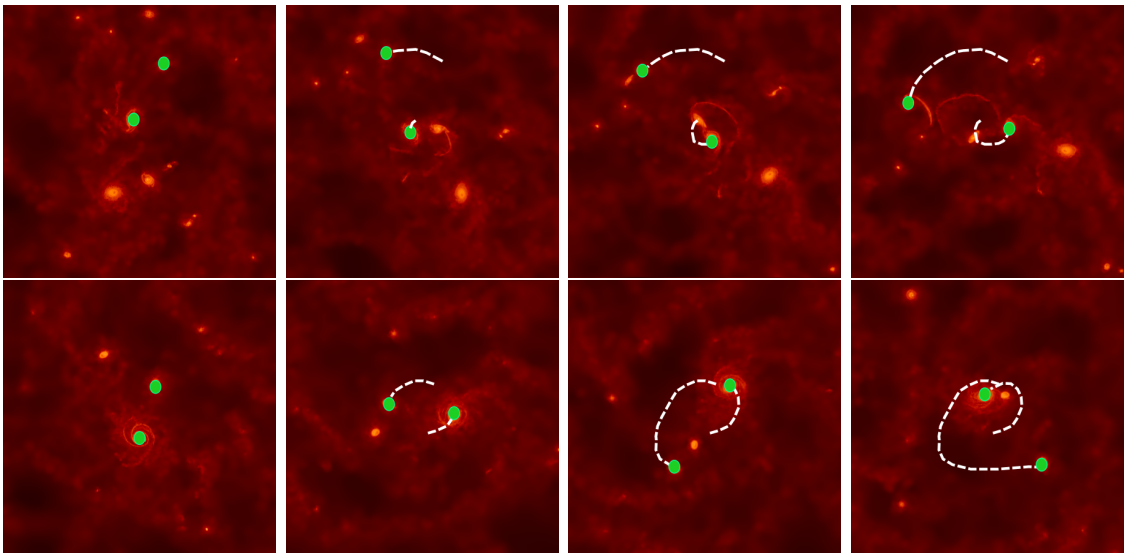

Figura 4.10: Distribution of gas in the plane of the disk, from left to right the time of the snapshots increases. The figures show the orbit of the black holes in the run C015_$\epsilon$.004. The upper row shows the evolution during the first large fluctuation on the SMBHs' separation (first red circle in figure 4.8D). The lower row shows the evolution at the moment of the second large fluctuation on the SMBHs' separation (second red circle in figure 4.8D).

in simulations with our recipes the orbital decay is sometimes slower than in simulation E05, even though the gas density in these simulations is higher than in simulation E05. This happen because in these simulations, the CND is fragmented in a few tens of high density ($\sim 10^6 - 10^9$ cm$^{-3}$) gaseous clumps, which erratically perturb the orbits of the SMBHs, delaying their orbital decay.

The density of these gaseous clumps are extremely high compared to the observed density of molecular clouds in isolated galaxies (Mathis 1990; Struve & Conway 2010) or ULIRGs (Downes & Solomon 1998; Schulz et al. 2007), which is typically on the order of $\sim 10^2 - 10^5 \mathrm{cm}^{-3}$. The reason for this discrepancy is that we don't include all the different physical process that sculpt the properties of the gas clumps. For example, to properly model the formation of gas clumps in the CND, we need to consider a more realistic cooling function which computes the effects of photons trapped inside the optically thick clumps, or follow the radiative transfer of these photons inside the clumps. Also, we have to include heating due to the stars and the accretion disks of the SMBHs, which can have an important effect on the temperatures and densities of the gas clumps. As the gas clumps are regions of vigorous star formation, we also expect that they will be highly turbulent. This turbulence, which would sustain the gas clumps against gravitational collapse, is also a missing ingredient in our simulations since it is damped in SPH codes like `Gadget-3`.

We also found that in simulations with our recipes, the density of the gas clumps is comparable to or greater than the effective mass density of the SMBHs, which we define as $\rho_{\rm BH} = 3\,M_{\rm BH}/(4\pi\epsilon_{\rm BH}^3)$ (for $\epsilon_{\rm BH} = 4$ pc, this density is $\rho_{\rm BH} = 3.8\,m_{\rm H} \times 10^6 \mathrm{cm}^{-3}$). We ran simulations where the gravitational softening of the SMBHs is smaller, and hence their effective mass density higher. With these simulations we show that the outcome of a close encounter, within a distance comparable with the gravitational softening, depends on the force resolution of the SMBHs. If the force resolution (i.e. gravitational softening) is such that the effective density of the SMBHs is smaller than the density of the gas clumps, a close encounter results in the scattering of the SMBH. On the other hand, if the force resolution is such that the effective density of the SMBHs is higher than the density of the gas clumps, a close encounter results in the tidal disruption of the gas clump and the SMBH orbit is less affected.

Recently, it has been argued that the orbital evolution of a pair of SMBHs in a clumpy CND has a stochastic behavior, due to the gravitational interaction of the SMBHs with high density gaseous clumps (Fiacconi et al. 2013; Roskar et al. 2014). However, in the simulations of these studies, as in our simulations, the densities of the denser gaseous clumps are higher than the densities of the observed, denser molecular clouds (Mathis 1990; Oka *et al* 2001; Struve & Conway 2010). Thus, in these simulations the effect of the denser gaseous clumps on the orbital evolution of the SMBHs, which is density dependent, can be overestimated. So the delay produced on the orbital decay of the SMBHs by these gaseous clumps in real CNDs can be even smaller than the observed in simulations.

We emphasize that even though in our simulations the orbit-perturbing gravitational torques produced by these gaseous clumps are overestimated, the migration timescale is still at most a factor three longer than the migration timescale in simulations with

simpler gas physics (Escala et al. 2005; Dotti et al. 2006). Even with this overestimation, gravitational interaction with the gas with the SMBHs produces a migration timescale which is much shorter than the typical migration timescale due to gravitational interaction with a background of stars. Interaction with gas yields a migration timescale on the order of $10^7$ yr, while migration timescale is on the order of one to ten Gyr in the case of a triaxial distribution of stars (Berczik et al. 2006; Khan et al. 2011).

From our numerical study and previous studies of binaries embedded in gaseous circumbinary disks (Escala et al. 2005; Dotti et al. 2006; Cuadra et al. 2009), we conclude that from the moment the SMBHs are separated by hundreds of parsecs until shortly after they form a binary, SFR has a much smaller effect on their orbits than cavity formation in the CND does. (This cavity formation is the result of inefficient viscous dissipation of angular momentum extracted from the binary (del Valle & Escala 2012, 2014). Indeed, we show that for a two order of magnitude of difference on the SFR the migration timescale only change in a factor of two, and in comparison, the formation of a cavity in the CND can extend the migration timescale by two orders of magnitude. However, since we are limited by the resolution of our simulations, we don't explore for a sufficiently long period the effects of the star formation on the evolution of the SMBHs after they form a binary. Amaro-Seoane et al. (2013) have made advances in this direction by studying the evolution of an SMBH binary which resides inside the central cavity of a star-forming gaseous circumbinary disk. Their results indicate that star formation slows the orbital decay of the binary. However, they do not explore how star formation affects the evolution of an SMBH binary when it is embedded in a circumbinary disk without a gap, a regime in which the gravitational torque of the gas on the binary is stronger.

As a future work, the effects of the star formation on the orbital evolution of an SMBH binary embedded in a circumbinary disk without a gap should be explored. We also need to model the gas around the binary more realistically. Ultimately, we would like to determine if the gas can extract sufficient angular momentum from the SMBH binary to drive its separation down to scales small enough for gravitational radiation to take over, ensuring coalescence of the SMBHs.

*Acknowledgments.* L del V's research was supported by CONICYT-Chile through Grant D-21090518 and a Redes (12-0021) grant, DAS Universidad de Chile and proyecto anillo de ciencia y tecnologÃa ACT1101. A.E. acknowledges partial support from the Center of Excellence in Astrophysics and Associated Technologies (PFB 06), FONDECYT Regular Grant 1130458. J.C. acknowledges support from FONDECYT Regular Grant 1141175. The simulations were performed using the HPC clusters Markarian (FONDECYT 11090216) from the DAS, Geryon(2) (PFB 06, QUIMAL 130008 and Fondequip AIC-57 ) at the Center for Astro-Engineering UC and Damiana from the AEI. We used splash (Price 2007) for the SPH visualization in Figures 7, 8, 9, 15 and 16. We are grateful to V. Springel for allowing us to use the `Gadget-3` code.

# Capítulo 5

# Gap-opening criterion in simulations of galaxy mergers

In this chapter we apply our gap opening criterion to the SMBHB-disk systems that are formed in the nuclear region of galaxy mergers. With this purpose we run different simulations of galaxy mergers. These simulations include recipes to model the star formation, the feedback of supernovas and radiative cooling of optically thin gas. We use our gap opening criterion to determine how likely the SMBH binaries formed in these galaxy mergers will experience a fast shrinking, and how far they are from a slow shrinking regime.

## 5.1. Introduction

Central SMBHs are found in practically every galaxy with a significant bulge (Richstone et al. 1998, Magorrian et al. 1998, Gultekin et al. 2009). Within the currently accepted evolutionary model of the Universe the merger between galaxies is a common event (White & Frenk 1991, Springel et al. 2005). If the two galaxies involved in a merger host a SMBH we expect that both SMBHs will sink by dynamical friction to the innermost region of the core of the merger remnant. When the mass enclosed by the orbit of these two SMBHs is smaller than the sum of their masses, then they will form a SMBH binary (see chapter §1 for a more extended discussion of this picture).

Understand the further evolution of these SMBH binaries is crucial because if they are able to shrink their separation down to $a_{\rm GW} \sim 10^{-3}(M_{\rm MBHs}/10^6 M_\odot)$ pc, then the binary becomes an intensive emitter of gravitational waves (GW) which allows the binary to coalescence within $10^{10}$ yr (see chapter §1). Therefore, if we are able to determine what happens to SMBH binaries after galaxy mergers we will be able to determine the amount of sources of GW in the Universe and understand better the cosmic evolution of the population of SMBHs.

The problem is that after a galaxy merger the range of separations that has to be cover by the SMBHs, in order to reach a separation comparable with $a_{\rm GW}$, is enormous (from $\sim 100$ pc to $10^{-3}$ pc). This make the study of the fate of SMBHs after a galaxy merger very interesting but very challenging.

When the SMBHs binary in the nuclear region of the merger remnant is embedded in a distribution of stars, the stars extract angular momentum from the binary driving its in-spiral. If the stellar system is axisymmetric the migration timescale will be longer than the age of the Universe ("last parsec problem", Begelman, Blandford & Rees 1980). However, if the stellar distribution has some degree of triaxiality the shrinking timescale will be of the order of $1 - 10$ Gyr (Khan et al. 2011; Vasiliev, Antonini & Merritt 2015), timescale that is comparable or longer than the time between galaxy mergers (see chapter §1 for a extended discussion of this picture).

However, if the galaxies involved in the merger have at least 1 % of gas we expect that a mass of the order of 10 to 100 times the mass of the SMBHs will sink to the central kiloparsec of the merger remnant (Barnes 2002; Mayer et al. 2010; Downes & Solomon 1998; Ueda et al. 2014). This gas can efficiently extract angular momentum from the binary making the shrinking timescale as short as $10^7$ yr, down to a separation comparable with $a_{\rm GW}$. However, if the gas does not redistribute efficiently the extracted angular momentum from the binary then it will be pushed away, generating a region of low density or gap around the binary (Artymowicz & Lubow 1994). In this case, the binary will enter a regime of slow migration in which, for a SMBH binary of mass $\geq 10^7$ $M_\odot$, the migration timescale can be as long as the age of the Universe (Cuadra et al. 2009).

In two previous publications (del Valle & Escala 2012, 2014) we derive and test against SPH numerical simulation a gap-opening criterion that allow us to determine in which conditions a binary that is embedded in a gaseous disk will excavate a gap. Therefore, this criterion allow us to determine when the binary experience a fast or slow shrinking. Motivated by the result of these publications we want to apply these criterion to determine how likely is that the SMBHs binary/disk systems formed in situs in a galaxy merger will experience a fast shrinking.

In section §5.2 we present the gap opening criterion and how we will use this criterion to determine how likely the SMBHs binaries experience a fast shrinking. In section §5.3 we present the numerical method and initial setup of the galaxy mergers. In section §5.4 we apply our gap-opening criterion to the nuclear gaseous region of the merger remnant. In section §5.5 we estimate in which conditions the formation of a gap and the subsequent stalling of the fast shrinking occurs. Finally in section §5.6 we discuss and summarize our main results. Additionally in the appendix we analyze the merger remnant, their kinematics and characteristics of the nuclear region.

## 5.2. The position on the gap-opening criterion phase space

In del Valle & Escala (2012, 2014) we derive an analytical criterion that allow us to determine when a binary embedded in a gaseous disk opens a gap. When the binary opens this cavity it enters a regimen of slow shrinking and therefore this gap-opening criterion also allow us to determine when the binary experience a slow or fast shrinking.

The gap-opening criterion for an equal mass binary has the following form,

$$\frac{\Delta t_{\rm open}}{\Delta t_{\rm close}} = \frac{1}{0.33}\left(\frac{c_{\rm s}}{v}\right)\left(\frac{v}{v_{\rm bin}}\right)^2\left(\frac{H}{a}\right) \leq 1\,, \tag{5.1}$$

where $v_{\rm bin}^2 = G\mu/a$, $v$ is the rotational velocity of the binary-disk system and $a$ is the binary separation (del Valle & Escala 2014).

The interesting thing is that this criterion can be used not only to determine if a particular binary undergoes a fast shrinking but also can be used to determine how far is the binary from a slow shrinking regime. To illustrate this in figure 5.1 we present a representation of the gap opening criterion.

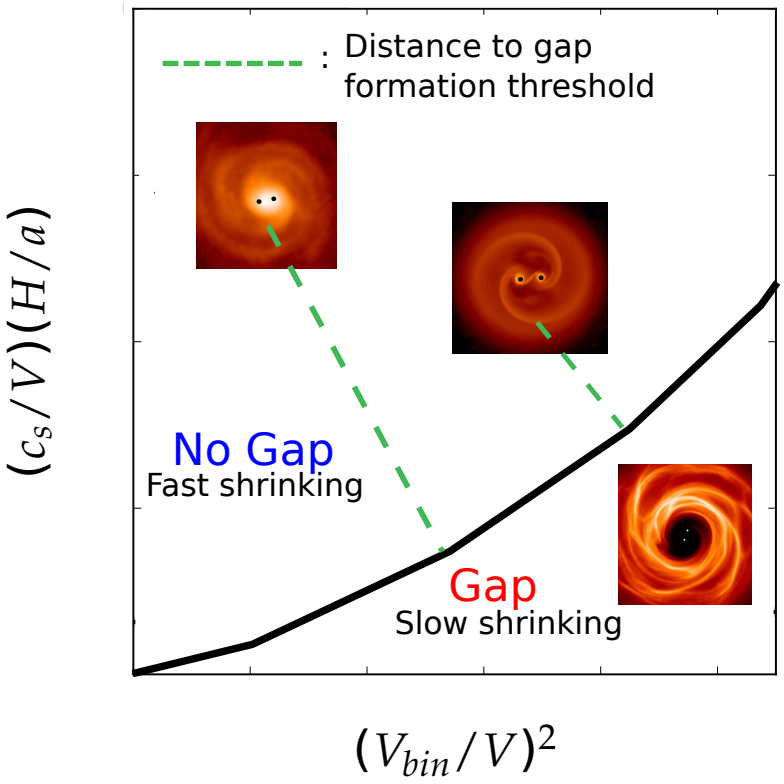


Figura 5.1: Representation of the gap-opening criterion in the space of parameters $(c_s/v)\,(H/a)$ vs $(v_{\rm bin}/v)$. The black dashed curve represent the gap-opening criterion on equation 5.1. Below this curve there are the combination of parameters for which the binary experience a slow shrinking and above the curve the combination of parameters for which the binary experience a fast shrinking. We show three representative cases, two in the fast shrinking regime and one in the slow shrinking regime. The green dashed curves represent the distance to the threshold line between the slow and fast shrinking regime.

In figure 5.1 the gap-opening criterion (equation 5.1) is represented by the thick black curve. Here we show three representative cases, one below the curve in which the binary

opens a gap, and therefore experience a slow migration (Cuadra et al. 2009), and two above the curve that represent two cases where the binary experience a fast shrinking. However, we note that the case that is closer to the black thick threshold line is closer from the slow shrinking regime. Therefore, if there is a change on the parameters that control the gap-opening criterion, for example a decrease on $c_{\rm s}$, it is more probable that the binary/disk system that is closer to the threshold line will reach the slow migration regime.

Therefore, from the position on the space of parameter of figure 5.1 we can determine how far a binary/disk system is from a slow shrinking regime. This distance tells us how much have to change the parameters of binary/disk system in order to enter in a slow shrinking regime. We use this approach to study for the first time the likelihood of fast shrinking of SMBHs binaries in simulation of galaxy merger in terms of their position in the space of parameters $(c_s/v)\,(H/a)$ vs $(v_{\rm bin}/v)$, and not only by following the evolution of their separation as is typically done (Callegari et al. 2011; Van Wassenhove et al. 2014; Roskar et al. 2015). This will allow us to make more robust conclusions about the shrinking timescale of SMBH binaries because we will be able to determine how far they are from a slow shrinking regime in the typical conditions of a galaxy merger. Also we will be able to determine which conditions has to fulfill the nuclear region of the merger remnant in order to make the SMBH binary experience a slow shrinking. We also explore if the geometry of the galaxy merger has some influence on the position of the binary/disk system on the phase space of the gap-opening criterion.

## 5.3. Initial conditions and numerical method

In this section we present the different simulations of galaxy merger that we will use in our study. All the simulations that we run consists of the merger of two equal-mass disk galaxies that collide on a parabolic orbit with pericentric distance $R_{\rm min} = 8kpc$. In the coordinate system that we use the orbital plane coincides with the $x$-$y$ plane. We run four mergers with different orientation of the disks of the galaxies relative to the plane of the parabolic orbit. We use the same geometry parameters defined by Barnes 2002: DIRect, RETrograde, POlar and INClined. In table 1 we present the different inclination $i$ between the galaxies and the orbital plane, and the pericentric argument $\omega$, measured in the orbital plane from the line of nodes to the $y$ axis, for the mergers DIRect, RETrograde, POlar and INClined.

| **Geometry** | $i_1$ | $\omega_1$ | $i_2$ | $\omega_2$ |
|---|---|---|---|---|
| DIRect | 0 | - | -71 | 30 |
| RETrograde | 180 | - | -109 | 30 |
| POlar | 71 | 90 | -109 | 90 |
| INClined | 71 | -30 | -109 | -30 |

Tabla 5.1: Geomerty parameters of galaxy mergers

The galaxies are initialized using the code GalactICS, in particular we use their "Milky Way model" D (see Kuijken & Dubinski 1995 for details). In each galaxy model, we in-

clude a gaseous disk with the same exponential profile as the stellar component (Kuijken & Dubinski 1995) and with a total gas mass corresponding to 10 % of the total stellar disk mass. In our simulations, we use the following units: [Mass]=$5.8 \times 10^{11} M_{\odot}$, [Distance]=1.2 kpc and G=1. The total number of particles per galaxy is 420,000, 200,000 for sampling the gas, 120,000 for the dark matter halo, 80,000 for the disk component, and 20,000 for the bulge. We also include a collisionless particle in the center of each galaxy that represent a SMBH.

For each merger setup (DIR, RET, PO or INC) we run two simulations where the mass of the SMBHs is different. For one set of simulations the SMBH has a mass that follows the $M_{\rm SMBH} - M_{\rm bulge}$ relation in their host galaxies. This set of simulations permit us to explore the gap formation likelihood under the assumption that the mass accretion of the SMBHs occurs before they coalesce to form a single SMBH ("late accretion" model, see 5.2). In the second set of simulations we assume that the sum of the masses of the SMBHs is proportional to the mass on stars of the inner 2 kiloparsecs of the merger remnant. This set of simulations permit us to study the gap formation likelihood under the assumption that the mass accretion onto the SMBHs occurs before they form a bound binary ("early accretion" model, see figure 5.2).

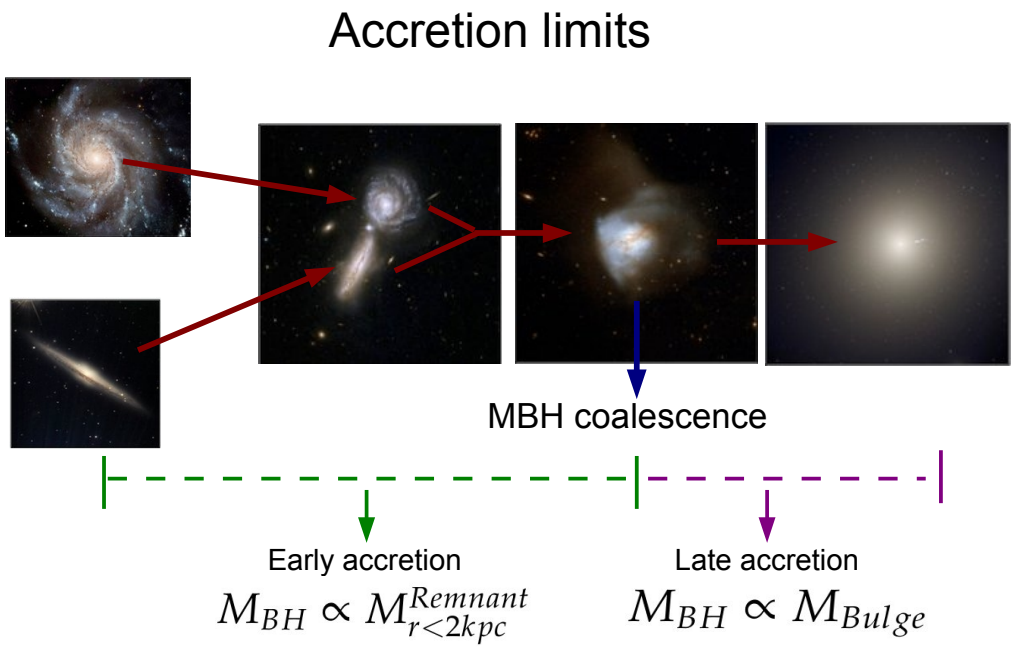


Figura 5.2: An scheme explaining the two accretion limits that we assume: The "early accretion" limit where the accretion occurs before the coalescence of the SMBH binary (period indicated by the green dashed line) and the "late accretion" limit where the accretion occurs after the coalescence of the binary (period indicated by the purple dashed line).

The gravitational softening of the dark matter halo particles and the initial stars is 50 parsecs. For the gas, the stars formed during the simulation and the SMBHs the initial softening is 10 parsecs and then is reduced down to 1 parsec when the separation of the SMBHs is $\sim$ 500 parsecs.

We evolve the merging galaxies using the code Gadget-3 (Springel *et al.* 2001; Springel 2005). This code evolves the system by computing gravitational forces with a hierarchical tree algorithm, and it represents fluids by means of smoothed particle hydrodynamics (SPH; e.g.Monaghan1992) We used the recipes for cooling, stellar feedback and star formation included in the code Gadget-3. These recipes assume that the star formation is self-regulated and is parameterized only by the star formation timescale $t_0$. We use the typical value for this parameter, $t_0$= 2.1, which provides a good fit to the Kennicutt law (Springel *et al* 2001)

## 5.4. The gap-opening criterion in remnants' CND

In this section we use the gap-opening criterion of equation 5.1 (del Valle & Escala 2014) to determine the position of the SMBH binaries, formed in situs in our simulations of galaxy mergers, on the gap-opening criterion phase space. In this way we will determine how likely is that SMBH binaries experience a fast shrinking ($\sim 10^7$ years). Also we will evaluate in which conditions these binaries can experience a slow shrinking.

### 5.4.1. Evaluating the gap-opening criterion

It was shown by Escala et al. 2005 that when the gravitational influence radius of two SMBHs embedded in a gaseous environment overlap they will generate a strong non-axisymmetric density perturbation in the gas, which principal axis lags behind the principal axis that pass trough the two SMBHs. This is the process that can drive the fast shrinking of the SMBH binary if the binary does not excavate a gap on the disk. Therefore, is only valid to apply our gap-opening criterion in binary/disk systems where the gravitational influence radius of two SMBHs are overlapped. This means that to evaluate our gap-opening criterion in our simulations of merging galaxies we need to know at what scales this overlap occurs.

In figure 5.3 we show the evolution of the gravitational influence radius $R_{\rm inf} = 2GM_{\rm BH}/(v_{BH}^2 + c_s^2)$ as a function of half the distance between the SMBHs. From this figure we can see that $R_{\rm inf}$ becomes equal to the binary separation when the binary separation is approximately 35 pc. Therefore, for binary separations on the scale of 35 pc and less the gravitational influence sphere of each SMBH overlap, region that is properly resolve by our simulations because our gravitational resolution for the gas and the SMBHs is $\sim$ 1 parsec. Also, we note that in this innermost region, below 100 parsecs, is where the conditions of the circum nuclear disks that are formed in our simulations match better the observations of ULIRGs (see the Appendix where we show the properties of the merger remnants).

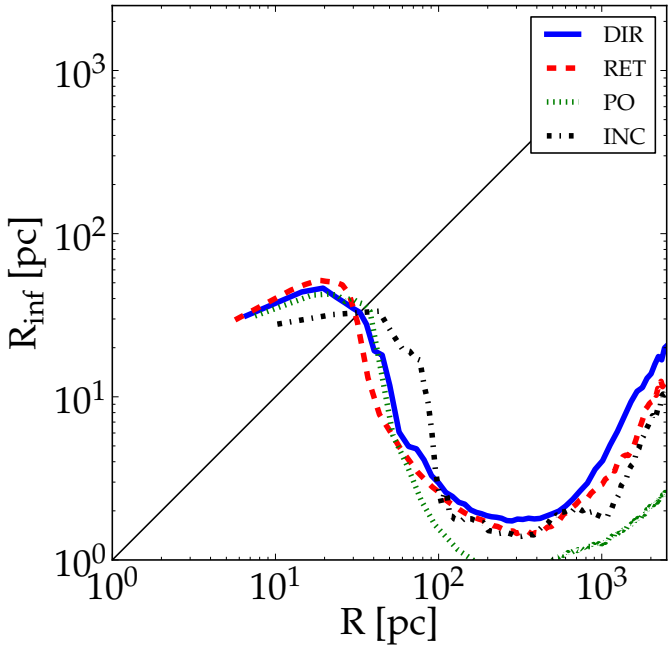


Figura 5.3: Gravitational influence radius $R_{\rm inf} = 2GM_{\rm BH}/(v_{BH}^2 + c_s^2)$ of the SMBHs in function of half the binary separation. The line represent the case when $R_{\rm inf} = R$. Above this line $R_{\rm inf} > R$ and therefore the gravitational influence sphere of each SMBH overlap.

Now that we know at what separations of the SMBHs our gap-opening criterion is valid, we will apply it to the SMBH binaries formed in our simulations of galaxy mergers. In figure 5.4 we plot the space parameter of the gap-opening criterion in an analogue way as was done by del Valle & Escala 2014. The black curve is the threshold between the region of the space of parameters where we expect that a gap will form (region below the curve) and the region where the viscous diffusion of the gas is fast enough to maintain the gap closed (region above the curve), as predict by our gap-opening criterion. This black curve correspond to the cases where $\Delta t_{\rm open} = \Delta t_{\rm close}$ (see equation 5.1).

From the result of our four mergers with a "late accretion" model, squares in figure 5.4, we see that they populate the region above the gap-opening threshold curve in the parameter space $((c_s/v)\,(H/a), (v_{\rm bin}/v))$ and therefore the formation of a gap on the disk in these simulations is unlikely. This is consistent with the evolution of the SMBH binaries that are formed in our simulations of galaxy mergers. All the SMBH binaries in these four simulations shrink their separation down to the gravitational resolution (softening $\sim 1$ pc), due to the extraction of angular momentum from the gas and background stars on the remnant's nuclear region, and they are never able to open a gap in this gaseous environment.

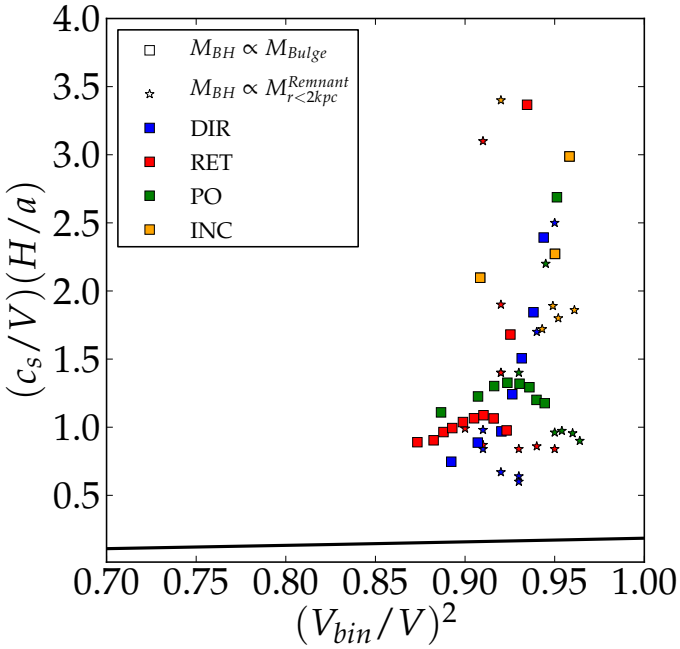


Figura 5.4: The space of parameter of the gap-opening criterion: the ratio of the sound speed of the gas and the velocity of the binary-disk system multiply by the ratio of the thickness of the disk and the binary separation $(c_s/v)(H/a)$, plotted against the quadratic ratio between the rotational velocity of the isolated binary and the rotational velocity of the binary-disk system $(v_{\rm bin}/v)$. The curve is the threshold between the region where we expect that a gap will form (region below the curve) and the region where no gap will form (region above the curves), as predict by our gap-opening criterion (del Valle & Escala 2012,2014). The squares markers are the results from our simulations of merging galaxies assuming the "late accretion" model. The stars markers are the results from our simulations of merging galaxies assuming the "early accretion" model. The blue, red, green and black colours design the different simulations DIR, RET, PO and INC respectively. All the square and star points are computed for the binary when it separation is smaller than 35 pc, which is the distance in which the gravitational influence radius of the SMBHs overlap.

From our simulations where the mass of the SMBHs is $M_{\rm BH} = 0.0013 * M^{\rm Remnant}_{r<2kpc}$ before the coalescence of the SMBH binary (star points on figure 5.4) we can see that they are still well above the gap-opening threshold curve and therefore the SMBHs binaries in these simulations are not able to excavate a gap on the circum nuclear disk.

Therefore, we can conclude from our gap opening-criterion that in the typical conditions on the central region of ULIRGs, and for a mass accretion that permits to the SMBHs fulfill the $M_{\rm BH} - \sigma$ condition at the end of the merger, is unlikely that the SMBH binary will excavate a gap on the gas, and therefore we expect that they will experience a fast shrinking. Indeed, we can see that the position of the binary/disk systems formed in all the galaxy mergers is well above the threshold line, meaning that the SMBHs binary are far away from the slow migration regime.

However, neither in our simulation nor estimations we include the effect of the black hole accretion feedback. In principle this effect may push away the gas around the SMBH binary, facilitating the formation of a gap, however, this feedback can also increase the sound speed of the gas around the binary, decreasing the viscous diffusion timescale and therefore making more difficult the formation of a gap (see figure 5.4 to see how a change on $c_s$ affects the likelihood of gap formation). Therefore the net effect of the AGN feedback on the gap formation process is unclear.

### 5.4.2. Conditions needed to open a gap and further evolution

Now we explore the necessary conditions to open a gap in the gaseous circum-nuclear disk. As we see in the previous section if the sound speeds and thickness are comparable with the values observed in ULIRGs and the SMBH binary ends with a mass that fulfills the $M - \sigma$ relation in the merger remnant, for a "early accretion" or "late accretion" model, the formation of a gap is improbable.

From our gap opening criterion, equation 5.1, we know that $\Delta t_{\rm close}/\Delta t_{\rm open}$ decrease with $c_s^{-1}$, $H^{-1}$ and $M_{\rm BH}$ and therefore for colder thinner disks and more massive SMBHs the formation of a gap is more probable. Therefore, we can evaluate for which values of these parameters the formation of a gap will occur.

We take the values from the simulation DIR (which is the one closer to the gap-opening threshold curve) as representative and we change the values of $c_s$ and $M_{\rm BH}$ to determine in which conditions a SMBH binary will excavate a gap reaching the slow shrinking regime.

From our gap opening criterion we know that a way to ensure gap formation is to reduce the sound speed of the gas, because this will reduce the speed with which the gas can fill a gap. We estimate that to ensure gap formation in the "late accretion" model the sound speed of the gas must be equal or smaller than 15 km s$^{-1}$, which is much smaller than the turbulent velocity in interacting galaxies, such as ULIRGs ($\sim$ 100 km s$^{-1}$), or the turbulent velocity on high redshift star forming galaxies ($\sim$ 50-80 km s$^{-1}$, Cresci et al. , 2009; Dekel, Sari & Ceverino 2009 and references therein) and is similar to the turbulent velocity in the inner region of local spirals ($\sim$ 5-10 km s$^{-1}$, Dickey et al. , 1990; Dib, Bell & Burkert 2006). We plot with blue triangles in figure 5.5 the position of the DIR "late accretion" simulation in the $((c_s/v)\,(H/a),(v_{\rm bin}/v))$ assuming that $c_{\rm s} \sim 15$ km s$^{-1}$.

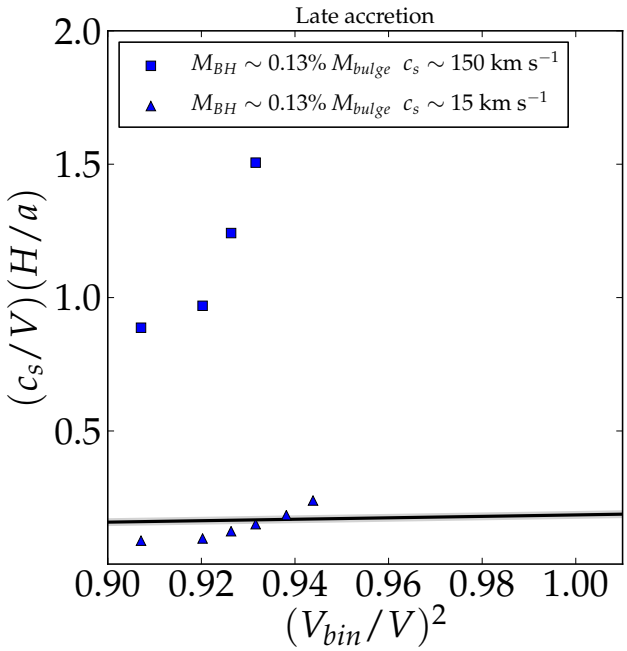


Figura 5.5: Same as figure 5.4. Here the different points represent the values on this space of parameters of the simulation DIR for different values of $c_s$. The squares are the same from figure 5.4, the "late accretion" model in which we initialize the mass of the SMBHs as $M_{\rm BH} \sim 0.13\,\% M_{bulge}$. The triangles are the values on this space of parameters of the simulation DIR with the "late accretion" model assuming $c_s \sim 15$ km s$^{-1}$.

In figure 5.6 we plot the values on the gap-opening space parameter ( $(c_s/v)\,(H/a)$, $(v_{\rm bin}/v)$ ) for the simulation DIR, assuming the "early accretion" model. From this figure we estimate that to ensure gap formation in typical conditions of a ULIRGs ($H$ ∼100 pc and $c_{\rm s} \sim 100$ km/s) the black holes need to grow their mass to a mass comparable with 2 % the mass of the remnant's bulge ($M_{\rm BH} \sim 2\,\% M_{\rm Remnant}(r < 2kpc)$). This mass growth will produce a SMBH with a mass one order of magnitude greater than the expected from the observed $M_{\rm BH} - M_{\rm bulge}$ relation (Magorrian *et al.* 1998 ; Marconi & Hunt 2003; Novak, Faber & Dekel 2006). Assuming that the SMBHs gain this mass over the ∼ 100 Myr that pass from the beginning of the merger (where we assume the beginning of the merger as the moment when the separation between the dark matter halos of the galaxies is comparable with the size of the dark matter halos) to the moment when the two SMBHs form a bound binary, the SMBHs need to accrete at a rate much greater than the typical accretion rate derived from observations (Di matteo et al. 2002; Dotti, Merloni & Montuori 2015 and references there in). Also, from figure 5.6 we estimate that for the "early accretion" model (assuming $M_{\rm BH} \sim 0.13\,\% M_{\rm Remnant}(r < 2kpc)$) a sound speed smaller than 30 km s$^{-1}$ will ensure the formation of a gap. Then, for both accretion models the sound speed needed to form a gap is smaller than the typical turbulent velocity observed in the inner region of ULIRGs which is of the order of 100 km s$^{-1}$, therefore we may expect that in typical conditions of ULIRGs such low turbulent velocity are not reached by the gas.

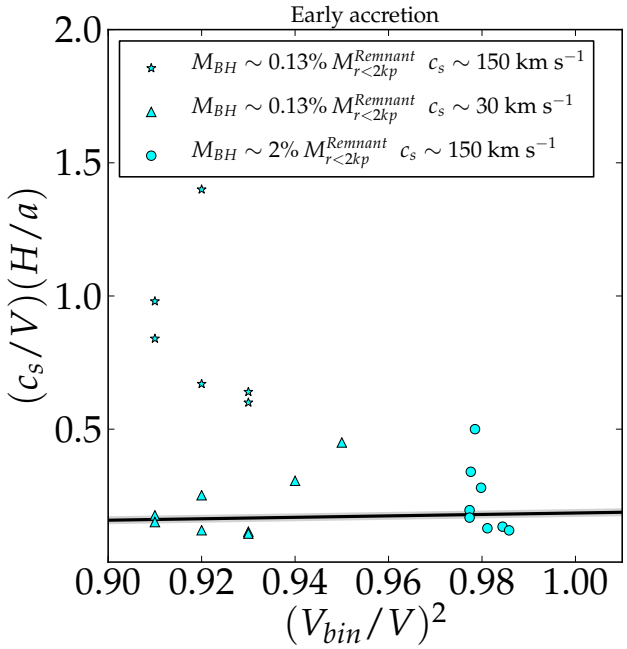


Figura 5.6: Same as figure 5.4. Here the different points represent the values on this space of parameters of the simulation DIR for different assumptions of $M_{\rm BH}$ and $c_s$. The stars points are the same from figure 5.4, the "early accretion" model in which we initialize the mass of the SMBHs as $M_{\rm BH} \sim 0.13\,\% M^{\rm Remnant}_{\rm r<2kpc}$. The triangles are the values on this space of parameters of the simulation DIR with the "early accretion" model assuming $c_s \sim 30$ km s$^{-1}$. The filled circles are the values on this space of parameters of the simulation DIR with the "early accretion" model assuming $M_{\rm BH} \sim 2\,\% M^{\rm Remnant}_{\rm r<2kpc}$.

## 5.5. Discussion and Conclusions

We study the fate of SMBHs in simulations of galaxy mergers. If the galaxies involved in these mergers have a gas fraction of at least 1 % we expect that a massive gaseous disk with a mass of ten to hundred times the mass of the SMBHs will be formed in the central kiloparsec of the merger remnant. The SMBHs in these nuclear region will form a SMBH binary which separation will experience a fast shrinking (in a timescale $\sim 10^7$ years) mainly due to the gravitational torque produced by the gaseous disk. However, if the gas does not redistribute efficiently the extracted angular momentum from the binary a cavity of low density of gas will be formed around the binary and the shrinking of the SMBH binary will be dramatically delayed.

We use the gap-opening criterion derived in del Valle & Escala (2012, 2014), that allow us to determine in which binary/disk system a gap is formed, to determine how likely is that the SMBHs binaries formed in our galaxy mergers will experience a fast or slow shrinking. Using this approach we also determine how far are the SMBHs binaries from the slow shrinking regime by studying their positions on the phase space of the gap opening criterion. This allow us to determine how much the properties of the binary/disk system (sound speed, ratio between the mass of binary and the disk, thickness

of the disk, velocity of the system) have to change in order to make the binary shift from a fast shrinking mode to a slow shrinking mode. From these estimations we make more robust conclusion about the shrinking timescales of SMBHs binaries in galaxy mergers.

The simulations of galaxies mergers that we run correspond to the merger of equal mass "Milky way" type galaxies in a parabolic orbit. The inclination between the plane of the galaxies and the plane of the orbit differ between simulations, we explore four different geometries which we call RET, DIR, PO and INC following the nomenclature of Barnes (2002). We evolve our galaxy merges using the SPH/N-body code Gadget-3 which include recipes for star formation, radiative cooling and supernovae heating. We find that all our merger remnants have properties consistent with observation of interacting galaxies within the central 100 pc (Sanders & Mirabel 1996; Downes & Solomon 1998; Medling et al. 2014; Ueda et al. 2014).

We find that the position of all SMBH binaries in the phase space of the gap opening criterion are within the fast shrinking regime and very far from the slow shrinking regime. This means that the SMBH binaries in our simulations will very likely experience a fast shrinking and that the properties of the gas around them have to change very radically in order to pass from the fast shrinking regime into the slow shrinking regime. This is in concordance with the actual evolution of the SMBHs in our galaxy merger simulations, where we observe that the SMBHs experience a fast migration until they reach a separation comparable with the gravitational softening without forming a gap.

However, in our simulations the SMBHs do not experience mass accretion. For this reason we run four additional simulations to estimate the gap-opening likelihood assuming that the mass of the SMBHs is proportional to the mass of the of the remnant's bulge, in concordance with the $M_{\rm BH} - M_{\rm bulge}$ relation. We find that even if the SMBHs reach this higher masses before they form a bound binary the formation of a gap is unlikely.

From our gap-opening criterion we find that the formation of a gap is more probable for more massive SMBHs (del Valle & Escala 2012, 2014) or disks with smaller sound speed. Hence we estimate the necessary SMBH's mass to form a gap and the necessary sound speed of the disk to form a gap. We find that the SMBH binary has to reach a mass comparable with 2 % the mass of the remnant's bulge before they form a bound binary in order to gap formation be possible. This condition can be translated to an accretion rate much higher than the typical accretion rate derived from observations (Di matteo et al. 2002; Dotti, Merloni & Montuori 2015 and references there in). We also find that the sound speed of the gas has to be smaller than 15 km $s^{-1}$ to gap formation occur, sound speed that is much smaller than the typical turbulent velocity on the inner region of ULIRGs which is of the order of 100 km $s^{-1}$ and which is more similar to the turbulent velocity in the inner region of a "Milky Way" type galaxy ($\sim$ 5-10 km $s^{-1}$, Dib, Bell & Burkert 2006).

We conclude that in standard conditions of the nuclear region of ULRIGs, and even for a relative high accretion rate, the formation of a gap is very unlikely to occur because in these conditions the SMBHs binaries/gaseous disk system are very far from the slow sh-

rinking regime in the phase space of the gap-opening criterion. Thus, we expect that after the merger of galaxies with a gas fraction of at least $1\,\% - 5\,\%$, the SMBHs will experience a fast shrinking (in a typical timescale of the order of $10^7$ yr) down to the scales where their final coalescence will be driving by the emission of gravitational waves ($\sim 10^{-3}$ pc), unless other processes strongly affect the distribution of the gas nearby the SMBH binary.

One of these processes that can stop the fast shrinking of the SMBH binary is the effect of the accretion luminosity of the SMBHs in the nearby gas. However, the effect of the accretion luminosity onto the gas is not clear, because some numerical works suggest that even for a super-Eddington regime the radiation is not strong enough to push all the gas that is nearby the SMBHs away from the SMBHs (Krumholz & Thompson 2012). Therefore we conclude that, if the accretion luminosity of the black holes does not push away a large portion of the gas nearby the SMBH binary, then the SMBH binaries are very likely to experience a fast shrinking. However, to make this statement more robust, further research of the characteristic of the gas in the nuclear region of merger remnants at sub parsec scales are needed. This research would allow us to put more secure constraints on the rate of merging SMBHs in the universe, which is a crucial ingredient in models of the evolution of the population of SMBHs in the Universe, and to determine the amount of gravitational waves sources that we expect to observe with the future European Laser Interferometer Space Antenna (eLISA, Amaro-Seoane et al. 2013).

*Acknowledgments.* L del V's research was supported by CONICYT-Chile through Grant D-21090518 and a Redes (12-0021) grant, DAS Universidad de Chile and proyecto anillo de ciencia y tecnología ACT1101. A.E. acknowledges partial support from the Center of Excellence in Astrophysics and Associated Technologies (PFB 06), FONDECYT Regular Grant 1130458. The simulations were performed using the HPC clusters Docorozco (FONDECYT 1130458) from the DAS and Geryon(2) (PFB 06, QUIMAL 130008 and Fondequip AIC-57 ) at the Center for Astro-Engineering UC. We are grateful to V. Springel for allowing us to use the `Gadget-3` code.

# Appendix: Structure of the merger remnant

## Kinematics of the merger remnant

In this appendix we describe the dynamical structure of the mergers remnants for our four simulations of galaxy mergers.

In fig 5.7 we show the distribution and kinematics of the gas at the end of each simulation. These figures show the radial velocity $v_r$ of the gas particles as a function of the radius $r$ for the four mergers that we simulate. We can see that the distribution of the particles in these figures is nearly symmetric with respect to $v_r = 0$ for radius smaller than $r \approx 1 - 10$ kpc. For larger radius all the simulations present narrow diagonal stripes that are not symmetric with respect to $v_r = 0$. These stripes are the tails of the merger which are form from extracted material from the disk of the galaxy when the galaxies experience a pericentric passage. The amount of material in each of these tails and their number depend on the orbital parameters of the merger. For example the merger INC in figure 5.7 (bottom right panel) shows more of these asymmetric features than the other mergers because, in this merger, there are two pairs of tails in different planes that coexist simultaneously. Instead in simulation DIR (upper left panel) there are only a pair of tails and in simulation RET (upper right panel) there are only two big tails and a third smaller tail which is in the same plane of the bigger tails. The PO merger (bottom left panel) shows only one of this asymmetric structures and in this case is not properly a tail but more an elongated puffier structure of gas.

The distribution of the gas that is nearby to $v_r = 0$ represents particles with nearly circular orbits and therefore are characteristic of the gas disc that is formed by the in-fall of material. The particles of gas with larger $v_r$ dispersion, symmetric respect to $v_r = 0$, represent the gas that follows more elongated eccentric orbits in this disk. For example, the remnants of the DIR and RET mergers have large amounts of gas with narrower $v_r$ distributions at radius smaller than 4 kpc and larger than 2.5 kpc. This narrower distribution represent a disk structure and they are not found in simulations PO and INC. In simulation PO there is no disk structure at this radius and the remnant has a more ellipsoidal geometry. For the case of the simulation INC at this radius the material on the tails is still falling and, comparing with the evolution of the tails of the RET and DIR mergers, we expect that at these radius the tails will settled down in a disk structure after a few Myr.

In radius smaller than 2.5 kpc we find the nuclear region which for simulations RET, DIR and INC has the shape of a disk. For the case of the RET and DIR simulations we can see that this nuclear disk have a larger $v_r$ dispersion than the disk in the region 2.5 kpc $< r <$ 4 kpc and therefore they consist of gas with more elongated orbits. The kinematics of the nuclear disk of the INC simulations its more difficult to recognize because its hidden by the gas tails. The simulation PO has a nuclear region that has a more ellipsoidal geometry with a larger $v_r$ dispersion however below 100 pc appears a narrower structure that can be identify as a disk.

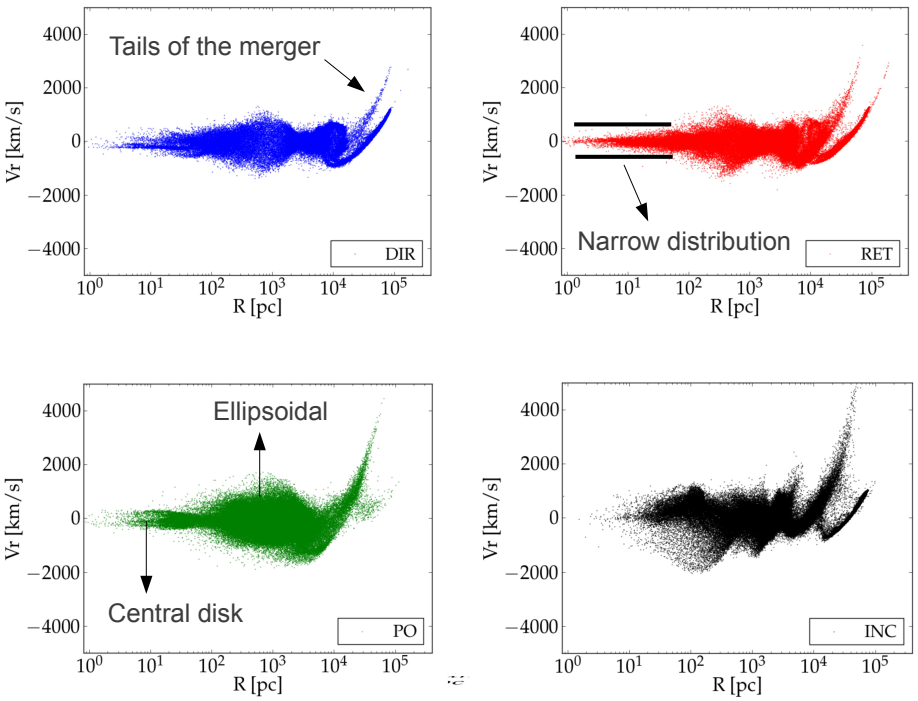


Figura 5.7: Radial velocities and distribution of gas in all merger remnants. In each plot, the horizontal axis is the radius in logarithmic scale, while the vertical axis is $v_r$. These figures show the distribution and kinematics of the gas at the end of each simulation.

## Properties of the nuclear region

In figure 5.8 we show the surface density of the gas in function of the radius (left panel) and the sound speed of the gas in function of the radius (right panel) for the nuclear region of our four simulations. In these two figures we compute the quantities on the plane perpendicular to the angular momentum of the central kiloparsec of the merger remnant. From these figures we can see that, although the exact form of the surface density and sound speed profile of the nuclear region differs between different simulations, the general trend is similar for the four mergers that we simulate.

In all our simulations the nuclear region of the merger remnant have surface densities that range between $10^{24} - 10^{25}$ cm$^{-2}$ which is consistent with the observed average surface density of the nuclear region of ULIRGs (Hodge et al. 2014; Iono et al. 2014; Xu et al. 2014). The surface density profile, in the four merger's remnant, roughly decay as $r^{-0.5}$, and therefore is less steeper than a typical Mestel density profile (see figure 5.8) which is used to model circum-nuclear disks in more idealized simulations (Escala et al. 2005, Dotti et al. 2006).

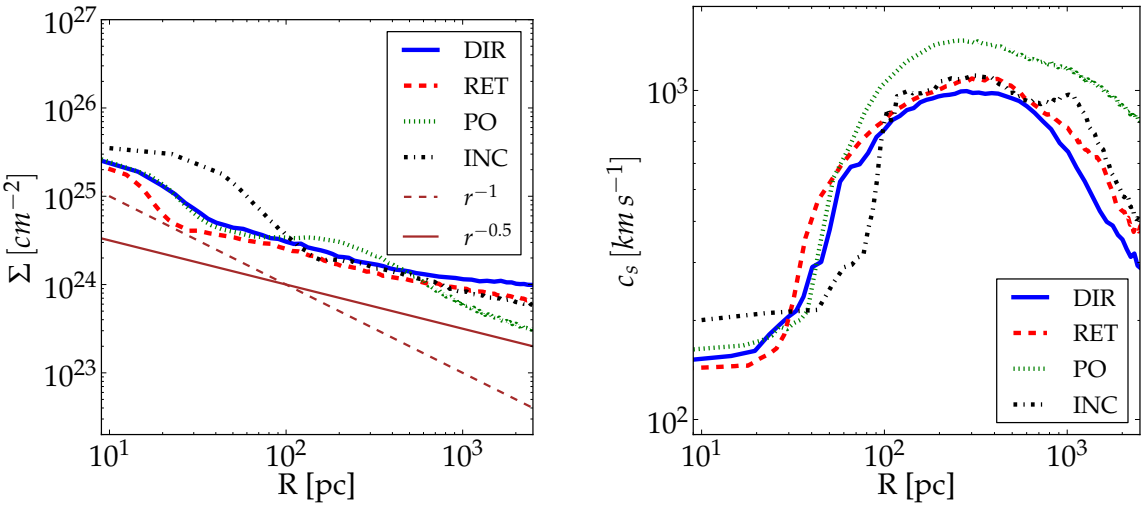


Figura 5.8: Left Panel: Surface density in function of radius for our for simulations of galaxy mergers with different orbital parameters. This surface density is computed on the plane perpendicular to the angular momentum of the central kiloparsec of the merger remnant. Right Panel: Sound speed as a function of radius for our for simulations of galaxy mergers.

The sound speed of the central 2.5 kpc of the four merger remnants range between 110 km $s^{-1}$ and 1200 km $s^{-1}$, however, in the innermost region (below 100 pc), which is the region where we will study the evolution of SMBH binaries, the sound speed is of the order of 100 km $s^{-1}$ which is consistent with the turbulent velocity of the gas observed in the central kiloparsecs of ULIRGs (Downes & Solomon 1998; Ueda et al. 2014). The higher sound speeds that we observe in the central kiloparsec of our simulations are consequence of the high star formation rate in these regions and the subsequent heating by supernova Type II explosion which typically heats the gas up to $10^8$ K which correspond to a sound speed of the order of 1000 km s−1.

In the left panel of figure 5.9 we show the enclosed mass in function of the radius. We can see from this figure that the enclosed mass follow a similar trend with radius for the four merger, also we can see that the enclosed mass inside 2.5 kpc is of the order of $10^{10}$ $M_\odot$ for the four mergers, which is consistent with the mass observed in the nuclear region of interacting galaxies such as ULIRGs (Sanders & Mirabel 1996; Downes & Solomon 1998; Engel et al. 2010; Medling et al. 2014; Ueda et al. 2014; Xu et al. 2014).

In all our mergers the total mass on gas of the two galaxies just before the first passage is approximately $5.8 \times 10^{10}$ $M_\odot$, therefore, from the left panel of figure 5.9 we found that the percent of this mass on gas that ends accumulated in the central 2.5 kpc of the remnants are 70 %, 36 %, 35 % and 18 %, for the merger DIR, INC, RET, and PO respectively. We note that these percents are smaller than the typical values that are found in other simulations of galaxy mergers because in these works it is not considered the consumption of gas by star formation (Barnes & Hernquist 1996; Mihos & Hernquist

1996; Barnes 2002) or, if there it is included a recipe for star formation, the density threshold to form stars is higher that the density threshold in our simulations (Mayer et al. . 2007, 2010).

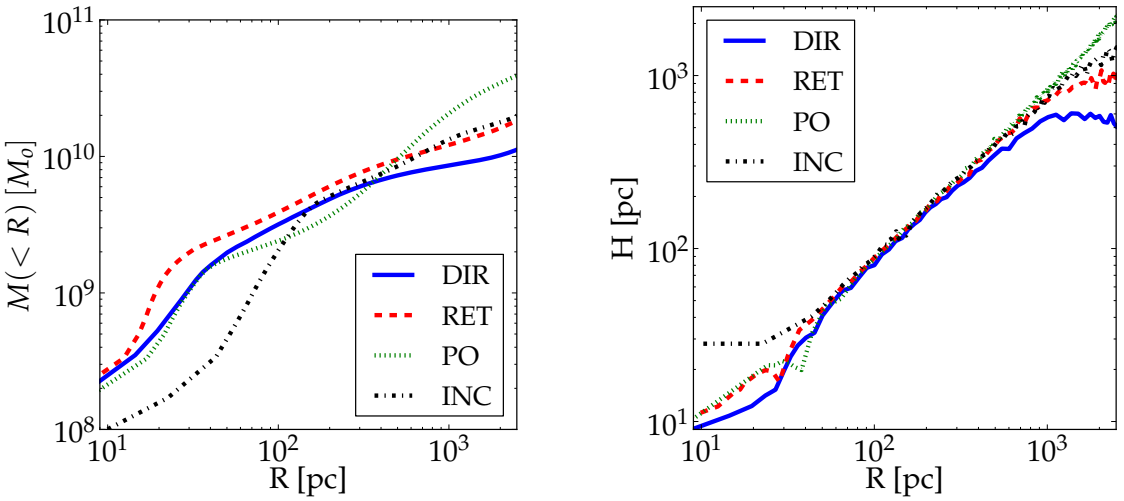


Figura 5.9: Left Panel: Enclosed mass in function of radius for our for simulations of galaxy mergers with different orbital parameters. Right Panel: Thickness of the central few kiloparsecs of the merger remnants as a function of the radius.

The right panel of figure 5.9 shows the thickness $H$ of the nuclear region in function of the radius for the four mergers remnants. We define $H(R)$ as the distance, in the direction of the angular momentum of the gas in the nuclear region, which enclose 95 % of the mass of an annulus of inner radius $R - \Delta R$ and outer radius $R$. We can see that the nuclear region of the DIR merger is the narrower with $H/R \sim 1/5$. The central nuclear region of simulations RET and INC are wider with $H/R \sim 1/2.5$ and $H/R \sim 1/1.7$ respectively. In the case of the PO merger we observe that the nuclear region, between one hundred parsecs and a few kiloparsecs, is even wider and clearly is consistent with an spherical/ellipsoidal distribution of gas, instead of a disk of gas, in concordance with the kinematic information of figure 5.7. We note that in our four simulations the thickness $H$ for radius below 100 parsecs is consistent with the thickness of the massive circum nuclear gas disks observed in ULIRGs even when the central kiloparsec of our merger remnants tends to have the geometry o a thick disk or an ellipsoid (Sanders & Mirabel 1996; Downes & Medling et al. 2014; Ueda et al. 2014).

# Capítulo 6

# Conclusions

In this thesis I study the evolution of SMBHs after a galaxy merger and how likely is that the SMBHs of the galaxies will coalescence after the merger. Within the context of hierarchical structure formation, where the merger between galaxies is a common event, and from the observational realization that a SMBH is harboured in the center of practically every galaxy with a significant bulge, I overview how the formation and evolution of SMBH binaries has become an established concept.

I discussed the standard theory of the evolution and merger of SMBH binaries in galactic nuclei based in the study of the long-term evolution of a SMBH binary at the center of a dense stellar system. In this picture the SMBHs sink to the center of the dense stellar system due to the gravitational drag generated by the background stars onto the SMBHs and then the distance between the SMBHs becomes small enough to form a binary. This SMBH binary continues shrinking due to the transfer of energy onto the stars, however this process kicks out stars of the system, depleting the number of stars that are able to extract energy from the binary and drive the further shrinking of the SMBH binary. This depletion of stars stalls the shrinking of the binary and only in the more favourable cases, were the closest regions of the binary are refilled with new stars, the coalescence of the SMBH binary is achieved in a timescale of the order of 1 Gyr.

I also review how the stars are not the only component of galaxies that can extract angular momentum from the SMBHs binary. Indeed, numerical simulations of merging galaxies and observations of ultra luminous infrared galaxies (ULIRGs) have shown that in galaxy mergers 60 % to 90 % of the total gas is driven to the central kilo parsec of the merger remnant forming a disk like structure (circum nuclear disk). Therefore, if the galaxies involved in the merger have at least 1 % of gas it is expected that the SMBH binary will end embedded in a gaseous environment with a mass comparable to or much greater than its own mass, this will have an important effect on its orbital evolution.

Different studies have shown that this huge accumulation of gas can dramatically shorten the typical timescale of the coalescence of the SMBH binary. For example, Escala *et al.* (2005) showed that when the gravitational spheres of the SMBHs overlap, a strong non axisymmetric density perturbation is produced in the gas with a principal axis that lags behind the principal axis of the binary. This offset produces a torque onto the SMBHs that drives the transfer of angular momentum from the binary to the gas.

Under these conditions, if the extracted angular momentum is efficiently redistributed by the gas, Escala *etal.* (2004, 2005) showed that the SMBH binary will experience a fast migration that will allow the binary to coalesce in a timescale of the order of 10 Myr. However, if the gas does not efficiently redistribute the extracted angular momentum it will be pushed away from the binary forming a gap or cavity of low density. In these conditions, numerical studies have shown that the gas will not be able to drive the SMBH binary to coalescence in a timescale shorter than the age of the universe (Cuadra *etal* 2009).

Therefore, the aim of this thesis is to derive a criterion to determine under which conditions the gas will be able to efficiently redistribute the extracted angular momentum from the binary (conditions for which a SMBH binary will experience a fast shrinking). Then, I use these criterion to determine how likely is that in real astrophysical systems the conditions that will permit the fast shrinking of SMBHs after a galaxy merger are fulfilled. These studies ultimately will allow us to set constraints to the likelihood of coalescence of SMBHs in the universe, will help us to reach a better understanding of the evolution of the population of SMBHs in the universe and will help us to determine the amount of gravitational waves expected to be observed by the future European Laser Interferometer Space Antenna (eLISA, Amaro-Seoane et al. 2013) or by means of millisecond pulsar timing arrays.

## 6.1. Main results

I derived an analytic criterion to determine when the gravitational torque exerted by a SMBH binary in a massive gaseous disk will produce the formation of a gap. In disks where this gap or cavity does not form, we expect that the extraction of angular momentum from the binary will ensure the coalescence of the binary in a timescale of the order of $10^7$ yr. In comparison, in systems where the gap is formed the coalescence timescale may be as long as $10^9$ yr. We ran forty one SPH simulations of binaries embedded on isothermal gaseous disks to test our gap-opening criterion and we found concordance between the predictions of our gap-opening criterion and the gaps formed in our simulations.

To estimate the likelihood of formation of a gap, and therefore of the coalescence of SMBHs in galaxy mergers, I run eight simulations of major merger with different orbital parameter to apply the gap-opening criterion to the in situ disk-binary system formed in these simulations. In the eight simulations of major galaxy mergers that I performed I found that more than 60 % of the gas of the two galaxies ends in the central kilo parsec of the merger remnant and that the mass of the gas in this central region is $M_{\rm gas} \approx 10^{10}$ M$_\odot$. Also, I found that in the central one hundred parsecs the conditions of the gas roughly matches the condition observed on interacting galaxies such as ULIRGs.

I evaluated my gap-opening criterion on these eight simulations and I found that the formation of a gap is unlikely even if the SMBHs accrete all the mass necessary to fulfill the $M_{\rm BH} - M_{\rm bulge}$ relation on the remnant galaxy before they form a bound binary.

Moreover, I estimate that gap formation would be possible only if the gas has a turbulent velocity of the order of 10 km $s^{-1}$ , which is comparable with the turbulent velocity in the inner region of local spiral galaxies. Also, the gap formation would be possible if the SMBHs accrete a mass that is of the order of 2 % the mass of the bulge of the remnant galaxy before they form a bound binary, mass that is one order of magnitude greater than the expected from the $M_{\rm BH} - M_{\rm bulge}$ relation. This implies that the SMBHs have to accrete mass at a rate much greater than the derived from observations. Therefore, we may expect that in typical conditions of the central kilo parsec of ULIRGs SMBH binaries will coalescence in a timescale of the order of $10^7$ yr.

In addition, I studied the effect of star formation in the dynamical evolution of a pair of SMBHs in the pre-binary epoch following the evolution of a pair of SMBHs with a initial distance of 500 pc inside a star forming circum-nuclear disk (CND). For this purpose I implemented in the code Gadget-3 recipes of star formation, cooling and supernova explosions that allowed me to simulate the multiphase structure of the gas. I found that the orbits of the SMBHs are perturbed by the presence of high density gas clumps and that the shrinking of the separation of the SMBHs from 500 pc down to 4 pc does not depend strongly on the star formation efficiency. Indeed, I proved that for a difference of a factor 20 in the star formation efficiency the migration timescale changes only in factor a 2.

## 6.2. Open issues

**Implemented recipes of SF, cooling and SN heating in galaxy mergers:** In chapter §2.2 I present my implementation of recipes for star formation, supernovae heating and cooling in the code Gadget-3. In chapter §4 I use these recipes to study the effect of the star formation efficiency in the migration of a pair of SMBHs in a star-forming circum nuclear disk. These recipes allow me to model in a better way the multiphase structure of the gas than the recipes that are included in the code Gadget-3.

As a future work I will simulate the same galaxy mergers that I simulate in chapter §5 but with the recipes that I implemented. These simulations will have a more clumpy and realistic ISM which will allow me to evaluate the likelihood of coalescence of SMBH binaries in the central region of interacting galaxies in a more realistic environment.

**Gap-opening criterion in other astronomical systems:** The gap-opening criterion that I derive in this thesis can be applied to other systems that are analogous to the SMBH binary-disk system. For example: the evolution of proto-stellar binaries and common envelope events which are produced when one of the stars enter in a giant phase (Passy et al. 2012).

For proto-stellar binary system the proto-stars will shrink their separation until they excavate a gap on the gaseous environment, in analogue way as SMBH binaries do. Therefore my gap-opening criterion can be used to determine the final separation of star binaries. Also knowing the timescale in which gap-formation occurs allows us to set constraints to the evolution of the gas-dust distribution around binary stars, constraints that

are crucial to models of planet formation around binary stars. For example some studies show that the dimensionless viscosity parameter (Shakura & Sunyaev 1973) of the gas in a proto-planetary disk is higher than the dimensionless viscosity parameter of the dust (Johansen & Klahr 2005), meaning that gap formation can occur first in the dust, producing a decoupling between gas and dust.

**Viscous dissipation in the gap opening criterion:** From the gap-opening criterion of chapter §3 we can see that in a gaseous disks where viscous dissipation is faster, it is harder for the binary to excavate a gap. This happens because with a faster viscous dissipation the gas is able to redistribute the extracted angular momentum from the binary.

In my derivation of the gap-formation I used the dimensionless viscosity parameter $\alpha_{\rm ss}$ of Shakura & Sunyaev (1973) to parametrize the viscous dissipation ($\nu_{\rm visc} \sim \alpha_{\rm ss}\, c_{\rm s}$), which in my simulations is $\alpha_{\rm ss} \approx 0.008 - 0.016$. However, the presence of magnetohydrodynamic stresses can significantly increase the viscous torques, with an effective dimensionless viscosity parameter $\alpha \geq 0.2$ (Shi et al. 2012). Moreover, global instability of the gas in massive gaseous also increase the torques, leading to an effective $\alpha_{\rm ss}$ of order unity (Krumholz et al. 2007, Escala et al. 2007).

From these estimates, we expect that the value of $\alpha_{\rm ss}$ in real gas-rich astrophysical systems, like the nuclear disk in ULRIGs (Downes & Solomon 1998) and Sub-millimeter Galaxies (Chapman et al. 2003, 2005; Takoni et al. 2006; Swinbank et al. 2010), will be one or two orders of magnitude greater than in my simulations. Therefore, from the gap-opening criterion we can conclude that in the nuclear region of the gas-rich merging galaxies, it is more likely that a SMBH binary will not be able to excavate a gap on the gas, allowing the gravitational torques from the gas to shrink the SMBH binary separation down to scales where gravitational wave emission can drive the final coalescence of the binary within a Hubble time. For this reason it will be very interesting to test the dependence between the gap-opening criterion and the strength of the viscous torques, in order to determine if these important predictions of the gap-opening criterion are correct.

**Black hole accretion luminosity:** From a simple estimation we can compare the luminosity associated to an AGN with the luminosity produced by several supernova explosions in the vicinity of a SMBH binary. Assuming that the energy released by a population of stars per unit of mass is $\sim 7.65 \times 10^{47}$ erg $M_{\odot}^{-1}$ (Stinson et al. 2006) and that the typical timescale for supernova explosions is of the order of $10^6$ years, we find that the luminosity associated to supernova explosions in a stellar population of total mass $M_{\rm stars}$ is $\sim 3 \times 10^{35}\, (M_{\rm stars}/M_{\odot})$ erg s$^{-1}$. Also, we can assume that at the beginning of the binary evolution a total mass of stars comparable with the mass of the SMBHs is inside the orbit of the binary. In this case, for a SMBH binary of mass $\sim 10^8$ M$_{\odot}$ the supernova luminosity associated to the stars, inside the orbit of the binary, is $\sim 3 \times 10^{43}$ erg s$^{-1}$. On the other hand, a SMBH of mass $\sim 10^8$ M$_{\odot}$ accreting at the Eddington limit has an accretion luminosity of the order $\sim 10^{46}$ erg s$^{-1}$, which is much greater than the luminosity associated to the supernovas (note that the luminosity of AGNs range between $10^{42} - 10^{48}$ erg s$^{-1}$, e.g: Hopkins, Richards & Hernquist 2007). Therefore, we can assume that the effect of the black hole accretion luminosity in the gas around the SMBH binary

would be another important process worthy of being studied.

Although this process is typically included in some simulation of galaxy merger, the recipes used to model the AGN feedback assume that the gas is efficiently heated by the radiation produced by the accretion onto the black holes. However, how coupled is the gas to the AGN feedback is not clear. Indeed, some works suggest that even for a super-Eddington regime the radiation is not strongly enough to push away the gas that is near the SMBHs (Krumholz & Thompson 2012).

Determine the effect of the AGN feedback onto the gas around a SMBH binary is crucial to determine if this feedback can make easier or more difficult the formation of a cavity. In principle, if the gas is pushed away from the binary then we can think that the AGN feedback will make easier the formation of a gap, however, as the gas is also heated by the AGN feedback, and the gap formation is more difficult in a hotter gas, it is not clear whether the AGN feedback will facilitate or not the formation of a gap. Therefore, an interesting subject to future research is to study the effect of AGN feedback in the likelihood of gap formation and its consequence in the shrinking timescale of SMBH binaries.

**The SMBHs coalescence likelihood in semi analytical models:** Another interesting study would be use what we learn from detailed simulations of galaxy mergers in semi-analytical models of galaxy evolution. We can export the information of the likelihood of coalescence of SMBH and its dependence on the parameters of the galaxy merger to semi-analytical models. Using this information we can determine in a more consistent way the evolution on mass of the population of SMBHs. This information will also permit us to compute the gravitational wave background on the universe that is expected to be observed using millisecond pulsar timing arrays.

### 6.2.1. SMBHs in the context of hierarchical structure formation

In the ΛCDM cosmological model, the currently accepted evolutionary model for the universe, lower mass self-gravitating systems form first later, following a hierarchical process of mass accretion and mergers, more massive gravitationally bound systems appear in the Universe. In this evolutionary picture of the Universe the host galaxies of SMBHs experience multiple mergers during their lifetime (Menou, Haiman & Narayanan 2001). In these mergers SMBHs will sink together with the core of each galaxy and ultimately they will form binary systems inside the core of the mergers remnants.

From the hierarchical structure formation model we may expect that, if the shrinking of these binaries is not fast enough then SMBH binaries may be widespread in the Universe and, as Volonteri, Haardt & Madau (2003) show, they may contribute up to 10 % of the total population of SMBHs today and even more in the past. Indeed, if the binary shrinks only due to the gravitational interaction with stars the shrinking timescales is $t_{\rm s} \sim 1 - 10$ Gyr, which is comparable to or greater than the timescale between galaxy mergers. These means that triple SMBH interactions after a major merger are very likely, which will result in a population of massive SMBHs wandering in galaxy halos and in the intergalactic medium at the present epoch (Volonteri, Haardt & Madau 2003).

The results that I present in this thesis naturally suppress these predictions because they support that the shrinking timescale of SMBHs after a galaxy merger is of the order of $t_s \sim 10$ Myr thanks to the presence of gas that extracts angular momentum from the binary in a efficient way. Indeed, I found that for higher redshifts where the amount of gas is greater and the turbulent velocity of the gas higher is more likely that the shrinking of the SMBH binary will be faster, making the existence of a high rate of triple SMBH interactions very unlikely at high redshifts. Therefore, we expect not to observe this population of wandering SMBHs at redshift zero. A population of this type is more likely made of a collection of recoiling SMBHs: black holes that are the result of the coalescence of two black holes (2 MBHs $\rightarrow$ 1 MBH) and that experience a velocity kick due to the anisotropies of the gravitational waves emitted in the coalescence event (Bonning, Shields & Salviander 2007).

In addition like the merger rate of galaxies is $\propto (1+z)^{2-3}$ (Fakhouri & Ma 2008, Lotz et al. 2011), and for higher redshifts the conditions for a fast shrinking are more favorable (higher gas fraction and more turbulence) thus, the results of my thesis suggest that in most major galaxy mergers ($z > 1$) the SMBH binary will coalescence in a timescale much shorter than the time between mergers. Meaning that the number of SMBHs binaries at this redshifts will be very low, setting important constraints to the evolution of the population of SMBHs and the expected number of SMBH binaries in the Universe.

# Capítulo 7

# Bibliography


Amaro-Seoane P., Aoudia S., Babak S. et al. , 2013, *GW Notes*, **6**, 4

Amaro-Seoane P., Brem P., Cuadra J., 2013, *ApJ*, **764**, 14

Armitage, P., Natarajan, P. 2002, *ApJ*, **567L**, 9

Armitage, P., & Rice, W. K. M. 2005, *Proc. of the STScI May Symp. 2005: A Decade Of Extrasolar Planets Around Normal Stars* p 66 , vol 19, Livio et al. (New York: Cambrige University Press), astro-ph/0507492

Artymowicz, P., Lubow, S.H. 1994, *ApJ*, **421**, 651

Artymowicz, P., Lubow, S.H. 1996, *ApJ*, **467L**, 77

Barnes, J. E. 2002, *MNRAS*, **333**, 481

Barnes, J., Hernquist, L. 1996, *ApJ*, **471**, 115

Barnes, J., Hernquist, L. 1992, *ARA&A*, **30**, 705

Baruteau C. & Masset F., 2013. *Recent developments in planet migration theory. In Tides in Astronomy and Astrophysics* (pp. **201-253**). *Springer Berlin Heidelberg.*

Bate, M. R. & Bonnell, I. A. 1997, *MNRAS*, **285**, 33

Bate, M. R., Lubow, S.H., Ogilvie G. I., & Miller K. A., 2003, *MNRAS*, **341**, 213

Begelman M. C., Blandford R. D. & Rees M. J., 1980, *Nature*, **287**, 307

Berczik P., Merritt D., Spurzem R., Bischof H.-P., 2006, *ApJL*, **642**, L21

Binney J. & Tremaine S., 1987, Galactic Dynamics, *Princeton Univ.Press, New Jersey, USA.*

Boehm, C., Schewtschenko, J. A., Wilkinson, R. J., Baugh, C. M., & Pascoli, S., 2014 *MNRAS*Letters, **445**, L31

Boyle B.J., Shanks, T. et al. , 2000, *MNRAS*, **317**, 1014

Bon E., Jovanovic P., Marziani P. et al. , 2012, *ApJ*, **759**, 118

Boroson, T.A. & Lauer T.R., 2009, *Narure*, **458**, 53

Bromm V., Coppi P.S. & Larson R.B., 2002, *ApJ*, **564**, 23

Callegari S., Kazantzidis S., Mayer L., Colpi M., Bellovary J. M., Quinn T., Wadsley J., 2011, *ApJ*, **729**, 85

Ceverino D. & Klypin A., 2009, *ApJ*, **695**, 292

Chapman S. C., Blain A. W., Ivison R. J. & Smail I. R., 2003, *Nature*, **422**, 695

Chapman S. C., Blain A. W., Smail I. R. & Ivison R. J., 2005, *ApJ*, **622**, 772

Chandrasekhar S., 1943, *ApJ*, **97**, 255

Christensen C. R., Quinn, T., Stinson G., Bellovary J. et al. , 2010, *ApJ*, **717**, 121

Cresci G., Hicks E. K. S., Genzel R., FÃ¶rster-Schreiber N. M., Davies R., *et al.* 2009 ,*ApJ*, **697**, 115

Cuadra J., Armitage P. J., Alexander R. D., et al. , 2009, *MNRAS*, **393**, 1423

Comerford J., Gerke B., Stern D., Cooper M., & Weiner, B., Newman J., Madsen, K., & Barrows, R. 2012, *ApJ*, **753**, 42

Chapman S. C., Blain A. W., Ivison R. J., & Smail Ian R., 2003, *Nature*, **422**, 695

Chapman S. C., Blain A. W., Smail Ian R. & Ivison R. J., 2005, *ApJ*, **622**, 772

Chapon D., Mayer L. & Teyssier R. 2011, submitted eprint arXiv:1110.6086

Dekel A., Sari R. & Ceverino D., 2009, *ApJ*, **703**, 801

del Valle L., Escala A., 2012, *ApJ*, **761**, 31

del Valle L., Escala A., 2014, *ApJ*, **780**, 84

Dib, S., Bell, E., & Burkert, A. 2006, *ApJ*, **638**, 797

Dickey J. M., Hanson M. M. & Helou G., 1990, *ApJ*, **352**, 522

Di Matteo T., Allen S. W., Fabian A. C. et al. , 2002, *in Lighthouses of the Universe: The Most Luminous Celestial Objects and Their Use for Cosmology*, Gilfanov M., Sunyeav R., Churazov E., eds., p. 443

Dotti M., Colpi M., & Haardt, F. 2006, *MNRAS*, **367**, 103

Dotti M., Sesana A. & Decarli R. 2011, *Advances in Astronomy* Volume 2012, Article ID 940568,

Dotti M., Merloni A. & Montuori C., 2015, *MNRAS*, **448**, 3603

Downes D., Solomon P. M., 1998, *ApJ*, **507**, 615

Eracleous, M., Boroson, T.A., Halpern, J.P. & Liu J., 2011, arXiv:1106.2952

Escala A., Larson R. B., Coppi P. S., Mardones D., 2004, *ApJ*, **607**, 765

Escala A., Larson R. B., Coppi P. S., Mardones D., 2005, *ApJ*, **630**, 152

Escala, A., 2007 *ApJ*, **671**, 1264

Evans II, P. J., 1999, *ARA&A*, **37**, 311

Fabian A. C., Wilman R. J., & Crawford C. S., 2002, *MNRAS*, **329**, L18

Fabbiano G., Wang J., Elvis M. & Risaliti G., 2011, *Nature*, **477**, 431

Fakhouri O. & Ma C., 2008, *MNRAS*, **386**, 577

Farris B. D., Duffell P., MacFadyen A. I., Haiman Z., 2014, *ApJ*, **783**, 134

Ferrarese L. & Merritt D. A, 2000, *ApJ*, **539**, 12

Ferrarese L. & Ford H, 2005, *Space Science Reviews*, **116**, 523

Fiacconi D., Mayer L., Roskar R., Colpi M., 2013, *ApJL*, **777**, L14

Foreman, G., Volonteri, M. & Dotti, M., 2009, *ApJ*, **693**, 1554

Garay G. *et al.*, 2004, *ApJ*, **610**, 313

Gerritsen J. P. E & Icke V., 1997, *aap*, **325**, 972

Gingold R. A. & Monaghan J. J., 1977, *MNRAS*, **181**, 375

Goldreich P., Tremaine S. 1980, *ApJ*, **241**, 425

Goldreich P., Tremaine S. 1982, *ARA&A*, **20**, 249

Gold R., Paschalidis V., Etienne Z. B., Shapiro S. L., & Pfeiffer H. P., 2013, arXiv:1312.0600.

Goodman J. & Tan J. C., 2004, *ApJ*, **608**, 108

Gould A. & Rix H.W, 2000, *ApJ*, **532**, L29

Guedes J., Callegari S., Madau P. & Mayer L., 2011, **742**, 76

Gultekin *et al.*, 2009, *ApJ*, **698**, 198

Gunther, R., & Kley, W. 2002, *A&A*, **387**, 550

Hayasaki, K., Mineshige, S., & Sudou, H. 2006, *arXiv preprint astro-ph/0609144.*

Hayasaki K., Saito H. & Mineshige S., 2013, *pasj*, **65**, 4

Heckman T. & Best P., 2014, *Annu. Rev. Astron. Astrophys.*, **52**, 589

Hodge J. A., D. Riechers D., R. Decarli R., et al. , 2014, *ApJ*, **748**, L18

Hopkins P., Richards P. & Hernquist L. 2007, *ApJ*, **654**, 753

Hopkins P. F. & Quataert E., 2010, *MNRAS*, **407**, 1529

Hoyle F., & Fowler, W. 1963, *MNRAS*, **125**, 169

Iono D., Wilson C.D., Takakuwa S., et al. , 2007, **659**, 283

Ivanov P. B., Papaloizou J. C. B., & Polnarev A. G., 1999, *MNRAS*, **307**, 79

Johansen A. & Klahr H., 2005, *ApJ*, **634**, 1353

Kaspi, S., Smith, P. S., Netzer, H., et al. , 2000,*ApJ*, **533**, 631

Katz N., Weinberg D. H., Hernquist L., 1996, *apjs*, **105**, 19

Kazantzidis, S., et al. 2005, *ApJ*, **623L**, 67

Kennicutt Jr. R. C., 1998, *ApJ*, **498**, 541

Khan F. M., Just A., Merritt D., 2011, *ApJ*, **732**, 89

Kazantzidis S., Mayer L., Colpi M., Madau P., Debattista V. P,, Wadsley J., Stadel J., Quinn T., and Moore B. *ApJ*, **623**, 67

Khan F. M., Preto M., Berczik P., Berentzen I., Just A., & Spurzem. R., 2012, *ApJ*, **749**, 147

Kim H., Kim W.-T., 2007, *ApJ*, **665**, 432

Kormendy J., Ho L. C., 2013, araa, **51**, 511

Komossa S., Burwitz V., Hasinger G., Predehl P., Kaastra J. S. & Ikebe Y., 2003, *ApJL*, **582**, L15

Kocsis B., Haiman Z. & Loeb A., 2012a, *MNRAS*, **427**, 2680

Kocsis B., Haiman Z. & Loeb A., 2012b, *MNRAS*, **427**, 2660

Komosa S., Zhou H. & Lu H., 2008, *ApJ*, **678**, 81

Krumholz M., Klein R. & McKee C., 2007, *ApJ*, **656**, 959

Krumholz, M. & Thompson T., 2012, *ApJ*, **760**, 155

La Franca F., Fiore F., Comastri A., et al. , *ApJ*, 2005, **635**, 854

Lehto H. & Valtonen M., 1996, *ApJ*, **460**, 207

Levin Y., 2007, *MNRAS***374**, 515

Liu X., Greene J., Shen Y. & Strauss A., 2010, *ApJL*, **715**, 1

Liu X., Greene J., Shen Y. & Strauss A., 2011, *ApJL*, **737**, 2

Lin, D. N. C., Papaloizou, J. 1979, *MNRAS*, **186**, 799

Lin, D. N. C., Papaloizou, J. 1986, *ApJ*, **309**, 846

Lodato, G., & Price, D. J. 2010, *MNRAS*, **405**, 1212

Lodato G., Nayakshin S., King A. R., Pringle J. E., 2009, *MNRAS*, **398**, 1392

Lucia G. & Blaizot J., 2007, *MNRASsoc*, **375**, 2

Lucy L. B., 1977, *ApJ*, **82**, 1013

Lupi A., Haardt F., Dotti M., 2015, *MNRAS*, **446**, 1765

Lodato G., & Price D. J., 2010, *MNRAS*, **405**, 1212

Lotz J. M, Jonsson P., Cox T.J., Croton D., 2011, *ApJ*, **742**, 103

Lynden-Bell D. 1969, *Nature*, **223**, 690

Lynden-Bell D. & M.J. Rees, 1971 *MNRAS***152**, 461

Lynden-Bell D., 1978, *Physica Scripta*, **17**, 185

MacFadyen A. I. & Milosavljevic M., 2008, *ApJ*, **672**, 83

Madau P. & Rees M. J., 2001, *ApJLet.* **551**, L27

Magorrian J., Tremaine S., Richstone D. et al. , 1998, *ApJ*, **115**, 2285.

Mathis J. S., 1990, araa, **28**, 37

Marconi A. & Hunt L. K, 2003, *ApJ*, **589**, L21

Mayer L., Kazantzidis S., Madau P., Colpi M., Quinn T., & Wadsley J. 2007, *Science*, **316**, 1874

Makino J., Funato Y., 2004, *ApJ*, **602**, 93

Mashchenko S., Wadsley J. & Couchman H. M. P., 2008, *Science*, **319**, 174

Mayer L., Kazantzidis S., Escala A., Callegari S., 2010, *Nature*, **466**, 1082

Mayer L. *et al.*, 2007, *Science*, **316**, 1874

McKee C. F. & Ostriker J. P., 1977, *ApJ*, **218**, 148

McKee C .F. & Ostriker E. C., 2007, *ARA&A*, **45**, 565

Medling A. M., U V., Guedes J., Max C. E. et al. , 2014, *ApJ*, **784**, 70

Menou K., Haiman Z. & Narayanan V. K., 2001, *ApJ*, **558**, 535

Merloni A., 2004, *MNRAS*, **353**, 1035

Merloni A. & Heinz S., 2008, *MNRAS*, **388**, 1011

Mestel, L. 1963, *MNRAS*, **126**, 553

Mihos J. C., Hernquist L., 1996, *ApJ*, **464**, 641

Milosavljevic M., & Phinney E. S., 2005, *ApJ*, **622**, L93

Miralda-Escude J., Kollmeier J. A., 2005, *ApJ*, 619, 30

Miller G. E. & Scalo J. M., 1979, *apjs*, **41**, 513

Monaghan J. J., 1992, *ARA&A*, **30**, 543

Murray, J. R. 1996, *MNRAS*, **279**, 402

Muñoz D. J. *et al.*, 2007, *ApJ*, **668**, 906

Myers A. D et al. , 2007, *ApJ*, **658**, 99

Myers A. D et al. , 2008, *ApJ*, **678**, 635

Netzer, H., 2003, *ApJ*Letters, 583,

Novak G. S., Faber S. M. & Dekel A., 2006, *ApJ*, **637**, 96

Oka, T., Hasegawa, T., Sato, F., *et al.* 2001, *ApJ*, **562**, 348

Ostriker E. C., 1999, *ApJ*, **513**, 252

Ozel F., Psaltis D., Narayan D., & McClintock J., 2010, *ApJ*, **725**, 1918

Passy JC., De Marco O., Fryer C. L., Herwig F. et al. , 2012, *ApJ*, **744**, 52

Peters P. C. & Mathews J., 1963, *Phys. Rev.* **131**, 435

Peters P. C., 1964, *Phys. Rev.*,**136**, 1224

Plummer, H. C. 1911, *MNRAS*, **71**, 460

Preto M., Berentzen I., Berczik P. & Spurzem, R., 2011, *ApJL*, *732*, L26

Price D. J., 2007, pasa, **24**, 159

Raiteri C. M., Villata M., Navarro J. F., 1996, aap, **315**, 105

Richstone D. *et al.*, 1998, *Nature*, **395**, A14

Richards G.T., Strauss M. A. & Fan, 2006, *ApJ*, **131**, 2766

Rodriguez C., Taylor G. B., Zavala R. T. et al. , 2006, *ApJ*, **649**, 49

Roedig C., Dotti M., Sesana A., Cuadra J., & Colpi M., 2011, *MNRAS*, **415**, 3033

Roedig, C., Sesana, A., Dotti, M., Cuadra, J., Amaro-Seoane, P. & Haardt F., 2012, å, **545**, 127

Roskar R. *et al.*, 2014, ArXiv e-prints

Salpeter, E. E., 1964, *ApJ***140**, 796

Sanders D. B., Mirabel I. F., 1996, araa, **34**, 749

Saitoh T. R. et al. , 2008, *pasj*, **60**, 667

Saitoh T. R. *et al.*, 2010, in Astronomical Society of the Pacific Conference Series, Vol. 423, Galaxy Wars: Stellar Populations and Star Formation in Interacting Galaxies, Smith B., Higdon J., Higdon S., Bastian N., eds., p. 185

Scannapieco, C., White, S., Springel, V. & Tissera, P., 2009,*MNRAS*, **396**, 696

Schulz A. *et al.*, 2007, aap, **466**, 46

Shakura, N. 1., & Sunyaev, RA., 1973, *A&A*, **24**, 337

Shaver P. A., Wall J. V.,Kellerman K. I. et al. 1996, *Nature*, **384**, 439

Shu F. H., Adams F. C. & Lizano S., 1987, *ARA&A*, **25**, 23

Shi J., Krolik J., Lubow S., & Hawley J., 2012, *ApJ*, **749**, 118

Sillanpaa A., Haarala S., Valtonen M. J. et al. , 1988, *ApJ*, **325**, 628

Soltan A., 1982, *MNRAS*, **200**, 115

Springel V., Yoshida N. & White S. D. M., 2001, *NewA*, **6**, 79

Springel V., Hernquist L., 2003, *MNRAS*, **339**, 289

Springel V., Di Matteo T. & Hernquist L., 2005, *MNRAS*, **361**, 776

Springel V., 2005, *MNRAS*, **364**, 1105

Springel V. *et al.*, 2005b, *Nature*, **435**, 629

Stinson G. et al. , 2006, *MNRAS*, **373**, 1074

Struve C., Conway J. E., 2010, aap, **513**, A10

Swinbank, A., Smail, I., Longmore, S., Harris, A., Baker, A., De Breuck C., Richard, J., Edge, A., Ivison, R., Blundell, R., Coppin, K., Cox, P., Gurwell, M., Hainline, L., Krips, M., Lundgren, A., Neri, R., Siana, B., Siringo, G., Stark, D., Wilner, D., & Younger, J., 2010, *Nature*, **464**, 733

Takeuchi, T. & Lin, D. N. C., 2002, *ApJ*, **581**, 1344

Takoni, L., Neri, R., Chapman S., Genzel R., Smali, I., Ivison, R., Bertoldi, F,. Blin A., Cox P., Greve T. & Omont A., 2006, *ApJ*, **640**, 228

Tasker E.J. & Bryan G.L., 2006 ,*ApJ*, **641**, 878

Taylor, P. & Miller J., 2011, arXiv:1112.5120v3 [astro-ph.IM]

Tzalmantza, P., Decarli, R., Dotti, M, & Hogg D.W., 2011, *ApJ*, **738**, 20

Ueda J., Iono D., Yun M. S., Crocker A. F. *et al.*, 2014, apjs, **214**, 1

Valtonen, M., Lehto J. H., Nilsson K., et al. , 2008, *Nature*, **452**, 851

Van Wassenhove S., Volonteri M., Mayer L. & Dotti M.,2012, *ApJL*, **748**, L7

Vasiliev E., Antonini F. & Merritt D., 2014, *ApJ*, **785**, 163

Vasiliev E., Antonini F. & Merritt D., 2015, *ApJ*, **810**, 49

Volonteri M., Haardt F. & Madau P., 2003, *ApJ*, **582**, 559

Wada K. & Norman C., 2000, *ApJ*, **547**, 172

Wadsley J. W., Stadel J., Quinn T., 2004, *Nature*, **9**, 137

Ward, W. R, & Hourigan, K. 1989, *ApJ*, **347**, 490

Ward, W. R. 1997, *Icarus*, **126**, 261

White, S. D., & Frenk, C. S., 1991, *ApJ*, **379**, 52

Xu C. K., Cao C., Lu N., et al. , 2014, *ApJ*, **787**, 48

Yu Q. & Tremaine S., 2002, *MNRAS*, **335,4** 965

ZelDovich, Y. B. & Novikov, I. D., 1964, *Soviet Physics Doklady*, **9**, 246